FOSSIL ENERGY

MEASUREMENT AND MODELING OF ADVANCED COAL CONVERSION PROCESSES

13th Quarterly Report #523043-42
October 1, 1989 to December 31, 1989

By
Peter R. Solomon
Michael A. Serio
David G. Hamblen
L. Douglas Smoot
B. Scott Brewster

Work Performed Under Contract No. DE-AC21-86MC23075

For
U.S. Department of Energy
Office of Fossil Energy
Morgantown Energy Technology Center
Morgantown, West Virginia
Dr. Richard Johnson
COTR

By

Contractor

Advanced Fuel Research, Inc.
87 Church Street
East Hartford, CT 06108
(203) 528-9806

Program Director

Peter R. Solomon
President

Subcontractor

Brigham Young University
Provo, Utah 84602
(801) 378-4326

Program Director

L. Douglas Smoot
Dean and Professor

DOE/MC/23075--2814

DE90 010628

DISCLAIMER

PATENT STATUS

ABSTRACT

The overall objective of this program is the development of predictive capability for the design, scale up, simulation, control and feedstock evaluation in advanced coal conversion devices. This technology is important to reduce the technical and economic risks inherent in utilizing coal, a feedstock whose variable and often unexpected behavior presents a significant challenge. This program will merge significant advances made at Advanced Fuel Research, Inc. (AFR) in measuring and quantitatively describing the mechanisms in coal conversion behavior, with technology being developed at Brigham Young University (BYU) in comprehensive computer codes for mechanistic modeling of entrained-bed gasification. Additional capabilities in predicting pollutant formation will be implemented and the technology will be expanded to fixed-bed reactors.

The foundation to describe coal-specific conversion behavior is AFR's Functional Group (FG) and Devolatilization, Vaporization, and Crosslinking (DVC) models, developed under previous and on-going METC sponsored programs. These models have demonstrated the capability to describe the time dependent evolution of individual gas species, and the amount and characteristics of tar and char. The combined FG-DVC model will be integrated with BYU's comprehensive two-dimensional reactor model, PCGC-2, which is currently the most widely used reactor simulation for combustion or gasification. The program includes: i) validation of the submodels by comparison with laboratory data obtained in this program, ii) extensive validation of the modified comprehensive code by comparison of predicted results with data from bench-scale and process scale investigations of gasification, mild gasification and combustion of coal or coal-derived products in heat engines, and iii) development of well documented user friendly software applicable to a "workstation" environment.

Success in this program will be a major step in improving the predictive capabilities for coal conversion processes including: demonstrated accuracy and reliability and a generalized "first principles" treatment of coals based on readily obtained composition data.

The progress during the thirteenth quarterly of the program is summarized below.

For Subtask 2.a., a significant amount of work was done in the area of tar transport, work was resumed on the addition of polymethylenes to the FG-DVC model, and work also continued on the swelling model.

In addition, work continued on examining a percolation theory approach to doing the network decomposition calculations. A version of the model was developed which incorporates two different types of bonds, the so-called two-σ model. The Monte Carlo and two-σ predictions of the tar yield and of the coal fluidity data agree reasonably well with each other and with the data.

Work also continued on examining the rank dependence of the pyrolysis kinetic rates. So far, comparisons have been made with Pittsburgh Seam bituminous coal TG-FTIR data from experiments at four different heating rates. In this case, rank dependent kinetics have been determined which provide an excellent fit to the evolution profiles and yields for each heating rate.

Finally, a comparison was made of intrinsic reactivity measurements for Montana Rosebud coal determined from the non-isothermal test to the plot

developed by Smith (1982) for a range of carbons over a wide range of temperatures. The agreement at low temperatures was within a factor of two when compared to Smith's data for brown coal chars. When the results were extrapolated to high temperatures using E = 35 kcal/mole, again good agreement was obtained with Smith's data for coal chars (within a factor of two).

For Subtask 2.b., work continued on developing the optical particle-imaging system for the HPCP reactor. A new particle injection probe with smaller diameter and thicker insulation is being fabricated to reduce the thermal impact of the probe on the preheated inlet stream. A suction pyrometer for reactor centerline temperature characterization is also being fabricated. Work continued on the analytical procedure to measure titanium content for determining char burnout.

For Subtask 2.c., work continued on doing coal flame experiments in the transparent wall reactor (TWR). For a Montana Rosebud flame, tomographic reconstruction techniques were applied to line-of-sight FT-IR Emission/Transmission (E/T) measurements to derive spectra that correspond to small volumes within a coal flame. From these spectra, spatially resolved point values for species temperatures and relative concentrations can be determined as functions of distance from the flame axis and height above the coal injector nozzle. Initial measurements (reported last quarter) were made at 6 cm and 12 cm above the coal injector nozzle, with the ignition point occurring at 10 cm. During this quarter, two more slices of data, at 16 cm and 20 cm above the nozzle were collected and tomographically reconstructed.

For Subtask 2.d., the work on the study of mineral transformations in the entrained flow reactor (EFR) was temporarily suspended due to manpower and funding constraints. Temperature Programmed Desorption (TPD) experiments were done in air for chars produced from all of the Argonne coals. The CO_2 desorption and the O_2 adsorption show a consistent trend with the char reactivity as measured by the Critical Temperature (T_{cr}).

For Subtask 2.e., the work on the AFR fixed-bed reactor (FBR) system was continued. Experiments were done at two bed depths and two flow rates with samples of Illinois No. 6, Pittsburgh No. 8, and Upper Freeport bituminous coals. Over the range of bed depths examined, there did not appear to be a large effect on tar yield and composition. We were restricted from using larger bed depths because problems with tar deposition in the gas cell. However, the ability to bypass some of the tar from the cell has recently been added which will allow larger samples to be used.

For Subtask 2.f., work was initiated on this subtask. A literature search of large particle oxidation and high-pressure reactor systems was conducted. An experimental approach was selected which includes using reactor tubes containing fixed beds of large char particles inserted in the HPCP reactor from Subtask 2.b.

For Subtask 2.g., work continued on evaluating the thermal NO submodel using data from the BYU/ACERC laboratory-scale reactor. Problems with the high gas temperature previously predicted by PCGC-2 have been resolved, and thermal NO predictions have been compared with experimental data. The NO concentration is underpredicted by approximately 30 percent, but it is not certain that this disparity is a result of neglecting prompt NO. Several coal gasification cases have been simulated, and the gas temperature and major species concentrations

agree reasonably well with the experimental data. Evaluation of the combined fuel and thermal NO mechanism is ready to begin.

For Subtask 3.a., several improvements in PCGC-2 were made during the last quarter. A major error was discovered and corrected in the radiation submodel. This correction apparently resolved the previously reported problem with unreasonably high temperature predictions in some cases. A new option was also added to the code for solving the radiation submodel for gaseous combustion (no particles). Converged solutions were then obtained for several cases being used in Subtask 2.g to evaluate the extended NO_x submodel, and for the gasification case chosen previously as a standard test case. Additional model validation data were also obtained from AFR, and work continued on modeling the TWR reactor facility. Development of a user-friendly, graphical interface on the Sun workstation was also continued.

For Subtask 3.b., work continued during the last quarter on coding chemical and physical submodels and model validation. Improved temperature profiles and pressure profiles have been obtained from the one-dimensional, fixed-bed code. Predictions and comparisons to experimental data include effluent gas compositions and temperatures, temperature profiles, and axial pressure variation. Additional predictions with comparison to limited data include carbon conversion, variable particle size, and species concentration profiles. The relative importance of char oxidation resistances to bulk film diffusion, ash diffusion, and chemical reaction are identified. For the cases examined, chemical resistance dominates in the cool regions at the bottom and top of the reactor while ash diffusion resistance competes with chemical resistance throughout most of the reactor.

For Subtask 4.a., this subtask has not been initiated.

For Subtask 4.b., work continued on collecting fixed-bed design and test data from organizations and individuals involved in fixed-bed research. Eighteen sets of data have been obtained, but some of the most important ones have not been obtained yet. Work also continued on collecting fixed-bed experimental data from the open literature. Further testing and validating of the advanced fixed-bed code developed in Subtask 3.b was performed.

MEASUREMENT AND MODELING OF COAL CONVERSION PROCESSES

Contract No. DE-AC21-86MC23075

Table of Contents

DISCLAIMER i

ABSTRACT ii

I. INTRODUCTION 1

I.A. Program Background and Description 1
I.B. Objectives 1
I.C. Approach 2
I.D. Critical Technical Issues 2
I.E. Third Year Progress 3

II. TASK 2 - SUBMODEL DEVELOPMENT AND EVALUATION 9

II.A. Subtask 2.a. - Coal to Char Chemistry Submodel 10
II.B. Subtask 2.b. - Fundamental High-Pressure Reaction Rate Data 26
II.C. Subtask 2.c. - Secondary Reaction of Pyrolysis Product and Burnout Submodels 33
II.D. Subtask 2.d. - Ash Physics and Chemistry Submodel 35
II.E. Subtask 2.e. - Large Particle Submodels 37
II.F. Subtask 2.f. - Large Char Particle Oxidation at High Pressures 39
II.G. Subtask 2.g. - SO_x-NO_x Submodel Development 43

III. TASK 3 - COMPREHENSIVE MODEL DEVELOPMENT AND EVALUATION 54

III.A. Subtask 3.a. - Integration of Advanced Submodels into Entrained-Flow Code, with Evaluation and Documentation 55
III.B. Subtask 3.b. - Comprehensive Fixed-Bed Modeling Review, Development Evaluation and Implementation 65

IV. TASK 4 - APPLICATION OF INTEGRATED CODES 67

IV.A. Subtask 4.a. - Application of Generalized Pulverized Coal Comprehensive Code 68
IV.B. Subtask 4.b. - Application of Fixed-Bed Code 69

V. REFERENCES 71

APPENDIX A - "FT-IR Emission/Transmission Tomography of a Coal Flame" 75

APPENDIX B - "Chemical and Physical Processes in Countercurrent Fixed-Bed Coal Gasification" 97

SECTION I. INTRODUCTION

I.A. PROGRAM BACKGROUND AND DESCRIPTION

During the past 5 years, significant advances have been made at Brigham Young University (BYU) in comprehensive two-dimensional computer codes for mechanistic modeling of entrained-bed gasification and pulverized coal combustion. During the same time period, significant advances have been made at Advanced Fuel Research, Inc. (AFR) in the mechanisms and kinetics of coal pyrolysis and secondary reactions of pyrolysis products. The proposed program presents a unique opportunity to merge the technology developed by each organization to provide detailed predictive capability for advanced coal conversion processes. This predictive capability will incorporate advanced coal characterization techniques in conjunction with comprehensive computer models to provide accurate process simulations.

The program will streamline submodels existing or under development for coal pyrolysis chemistry, volatile secondary reactions, tar formation, soot formation, char reactivity, and SO_x-NO_x pollutant formation. Submodels for coal viscosity, agglomeration, tar/char secondary reactions, sulfur capture, and ash physics and chemistry would be developed or adapted. The submodels would first be incorporated into the BYU entrained-bed gasification code and subsequently, into a fixed-bed gasification code (to be selected and adapted). These codes would be validated by comparison with small scale laboratory and PDU-scale experiments. The validated code could then be employed to simulate and to develop advanced coal conversion reactors of interest to METC.

I.B. OBJECTIVES

The objectives of this proposed study are to establish the mechanisms and rates of basic steps in coal conversion processes, to integrate and incorporate this information into comprehensive computer models for coal conversion processes, to evaluate these models and to apply them to gasification, mild gasification and combustion in heat engines.

I.C. APPROACH

This program will be a closely integrated, cooperative effort between AFR and BYU. The program will consist of four tasks: 1) Preparation of Research Plans, 2) Submodel Development and Evaluation, 3) Comprehensive Model Development and Evaluation, and 4) Applications and Implementation.

I.D. CRITICAL TECHNICAL ISSUES

To achieve the goals of the program, the computer models must provide accurate and reliable descriptions of coal conversion processes. This will require the reduction of very complicated and interrelated physical and chemical phenomena to mathematical descriptions and subsequently to operational computer codes. To accomplish this objective a number of technical issues must be addressed as noted below. The status of each of these tasks is also indicated.

A	Separation of Rates for Chemical Reaction, Heat Transfer, and Mass Transfer
A	Particle Temperature Measurements Using FT-IR E/T Spectroscopy
A	Functional Group Description of Coal, Char, and Tar
A	Tar Formation Mechanisms
I	Char Formation Mechanisms
A	Viscosity/Swelling
A	Intraparticle Transport
I	Pyrolysis of Volatiles and Soot Formation
I	Secondary Reaction of Tar
I	Particle Ignition
A	Char Reactivity
I	Ash Chemistry and Physics
A	Particle Optical Properties
I	Code Efficiency and Compatibility for Submodels
I	Coupling of Submodels with Comprehensive Codes
I	Comprehensive Code Efficiency
I	Turbulence
I	SO_x and NO_x
o	Generalized Fuels Model
I	Fixed-Bed Model

(o) to be addressed; (I) initiated; (A) almost completed.

These technical issues are addressed in the three Tasks as described in Sections II-IV.

I.E. THIRD YEAR PROGRESS

Subtask 2.a. Coal to Char Chemistry Submodel Development and Evaluation

A significant amount of work was done in the area of tar transport during the past quarter. The current vapor pressure law does a good job of predicting the relative amounts of the oligomers in each size classification from FIMS pyrolysis experiments. However, it predicts a shift in the temperature range of the oligomers as the size range increases in the case of bituminous coal pyrolysis/FIMS, which is not observed in the actual data. We believe this results from restricted diffusion of the large oligomers as the coal begins to resolidify.

Work was resumed on the addition of polymethylenes to the FG-DVC model. Some predictions were made of the tar hydrogen composition for coals of different rank and compared to measurements made by Freihaut et al. (1988). Good agreement was obtained except for the two lowest rank coals (Zap lignite, Wyodak subbituminous), where the predicted hydrogen composition was too high.

Work also continued on the swelling model. Additional bubble types (sizes) were introduced into the model in order to improve the prediction of surface area. However, this did not lead to better predictions, so other modifications to the model will be tried.

Work continued on examining a percolation theory approach to doing the network decomposition calculations. A version of the model was developed which incorporates two different types of bonds, the so-called two-σ model. Three important new features in our two-σ percolation theory are: (i) tar vaporization, (ii) molecular weight distribution of monomers, and iii) an approximation which allows the removal of tar. These features are basically treated the same way as in the original DVC model. The Monte Carlo and two-σ predictions of the tar yield and of the coal fluidity data agree reasonably well

with each other and with the data.

Work also continued on the rank dependence of the pyrolysis kinetic rates. So far, comparisons have been made with Pittsburgh Seam bituminous coal TG-FTIR data from experiments at four different heating rates. In this case, rank dependent kinetics have been determined which provide an excellent fit to the evolution profiles and yields for each heating rate.

A comparison was made of intrinsic reactivity measurements for Montana Rosebud coal determined from the non-isothermal test to the plot developed by Smith for a range of carbons over a wide range of temperatures. The agreement at low temperatures was within a factor of two when compared to the data of Smith (1982) for brown coal chars. When the results were extrapolated to high temperatures using E = 35 kcal/mole, again good agreement was obtained with Smith's data for coal chars (within a factor of two).

Subtask 2.b. Fundamental High-Pressure Reaction Rate Data

Work continued on developing the optical particle-imaging system for the HPCP reactor. A mass flow meter and flow controllers were installed in the inlet streams to enable more rapid testing. A new particle injection probe with smaller diameter and thicker insulation is being fabricated to reduce the thermal impact of the probe on the preheated inlet stream. A suction pyrometer for reactor centerline temperature characterization is also being fabricated. The facility was modified to enable insertion of the pyrometer from the bottom of the reactor. Work continued on the analytical procedure to measure titanium content for determining char burnout.

Under independent funding, work continued on the collection of tar/char/gas from devolatilization runs in the HPCP reactor. Four devolatilization runs were made with North Dakota lignite at atmospheric and elevated pressures. The collection system is being modified to improve the separation.

Subtask 2.c. Secondary Reaction of Pyrolysis Products and Char Burnout

Work continued on doing coal flame experiments in the transparent wall reactor (TWR). An attempt was made to use the Pittsburgh Seam bituminous coal.

However, some problems were experienced in feeding the coal and with flame stability. Consequently, a switch was made back to Montana Rosebud subbituminous coal.

For a Montana Rosebud flame, tomographic reconstruction techniques were applied to line-of-sight FT-IR Emission/Transmission (E/T) measurements to derive spectra that correspond to small volumes within a coal flame. From these spectra, spatially resolved point values for species temperatures and relative concentrations can be determined. Values for particle temperature, relative particle density, relative soot concentration, the fraction of ignited particles, the relative radiance intensity, the relative CO_2 concentration and the CO_2 temperature have been obtained as functions of distance from the flame axis and height above the coal injector nozzle. Initial measurements (reported last quarter) were made at 6 cm and 12 cm above the coal injector nozzle, with the ignition point occurring at 10 cm. During this quarter, two more slices of data, at 16 cm and 20 cm above the nozzle were collected and tomographically reconstructed. An in-depth discussion of the four measurement positions can be found in Appendix A, which is a copy of our paper entitled **"FT-IR Emission/ Transmission Tomography of a Coal Flame"**, which has been submitted to the **23rd Symposium (Int) on Combustion, France, (1990).**

Subtask 2.d. Ash Physics and Chemistry Submodel

The work on the study of mineral transformations in the entrained flow reactor (EFR) was temporarily suspended due to manpower and funding constraints.

Temperature Programmed Desorption (TPD) experiments were done in air for chars produced from all of the Argonne coals. The CO_2 desorption and the O_2 adsorption show a consistent trend with the char reactivity as measured by the Critical Temperature (T_{cr}). The more reactive chars adsorb more O_2 and give off CO_2 earlier. These experiments will be repeated with chars produced from demineralized samples of these coals and experiments will also be done in CO_2.

Samples of char were collected from the Montana Rosebud coal flame experiments in order to do reactivity measurements. Since the samples at high levels of burnout had high ash contents, the non-isothermal reactivity measurement technique (which determines the "critical" temperature) had to be

modified to account for this.

Subtask 2.e. Large Particle Submodels

The work on the AFR fixed-bed reactor (FBR) system was continued. Experiments were done at two bed depths and two flow rates with samples of Illinois No. 6, Pittsburgh No. 8, and Upper Freeport bituminous coals. Over the range of bed depths examined, there did not appear to be a large effect on tar yield and composition. We were restricted from using larger bed depths because problems with tar deposition in the gas cell. However, the ability to bypass some of the tar from the cell has recently been added which will allow larger samples to be used.

It was also found that the temperature of the maximum evolution rate of tar and CH_4 decreased with increasing bed depth. This was due to low levels of oxygen contamination. The contamination problems have recently been solved.

Subtask 2.f. Large Char Particle Oxidation at High Pressure

Work was initiated on this subtask. A literature search of large particle oxidation and high-pressure reactor systems was conducted. An experimental approach was selected which includes using reactor tubes containing fixed beds of large char particles inserted in the HPCP reactor from Subtask 2.b.

Subtask 2.g. SO_x-NO_x Submodel Development

Work continued on evaluating the thermal NO submodel using data from the BYU/ACERC laboratory-scale reactor. Problems with the high gas temperature previously predicted by PCGC-2 have been resolved, and thermal NO predictions have been compared with experimental data. The presence of prompt NO in gaseous hydrocarbon flames has made it difficult to evaluate the results. Relatively high levels of HCN and NH_3 have been measured in the near-burner region, which supports the formation of prompt NO on the fuel-lean side of the flame. The NO concentration is underpredicted by approximately 30 percent, but it is not certain that this disparity is a result of neglecting prompt NO. Expressions for estimating radical oxygen, for example, have been shown to be sensitive to temperature. Several coal gasification cases have been simulated, and the gas

temperature and major species concentrations agree reasonably well with the experimental data. Evaluation of the combined fuel and thermal NO mechanism is ready to begin.

Subtask 3.a. Integration of Advanced Submodels into Entrained-Flow Code, with Evaluation and Documentation

Several improvements in PCGC-2 were made during the last quarter. A major error was discovered and corrected in the radiation submodel. This correction apparently resolved the previously reported problem with unreasonably high temperature predictions in some cases. A new option was also added to the code for solving the radiation submodel for gaseous combustion (no particles). Other improvements were made in the full energy equation option, the SIMPLE-based numerical algorithm used for solving the fluid flowfield, and the tri-diagonal matrix solver used by SIMPLE. Converged solutions were then obtained for several cases being used in Subtask 2.g to evaluate the extended NO_x submodel, and for the gasification case chosen previously as a standard test case. Additional model validation data were also obtained from AFR, and work continued on modeling the TWR reactor facility. Development of a user-friendly, graphical interface on the Sun workstation was also continued.

Subtask 3.b. Comprehensive Fixed-Bed Modeling Review, Development, Evaluation, and Implementation

Work continued during the last quarter on coding chemical and physical submodels and model validation. Improved temperature profiles and pressure profiles have been obtained from the one-dimensional, fixed-bed code. The fixed-bed model considers separate gas and solid temperatures, partial equilibrium in the gas phase, variable bed void fraction, coal drying, devolatilization based on chemical functional group composition, oxidation and gasification of residual char with an ash layer, and axially variable solid and gas flow rates. Predictions and comparisons to experimental data include effluent gas compositions and temperatures, temperature profiles, and axial pressure variation. Additional predictions with comparison to limited data include carbon conversion, variable particle size, and species concentration profiles. The relative importance of char oxidation resistances to bulk film diffusion, ash diffusion, and chemical reaction are identified. For the cases

examined, chemical resistance dominates in the cool regions at the bottom and top of the reactor while ash diffusion resistance competes with chemical resistance throughout most of the reactor. The importance of adequate treatment of devolatilization, gas phase chemistry, and variable bed void fraction is identified.

Subtask 4.a. Application of Generalized Pulverized Coal Comprehensive Code

This subtask has not been initiated.

Subtask 4.b. Application of Fixed-Bed Code

Work continued on collecting fixed-bed design and test data from organizations and individuals involved in fixed-bed research. Eighteen sets of data have been obtained, but some of the most important ones have not been obtained yet. Requests for data were sent again to a number of individuals and organizations who had not responded to the first request. Work also continued on collecting fixed-bed experimental data from the open literature. Further testing and validating of the advanced fixed-bed code developed in Subtask 3.b was performed. The test case was the same as one used before - the test run of the Wellman-Galusha gasifier with Jetson high volatile B bituminous coal. Improved predictions of temperature and pressure profiles were obtained, but the need for further improvement of the advanced fixed-bed code is still evident.

SECTION II. TASK 2. SUBMODEL DEVELOPMENT AND EVALUATION

Objectives

The objectives of this task are to develop or adapt advanced physics and chemistry submodels for the reactions of coal in an entrained-bed and a fixed-bed reactor and to validate the submodels by comparison with laboratory scale experiments.

Task Outline

The development of advanced submodels for the entrained-bed and fixed-bed reactor models will be organized into the following categories: a) Coal Chemistry (including coal pyrolysis chemistry, char formation, particle mass transfer, particle thermal properties, and particle physical behavior); b) Char Reaction Chemistry at high pressure; c) Secondary Reactions of Pyrolysis Products (including gas-phase cracking, soot formation, ignition, char burnout, sulfur capture, and tar/gas reactions); d) Ash Physics and Chemistry (including mineral characterization, evolution of volatile, molten and dry particle components, and ash fusion behavior); e) Large Coal Particle Effects (including temperature, composition, and pressure gradients and secondary reactions within the particle, and the physical effects of melting, agglomeration, bubble formation and bubble transport; f) Large Char Particle Effects (including oxidation); g) SO_x-NO_x Submodel Development (including the evolution and oxidation of sulfur and nitrogen species); and h) SO_x and NO_x Model Evaluation.

II.A. SUBTASK 2.a. - COAL TO CHAR CHEMISTRY SUBMODEL DEVELOPMENT AND EVALUATION

Senior Investigators - David G. Hamblen and Michael A. Serio
Advanced Fuel Research, Inc.
87 Church Street, East Hartford, CT 06108
(203) 528-9806

Objective

The objective of this subtask is to develop and evaluate, by comparison with laboratory experiments, an integrated and compatible submodel to describe the organic chemistry and physical changes occurring during the transformation from coal to char in coal conversion processes.

Accomplishments

A significant amount of work was done in the area of tar transport during the past quarter. The current vapor pressure law does a good job of predicting the relative amounts of the oligomers in each size classification from FIMS pyrolysis experiments. It also does a good job in predicting the direct vaporization of tar in the FIMS apparatus. However, it predicts a shift in the temperature range of the oligomers as the size range increases in the case of bituminous coal pyrolysis/FIMS, which is not observed in the actual data. We believe this results from restricted diffusion of the large oligomers as the coal begins to resolidify. We have developed a few simple approaches to addressing this problem but these have not been fruitful, so far, i.e., we were not able to fix this problem easily without creating problems in the other predictions.

Work was resumed on the addition of polymethylenes to the FG-DVC model. Some predictions were made of the tar hydrogen composition for coals of different rank and compared to measurements made by Freihaut et al. (1988). Good agreement was obtained except for the two lowest rank coals (Zap lignite, Wyodak subbituminous), where the predicted hydrogen composition was too high.

Work also continued on the swelling model. Additional bubble types (sizes) were introduced into the model in order to improve the prediction of surface area. However, this did not lead to better predictions, so other modifications

to the model will be tried.

Work continued on examining a percolation theory approach to doing the network decomposition calculations. A version of the model was developed which incorporates two different types of bonds, the so-called two-σ model. Three important new features in our two-σ percolation theory are: (i) tar vaporization, (ii) molecular weight distribution of monomers, and iii) an approximation which allows the removal of tar. These features are basically treated the same way as in the original DVC model. The Monte Carlo and two-σ predictions of the tar yield and of the coal fluidity data agree reasonably well with each other and with the data.

Work also continued on the rank dependence of the pyrolysis kinetic rates. During the past quarter, the transfer of TG-FTIR data to the Sun microsystems computer was successfully completed. This will allow a faster and more accurate comparison to the data. Criteria were established to assess the degree of fit to the evolution profiles and the yield data. So far, comparisons have been made with Pittsburgh Seam bituminous coal TG-FTIR data from experiments at four different heating rates. In this case, rank dependent kinetics have been determined which provide an excellent fit to the evolution profiles and yields for each heating rate. We will now do a systematic comparison of the same type of data for the remaining Argonne coals.

A comparison was made of intrinsic reactivity measurements for Montana Rosebud coal determined from the non-isothermal test to the plot developed by Smith (1982) for a range of carbons over a wide range of temperatures. The agreement at low temperatures was within a factor of two when compared to Smith's data for brown coal chars. When the results were extrapolated to high temperatures using E = 35 kcal/mole, again good agreement was obtained with Smith's data for coal chars (within a factor of two).

Tar Transport Model

The tar transport model assumes that the tars reach their equilibrium vapor pressure in the light gases and evolve with these gases as they are transported through the pores or by bubble transport. The details of the model are presented in Solomon et al. (1988a). We have used the vapor pressure correlation of

Suuberg et al. (1985) for the equilibrium vapor pressure. Since this vapor pressure law is a function of molecular weight and temperature, we tested the accuracy of our model in predicting the evolution of tar fragments of specific molecular weight as a function of temperature.

The experimental data used was obtained from FIMS analysis, where the FIMS apparatus is in line with a probe used to heat the sample. The FIMS analysis was performed by Ripudaman Malhotra at SRI International on coals, which pyrolyze in the apparatus (coal FIMS), and on already formed coal tar, which vaporizes in the apparatus (tar FIMS). We divided the tar oligomers (from both data and theory) into five different bins: 50-200 amu, 201-400 amu, 401-600 amu, 601-800 amu, and > 800 amu. The evolution with temperature of each bin is then plotted.

Tar FIMS - We found good agreement between the tar FIMS data and our simulation (Fig. II.A-1). A small mismatch is present for large molecular weight oligomers (> 800 amu), where the maximum of rate evolution occurs later in the simulation. The peak is also narrower, i.e. the temperature range of evolution is shorter than found experimentally. The vaporization of smaller oligomers is, however, well predicted. This validates the temperature and molecular weight dependence of the vaporization law (Suuberg et al., 1985) used in the model but not the absolute magnitude of the vapor pressure.

Coal FIMS - We compared the results of the simulation with coal FIMS data for two coals, Pittsburgh No. 8 and Wyodak. We found the best agreement when the Suuberg et al. (1985) correlation is multiplied by ten. For the Pittsburgh No. 8, the theory gave an accurate prediction for the evolution temperature of low molecular weight oligomers, as well as the relative amounts of all oligomer classes (Fig. II.A-2). It, however, predicted higher evolution temperatures for high molecular weight oligomers (> 600 amu), while the data showed a unique temperature of maximum evolution rates (T_{max}) for all molecular weights. A shift to higher T_{max} with higher molecular weight is consistent with the fact that large oligomers need higher temperatures to vaporize, as confirmed by the tar FIMS data. Since coal FIMS data doesn't present this feature, we suspect some additional limitations occur as the fluid coal melt resolidifies.

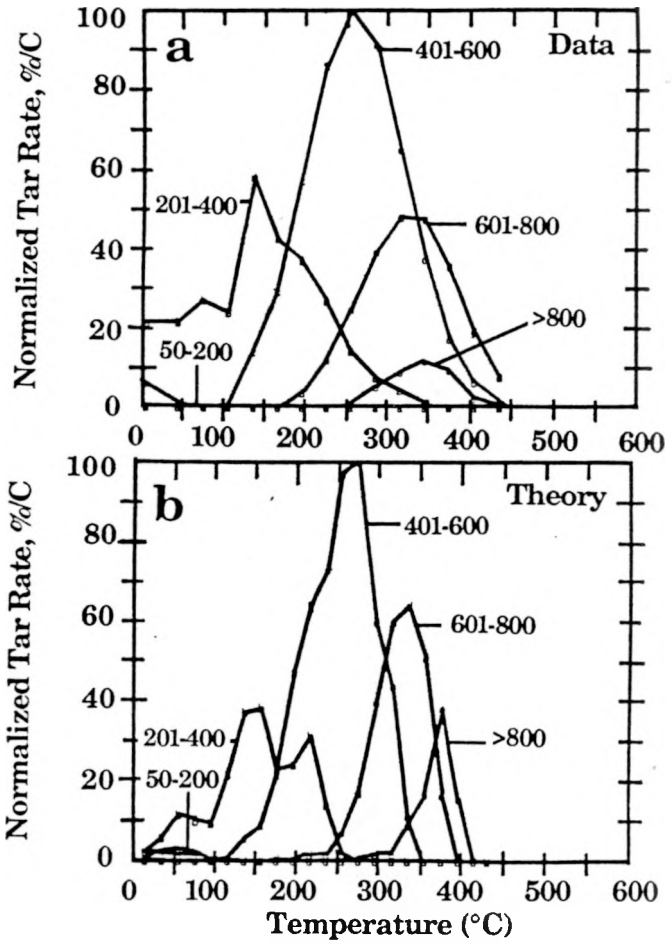

Figure II.A-1. Comparison of a) FIMS Data and b) Theory for Pittsburgh No. 8 Coal Tar.

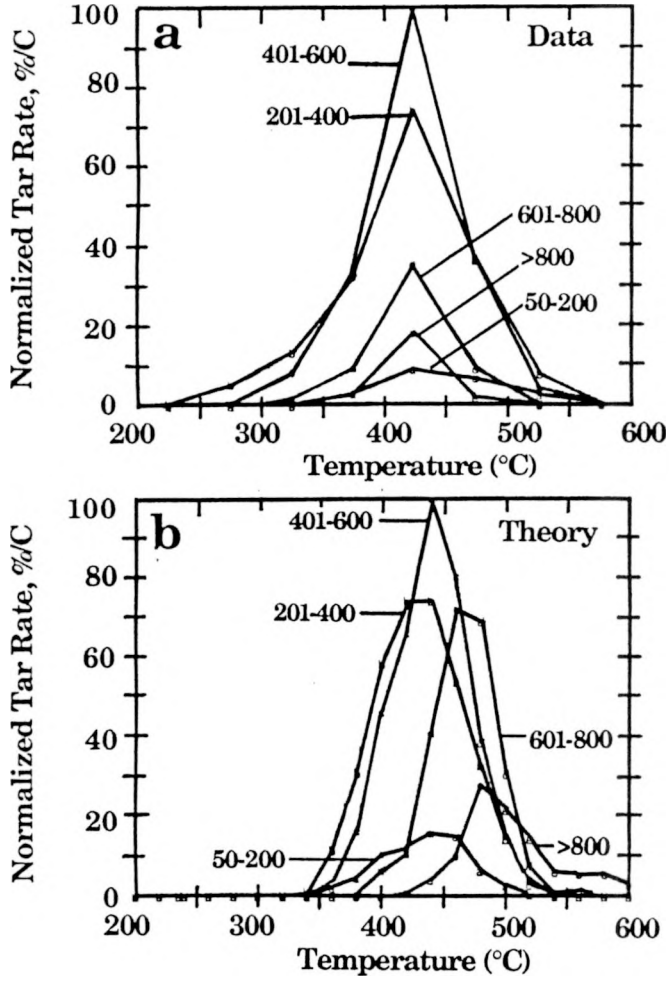

Figure II.A-2. Comparison of a) FIMS Data and b) Theory for Normalized Tar Rate for Pittsburgh No. 8 Coal Pyrolyzed in the FIMS.

The simulation for Wyodak coal gave a good prediction for the evolution of all molecular weight classes oligomers, including large ones (Fig. II.A-3). The data (Fig. II.A-3b) shows that the evolution of high molecular weight oligomers occurs slightly before the smaller oligomers. This also suggests the presence of additional limitations. In our simulation for low rank coals, the peak position is regulated by the low temperature cross-linking rate (which reduces the number of large oligomers which can vaporize) rather than by the vaporization law.

In order to obtain a better prediction for Pittsburgh No. 8, we considered additional transport limitations related to the reduction in the fluidity of the coal. However, none of the simple modifications tried gave a significant improvement in the model for both low and high rank coals. The current model gives good predictions for the relative amounts of the oligomers in each size classification. It also predicts accurately the evolution temperature of low molecular weight (< 600 amu) oligomers. The vapor pressure dependence on temperature and molecular weight is also validated by the good prediction of the tar FIMS data. The present model, therefore, uses the original FG-DVC transport assumption (Solomon et al., 1988a) with the Suuberg et al. (1985) vapor pressure correlation multiplied by ten.

Polymethylenes

Varying amounts (typically 0-9%, but in some cases as high as 18%) of long-chain aliphatics (polymethylenes) have been reported in pyrolysis products by Nelson (1987) and by Calkins and coworkers (1984a,b,c,d) and references quoted therein. The chains appear alone and attached to aromatic nuclei. The presence of these polymethylenes makes the tar more aliphatic than the parent coal. Also, for most coals, there is a low temperature tar peak which results from the vaporization of unattached small polymethylenes plus small aromatic ring clusters. This vaporization peak is illustrated in Fig. II.A-4 (from the Third Annual Report). Polymethylene chains can also crack or be released into the second tar peak. Further cracking of this material under more severe devolatilization conditions produces ethylene, propylene, and butadiene from which the concentration of polymethylenes may be determined (Calkins et al., 1984d). Originally, the polymethylenes were included in the FG model as part of the aliphatic functional group pool, which is assumed to decompose to produce

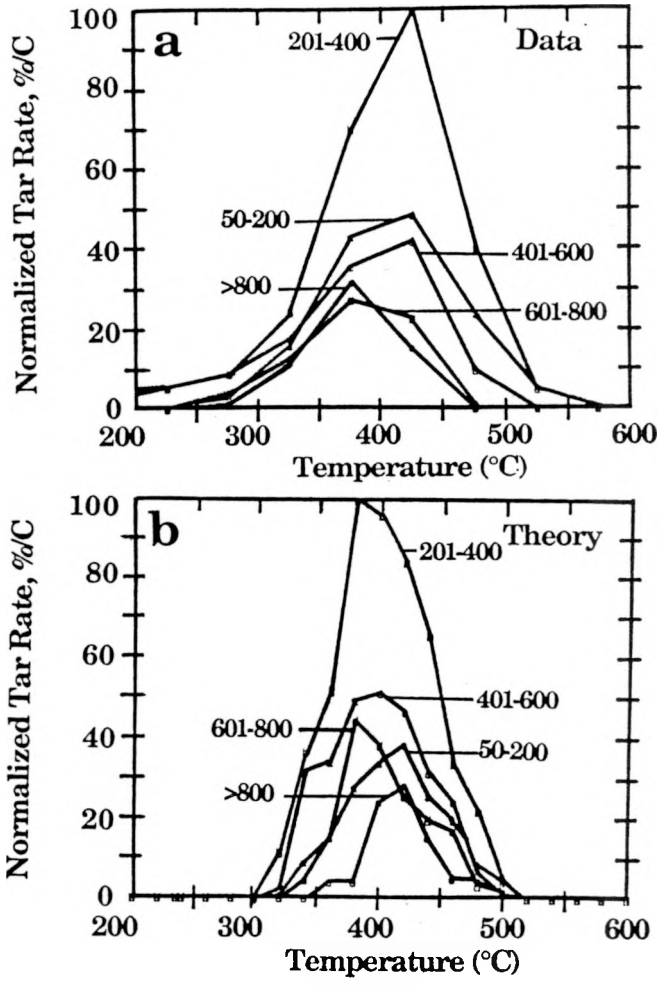

Figure II.A-3. Comparison of a) FIMS Data and b) Theory for Normalized Tar Rate for Wyodak Coal Pyrolyzed in the FIMS.

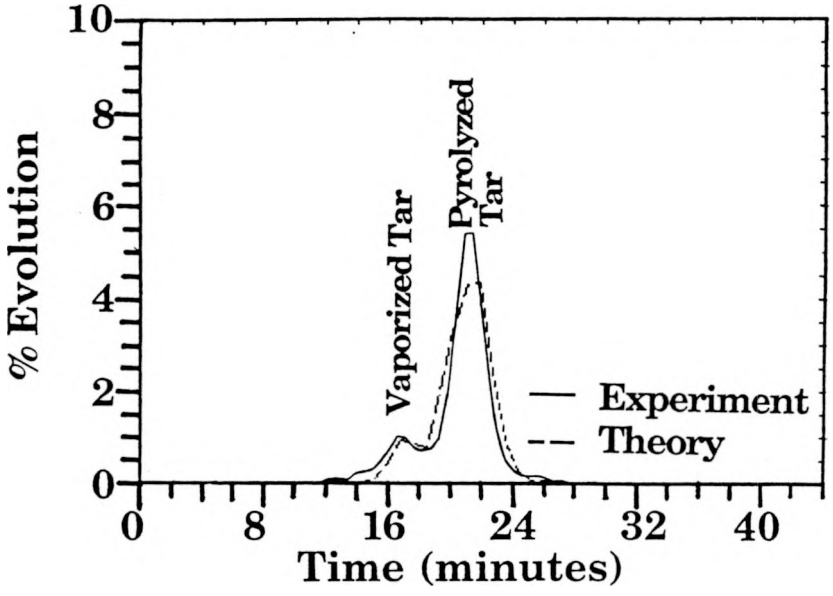

Figure II.A-4. Comparison of FG-DVC Model Predictions for Tar Evolution Rate from Upper Freeport Coal with TG-FTIR Data.

gas products, not tar. This leads to predicted H/C ratios in the tar for low rank coals which are lower than those measured by Freihaut et al. (1988).

Polymethylenes have now been added to the DVC part of the model as a second class of material whose molecular weight distribution and functional group composition are different from the main macromolecular network. The starting coal molecule now includes a distribution of oligomer sizes for polymethylenes and other guest molecules (with the chemical composition of the network). The vaporization of these molecules produces a peak which matches the early vaporization peak as shown in Fig. II.A-4. We also account for polymethylenes which are attached to the coal matrix and removed by bond breaking by including them as species in the FG model. Those polymethylenes are then added to the tar after vaporization.

The model requires a value for the total polymethylene content in the coal. Calkins determined that the yields of ethylene, butadiene, and propylene correlated well with the polymethylene content (1984d). It was decided that this is the most general and fruitful approach to take and we have used the coals which are in our set and Calkins' set to calibrate the method. As a first approximation, we arbitrarily chose to use polymethylene = 0.7 (C_2H_4). This gave $-CH_2-$ contents slightly above Calkin's values, but within 15% of Calkin's. The model also assumes that 50% of the polymethylenes are small enough to vaporize and are included in the oligomer pool while the other 50% are not and are included in the FG pool.

A prediction for the total tar yield including polymethylenes is compared in Fig. II.A-4 with measurements from a TG-FTIR experiment (Solomon et al., 1989a). The agreement is good. Comparisons between the predicted and measured (Freihaut et al., 1988) tar hydrogen compositions are shown in Fig. II.A-5. The prediction is good for high rank coals and shows the correct trend with rank. The tar hydrogen composition is, however, overpredicted for lower rank coals. This is due to the fact that the model underpredicts, for these coals, the tar yield at high heating rates. The relative contribution of polymethylenes is then more important. By improving the tar predictions with adjustments of DVC parameters, we should be able to obtain more accurate values of the tar hydrogen composition.

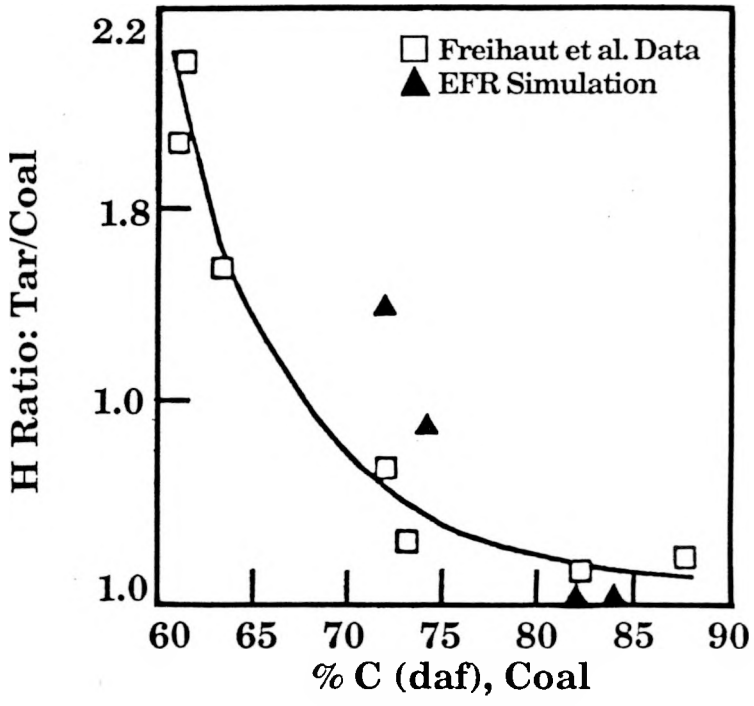

Figure II.A-5. Ratio of % H in Tar to % H in Coal as a Function of Coal Rank. (from Freihaut et al. (1988).

Swelling Model

Work also continued on the swelling model. We recently developed a multibubble approach to doing the swelling predictions. Since the swelling predictions depend on the fluidity model, some problems were introduced by the statistical variations in the fluidity model. This was solved by using a lookup table for the viscosity values based on averaging the results of several runs. Using a multi-bubble model with a single bubble size, reasonable predictions have been obtained for data on the swelling ratio and the porosity but not for surface area (too low). Additional bubble types (sizes) were introduced into the model in order to improve the prediction of surface area. However, this did not lead to better predictions, so other modifications to the model will be tried. The predictions are sensitive to the number of starting bubbles.

Percolation Theory

The statistical Monte Carlo method used in our FG-DVC model has been quite successful in predicting the depolymerization and crosslinking processes of the coal macromolecular network. However, the method has a few drawbacks. First, it is computationally time-consuming compared with other statistical methods. Second, its statistical nature presents a certain degree of fluctuation in the final results. The latter becomes increasingly significant and poses some difficulties for the modeling of coal fluidity and swelling.

To address these problems, attempts have been made to use the mathematics of percolation theory as an alternative to Monte Carlo calculations (Solomon et al., 1989b; Niksa and Kerstein, 1987; Grant et al., 1989). Percolation theory gives closed-form solutions for a Bethe lattice. Keeping in mind that an actual coal network contains some different features from the Bethe lattice (e.g. the Bethe lattice has no loops), we made use of some basic concepts of percolation theory while we further modified the mathematics of this theory to describe vaporization processes in coal devolatilization.

One of the key parameters of percolation theory is the coordination number, $\sigma + 1$ which describes the possible number of bridge attachments per ring cluster (monomer). A linear chain has $\sigma + 1 = 2$, while a rectangular "fish net" has $\sigma + 1 = 4$. The higher the coordination number, the more bridges must break to

create network fragments. In attempting to apply percolation theory to the FG-DVC model (Solomon et al., 1989b), it became obvious that the single coordination number lattice used in most applications of percolation theory was not appropriate to describe coal network decomposition. It appears from solvent swelling data (Sanada and Honda, 1966; Larsen and Kovac, 1978; Green et al., 1982; Lucht and Peppas, 1981,1987) and NMR data (Solum et al., 1989), that coal begins as a chain-like material with crosslinks every 2 to 8 ring clusters, i.e., $\sigma + 1$ between 2.2 and 2.5. So, its decomposition requires a low coordination number. However, crosslinking processes can occur at elevated temperature to increase the coordination number. Therefore, we extended the mathematics of percolation theory from a one-dimensional probability computation into a two-dimensional probability computation to describe the coal network as a lattice with two bond types per cluster, i.e., two coordination numbers. This modified theory is referred to as the two-σ model (Solomon et al., 1989b).

Two important new features in our two-σ percolation theory are: (i) tar vaporization and (ii) the molecular weight distribution of monomers. These features are basically treated the same way as in the original DVC model. The molecular weight of monomers is described by a probability distribution, which allows for the fact that monomers are made of various multi-ring structures. Tar molecules are removed out of the coal network using Suuberg's modified vaporization law. Molecular weight distributions of tar and char are kept track of during pyrolysis by a bookkeeping of the vaporization process in each mass bin. The percolation theory gives the mass fraction of all n-mers during pyrolysis. Combining this with a given molecular weight distribution of monomers, one can obtain the mass fraction of coal in each mass bin, which consists of two components: char and tar. Tar vaporization is computed for each mass bin. Tar in each mass bin monotonically increases and reduces the amount of char available for vaporization in the same bin until the char bin is emptied. Figure II.A-6 shows the comparison of predicted tar yields between the Monte Carlo method and the modified percolation theory. Also, a two-σ prediction of the fluidity for the same coal is included in Fig. II.A-7. The Monte Carlo and two-σ predictions agree reasonably well with each other and with the data.

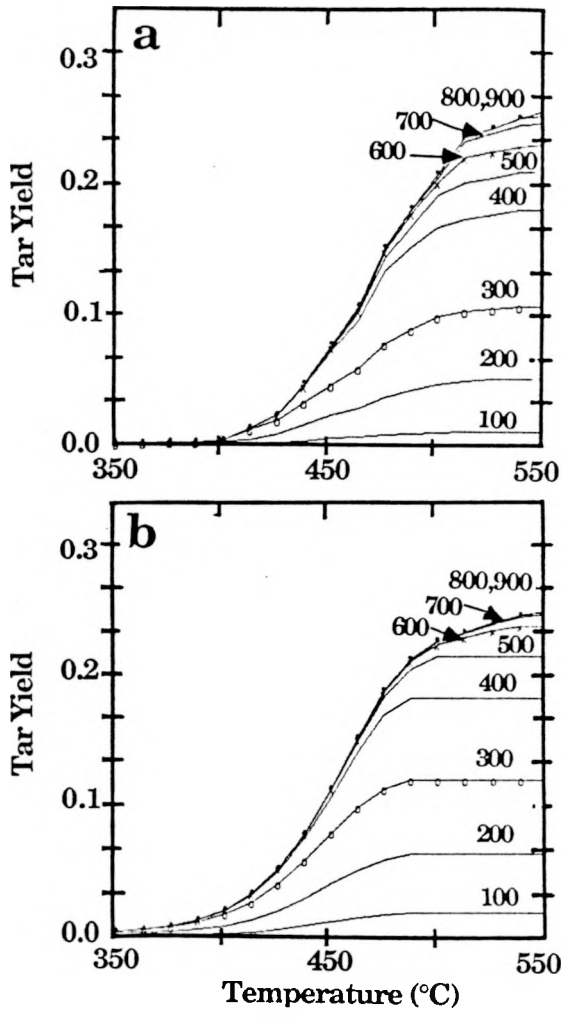

Figure II.A-6. Comparison of Tar Molecular Weight Distributions Predicted with: a) Monte Carlo Method and b) Two-σ Percolation Theory.

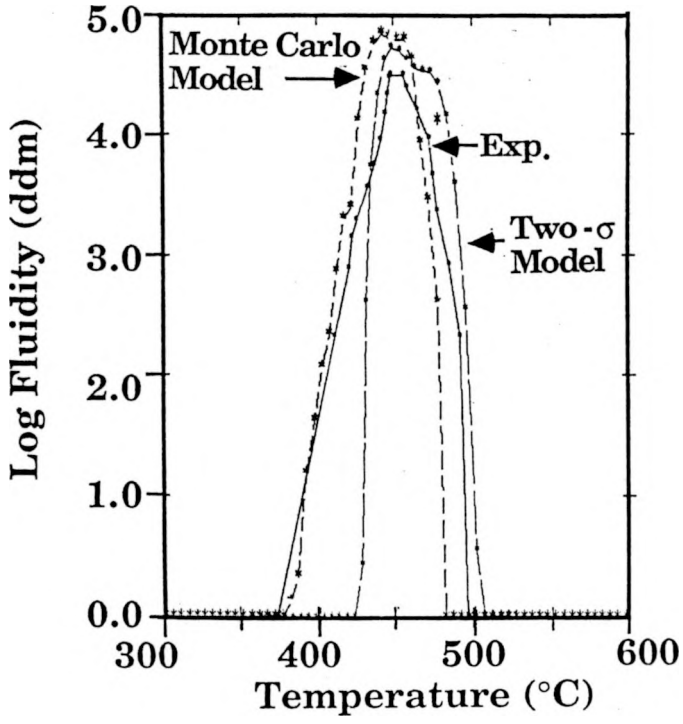

Figure II.A-7. Fluidity of Upper Freeport Coal: Experiment (solid), Monte Carlo Theory (dashed) and Percolation Theory (long dashed).

Rank Dependent Pyrolysis Kinetics

Work also continued on the rank dependence of the pyrolysis kinetic rates. During the past quarter, the transfer of TG-FTIR data to the Sun microsystems computer was successfully completed. This will allow a faster and more accurate comparison to the data. Criteria were established to assess the degree of fit to the evolution profiles and the yield data. So far, comparisons have been made with Pittsburgh Seam bituminous coal TG-FTIR data from experiments at four different heating rates. In this case, rank dependent kinetics have been determined which provide an excellent fit to the evolution profiles and yields for each heating rate. We will now do a systematic comparison of the same type of data for the remaining Argonne coals.

Correlation of T_{cr} Measurements with High Temperature Combustion Reactivities

A non-isothermal reactivity test has been used to make measurements of the critical temperature, T_{cr}, which is an index of relative char reactivities (Solomon et al., 1986; Serio et al., 1990). Of course the measurement of T_{cr} would not be of much good to those interested in p.f. combustion unless it can be shown that these measurements correlate with intrinsic reactivities measured at high temperatures. The T_{cr} measurement provides a temperature at which df/dt = 0.001 s^{-1}. For a ~ 60 μm mean diameter fraction of Montana Rosebud coal, the measured T_{cr} was 429°C (702K) while the measured CO_2 surface area was 152 m^2/g. The problems of using the BET surface area as a correlating parameter have been discussed previously (Best et al., 1987; Serio et al., 1989). However, since the intrinsic reactivity (R_i) data in the literature have been derived using such measurements, this approach is consistent. The CO_2 area varies the least over a wide range of burnoffs, for most coal chars, and is used here. Using the CO_2 surface area, one would calculate $R_i = 1.1 \times 10^{-10} g/cm^2 s$ at T_p = 702 K. The most comprehensive compilation of intrinsic reactivity data for a range of carbons is that provided by Smith (1982). The correlation of Smith would predict a value of $R_i = 1.0 \times 10^{-11}$ g/cm^2 s. However, this correlation underpredicts the data for brown coal chars and lignites in this temperature range, so the agreement is actually within a factor of 2 of the relevant data in Fig. 9 of Smith (1982). The extrapolation to high temperatures can be done by using E = 35 kcal/mole which gives $R_i = 2 \times 10^{-4}$ $g/cm^2 s$ at T_p = 1650K. This estimate is about a factor of two lower than Smith's correlation and about a factor of two higher than his data

for brown coal chars. A similar agreement is observed for the other chars that were studied. Consequently, it appears that the T_{cr} measurement is capable of giving meaningful results when extrapolated to high temperatures using an activation energy of E = 35 kcal/mole.

Recent work in our laboratory with a laminar coal flame experiment has shown a correlation of T_{cr} with the ignition point above the nozzle (Solomon et al., 1988b) and with the interval of time required to achieve 100% burnout (Solomon et al., 1989c).

Plans

The work on the development of rank dependent parameters will be continued for the rest of the Argonne coals. In addition, the work on the swelling model and the development of the percolation theory approach will also be continued. Work will be initiated on studying the evolution of sulfur and nitrogen species.

II.B. SUBTASK 2.B. - FUNDAMENTAL HIGH-PRESSURE REACTION RATE DATA

Senior Investigators - Geoffrey J. Germane and Angus U. Blackham
Brigham Young University
Provo, Utah 84602
(801) 378-2355 and 6536

Student Research Assistants - Charles Monson, Russell Daines,
and Gary Pehrson

Objectives

The overall objective of this subtask is to measure and correlate reaction rate coefficients for pulverized-coal char particles as a function of char burnout in oxygen at high temperature and pressure.

Accomplishments

Three components of the subtask have been identified to accomplish the objectives outlined above: 1) develop the laminar-flow, high-pressure, controlled-profile (HPCP) reactor, 2) prepare char at high temperature and pressure, and 3) determine the kinetics of char-oxygen reactions at high pressure. The HPCP reactor, capable of functioning at 400 psi (27 atmospheres), has been constructed to perform the fundamental reaction rate measurements required for the study. Data from another char oxidation study (atmospheric pressure) conducted at Brigham Young University will also be used.

Work continued during the last quarter on development of the high-pressure, controlled-profile (HPCP) reactor, the preparation and characterization of char, and the kinetics of char oxidation at high pressure. Most of the effort focused on development of the facility and analytical techniques in preparation for completion of the comprehensive test program. Some coal devolitalization tests of a coal identified for this study were conducted in connection with an independent research program, which has participated financially in the development of advanced instrumentation for the HPCP.

High Pressure Reactor Development and Characterization

Reactor Configuration - Following the initial reactor characterization and char tests, some modifications were found necessary to improve the operation of the reactor and the accuracy of the results. Many of these modifications were initiated during this reporting period, and are described below. Electronic mass flow meters were added to monitor the collection probe quench gas. The flow rate of this particular stream was difficult to obtain accurately when determined by difference using the total exit flow and the other inlet flows. Automatic control valves are being added to the inlet mass flow meters to allow easier stabilization and more consistent flow rates at elevated pressure. A smaller, water-cooled injection probe is also being fabricated. This new probe will have an outer diameter of 9.5 mm compared to an outer diameter of 13 mm for the original probe. The smaller size will allow the injection probe to be better insulated, which will reduce the load on the wall heaters and decrease the temperature drop of the gas flowing through the reaction tube.

In the past, gas temperatures have been measured with an unshielded, platinum-rhodium thermocouple that was inserted through the injection probe and moved along the centerline of the reaction tube. It was found that this probe resulted in temperatures approximately 50 K hotter than a radiation shielded probe inserted from the bottom of the reactor. The difference was due to both radiation and the large temperature gradient in the thermocouple leads as they entered the cooled injection probe. In order to obtain more accurate gas temperature measurements, a water-cooled, radiation-shielded suction pyrometer has been designed, and its fabrication is nearly complete. The test facility has also been modified to enable insertion of the suction pyrometer from the bottom of the reactor to provide gas temperature measurements along the reaction tube centerline without disturbing the upstream flow. Gas temperatures in the collection probe will also be obtained, providing information on quenching effectiveness.

Collection System - Under separate funding, the char/tar/gas separation and collection system is being modified to improve the separation and collection of tar, char and gas. Initial NMR analyses from collected tar samples indicated that the quench occurring in the collection probe has not been consistently sufficient to prevent secondary reactions. Further, a mass balance revealed that approximately 10 percent of the total collected tar was

found on the end of the collection probe that was without transpiration cooling, and on the walls of the impactor.

In order to improve collection efficiency, the collection probe is being redesigned to enhance the initial quench as the combustion particles exit the reaction zone to arrest all secondary reactions, and to lengthen the area of transpiration through the entire length of the collection probe to reduce the agglomeration of tar on the collection probe walls. In addition, the virtual impactor is being redesigned to reduce both the recirculation zones and the internal surface area to diminish the amount of tar sticking to the walls and to reduce the amount of char which collects before the cyclone. A backflush system is also being added to the cyclone to enhance char particle scavenging at low reactor pressure. Figure II.B-1 shows the modified collection system.

Char Preparation at High Temperature and High Pressure

Four devolatization runs were made on a North Dakota lignite to test the tar-char collection procedures. The runs were made at 1250 K and 1235 K, at pressures of 1 and 5 atmospheres, and at residence times of 50 and 200 ms. The distribution of the tar and char fractions are indicated in Table II.B-1. Two values for the tar, from two flow paths, are given in Runs 2-4. Path 1 carries the tar on the outside of the central tube in the impactor and is collected on a downstream filter. Path 2 carries the aerosol that goes through the central tube of the impactor and does not remain in the cyclone with the char, but is collected downstream of the cyclone on a separate filter. The tar and char fractions were analyzed for selected elements to determine whether or not any of these elements were selectively concentrated in either the tar or char fractions. Table II.B-1 shows percentages of calcium and iron in the tar and char fractions along with CHN analyses for these fractions. The detailed interpretations of these data are being made as part of a related, independent project.

From a previous determination of titanium content of a series of replicate samples it was observed that slight shifts in responses from the inductively-coupled plasma instrument for particular elements during analysis of several samples necessitated more frequent calibration. In this way the precision of the measurements has been improved. This will have application as additional oxidation kinetic runs are made in which the extent of reaction is measured by the titanium content of the oxidized chars.

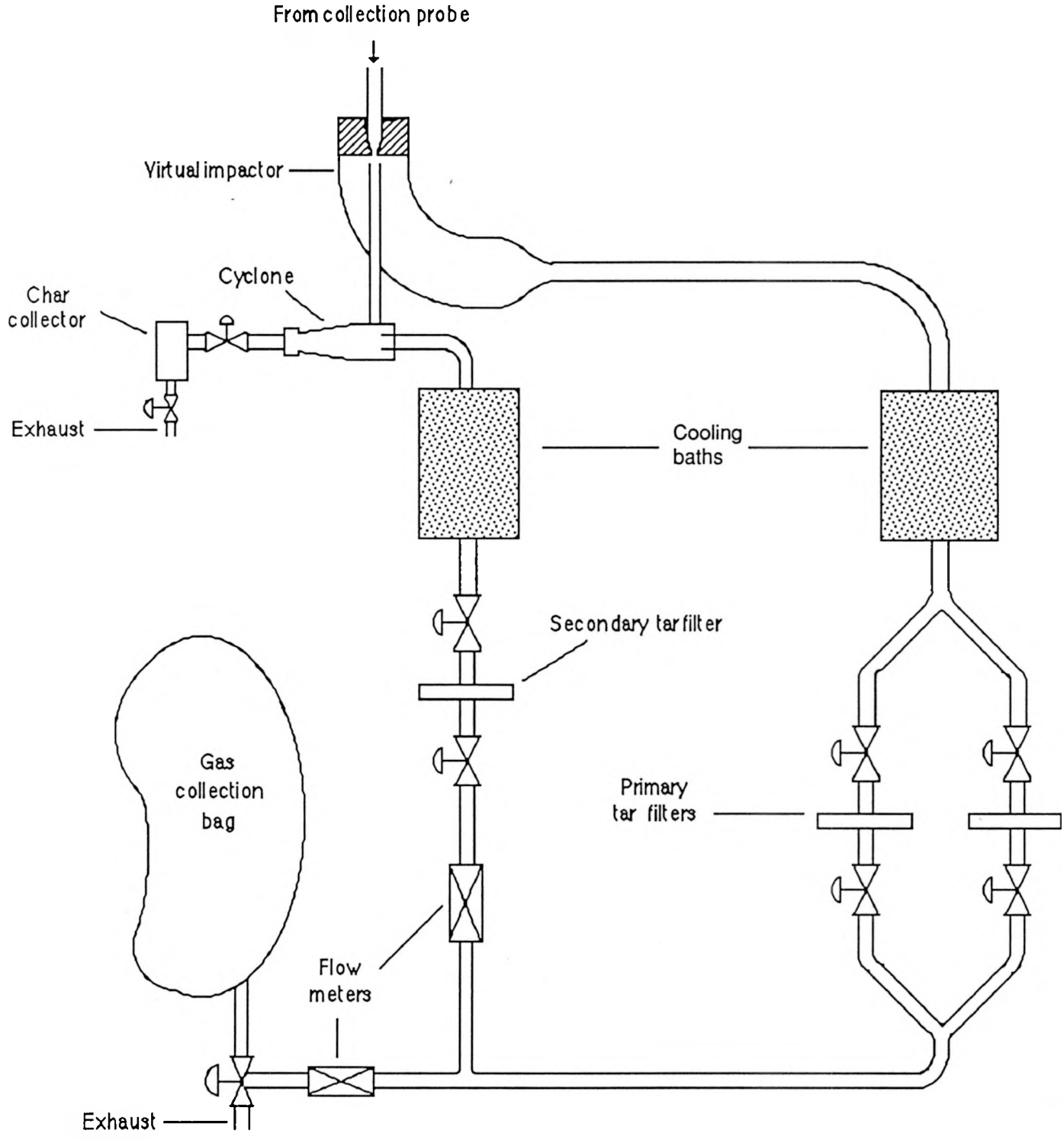

Figure II.B-1. Schematic of char/tar/gas separation and collection system.

Table II.B-1. Devolatilization of a North Dakota Lignite for Tar-Char Production

Run				Mass of Products (mg)	Tar Analyses (%)				
	Reaction Conditions								
No.	Pressure (atm)	Temp (k)	Residence Time (ms)	1. Tar-Path 1 2. Tar-Path 2 3. Char	Calcium	Iron	Carbon	Hydrogen	Nitrogen
1	1	1250	50	161	0.83	1.04			
				—	----	----			
				390	1.48	2.10	62.25	3.84	1.66
2	1	1250	50	180	0.82	1.08			
				40	1.19	1.77			
				974	1.29	2.08	62.19	3.70	1.51
3	5	1235	200	186	1.09	1.63			
				42	1.06	1.93			
				1360	1.26	2.40	61.93	3.58	1.61
4	5	1250	50	194	0.81	1.07			
				21	1.47	2.34			
				467	1.41	2.45	63.83	3.35	1.49
Coal					1.26	1.92	60.38	4.08	1.71

Kinetics of Char-Oxygen Reactions at High Pressure

Mitchell (1989) reported that char particles of the same size undergoing the same conditions have large variations in temperature and burning times. Samples of the same coal with most of the mineral matter removed exhibited a reduction in temperature and burning time variation. Mitchell concluded that variations in the ash content of the char were responsible for the differences in combustion. Catalytic effects of the mineral matter appeared to have little effect since the raw coal and cleaned samples both exhibited the same temperature dependence. Evidence was also found that the traditional kinetic model for char combustion may not be valid. These results may be very useful in helping to interpret results from the present study, since individual particle measurements of temperature will be made during char oxidation and extent of reaction will be determined from the collected particles.

Plans

The modifications to the HPCP reactor discussed previously will be completed during the next quarter. Completion of the suction pyrometer will allow better characterization of gas temperatures in the reaction tube. Previous conditions used for devolatilization and char oxidation experiments will be duplicated and temperature profiles will be measured to better characterize the particle temperatures encountered during the experiments. Components for the pyrometry and particle imaging system have been ordered and the system will be assembled and calibrated during the next reporting period.

During the upcoming quarter the remainder of the collection system will be reviewed. Based on the flow rates that will be employed in upcoming devolatilization and oxidation runs, design parameters of the cyclone will be determined to optimize collection efficiency of the char particles. To reduce the amount of tar that can condense on the tube walls, between the char separation and the collection filters, alternative methods of cooling the tar/gas flow will be examined. The method which employs the shortest possible length of tubing while maintaining the desired tar collection temperature will be selected.

Scanning electron micrographs of the coal samples used in previous tests indicated that the size classification of the particles needs to be improved. A relatively large number of particles that were smaller than the desired size

fraction were included in the samples because of agglomeration with particles of the desired size. Steps have been or will be taken to improve the sieving process, including prevention of agglomeration with an additive, and particle size measurements will be made with a Coulter counter. Selected devolitalization and char oxidation experiments using tight size fractions of Pittsburgh #8 bituminous and North Dakota lignite coal samples will be repeated. Further char oxidation experiments with these two coals will be conducted at a number of temperatures and elevated pressures.

II.C. SUBTASK 2.c. - SECONDARY REACTION OF PYROLYSIS PRODUCTS AND CHAR BURNOUT SUBMODEL DEVELOPMENT AND EVALUATION

Senior Investigator - James R. Markham and Michael A. Serio
Advanced Fuel Research, Inc.
87 Church Street, East Hartford, CT 06108
(203) 528-9806

Objective

The objective of this subtask is to develop and evaluate by comparison with laboratory experiments, an integrated and compatible submodel to describe the secondary reactions of volatile pyrolysis products and char burnout during coal conversion processes. Experiments on tar cracking, soot formation, tar/gas reactions, char burnout, and ignition will continue during Phase II to allow validation of submodels in Phase II.

Accomplishments

Work continued on doing coal flame experiments in the transparent wall reactor (TWR). An attempt was made to use the Pittsburgh Seam bituminous coal. However, some problems were experienced in feeding the coal and with flame stability. Consequently, a switch was made back to Montana Rosebud subbituminous coal.

For a Montana Rosebud flame, tomographic reconstruction techniques were applied to line-of-sight FT-IR Emission/Transmission (E/T) measurements to derive spectra that correspond to small volumes within a coal flame. From these spectra, spatially resolved point values for species temperatures and relative concentrations can be determined. Values for particle temperature, relative particle density, relative soot concentration, the fraction of ignited particles, the relative radiance intensity, the relative CO_2 concentration and the CO_2 temperature have been obtained as functions of distance from the flame axis and height above the coal injector nozzle. Initial measurements (reported last quarter) were made at 6 cm and 12 cm above the coal injector nozzle, with the ignition point occurring at 10 cm. During this quarter, two more slices of data, at 16 cm and 20 cm above the nozzle were collected and tomographically

reconstructed. An in-depth discussion of the four measurement positions can be found in Appendix A, which is a copy of our paper entitled **"FT-IR Emission/ Transmission Tomography of a Coal Flame"**, which has been submitted to the **23rd Symposium (Int) on Combustion, France, (1990).** The spectroscopic data are in good agreement with visual observations and thermocouple measurements. The data present a picture of the coal burning in a shrinking annulus which collapses to the center at the tip of the flame. CO_2 temperatures are highest in the rapid burning zone (2300 to 2900 K). The highest particle temperatures in this zone are 1900 to 2000 K, with temperatures up to 2400 K outside the zone.

Measurements are in progress or planned for 9.5, 10.5, 14, 18, and 25 cm above the nozzle for the Rosebud flame. With the local profiles we plan to produce pseudo-color images of the flame's central plane for temperature and relative concentrations fields in the manner we previously employed for tomography measurements in an ethylene diffusion flame (Ref. 3 in Appendix A).

Plans

Continue with tomography measurements at different heights in coal flames and compare tomography results for different coals. Continue characterization of TWR geometry and interact with BYU on PCGC-2 simulations of this system.

II.D. SUBTASK 2.d - ASH PHYSICS AND CHEMISTRY SUBMODEL

Senior Investigators - James Markham and Michael Serio
Advanced Fuel Research, Inc.
87 Church Street, East Hartford, CT 06108
(203) 528-9806

Objective

The objective of this task is to develop and validate, by comparison with laboratory experiments, an integrated and compatible submodel to describe the ash physics and chemistry during coal conversion processes. AFR will provide the submodel to BYU together with assistance for its implementation into the BYU PCGC-2 comprehensive code.

To accomplish the overall objective, the following specific objectives are: 1) to develop an understanding of the mineral matter phase transformations during ashing and slagging in coal conversion; 2) To investigate the catalytic effect of mineral matter on coal conversion processes. Data acquisition will be focused on: 1) design and implementation of an ash sample collection system; 2) developing methods for mineral characterization in ash particles; 3) developing methods for studying the catalytic effects of minerals on coal gasification.

Accomplishments

The work on the study of mineral transformations in the entrained flow reactor (EFR) was temporarily suspended due to manpower and funding constraints.

Temperature Programmed Desorption (TPD) experiments were done in air for chars produced from all of the Argonne coals. The CO_2 desorption and the O_2 adsorption show a consistent trend with the char reactivity as measured by the Critical Temperature (T_{cr}). The more reactive chars adsorb more O_2 and give off CO_2 earlier. These experiments will be repeated with chars produced from demineralized samples of these coals and experiments will also be done in CO_2.

Samples of char were collected from the Montana Rosebud coal flame experiments in order to do reactivity measurements. Since the samples at high

levels of burnout had high ash contents, the non-isothermal reactivity measurement technique (which determines the "critical" temperature) had to be modified to account for this.

Plans

Continue study of mineral effects on the reactivity of low and high rank coals. Continue analysis of material and element balances from ash collections in the entrained flow reactor.

II.E. SUBTASK 2.e. - LARGE PARTICLE SUBMODELS

Senior Investigator - Michael A. Serio
Advanced Fuel Research, Inc.
87 Church Street
East Hartford, CT 06108
(203) 528-9806

Objective

The objectives of this task are to develop or adapt advanced physics and chemistry submodels for the reactions of "large" coal particles (i.e., particles with significant heat and/or mass transport limitations) and to validate the submodels by comparison with laboratory scale experiments. The result will be coal chemistry and physics submodels which can be integrated into the fixed-bed (or moving-bed) gasifier code to be developed by BYU in Subtask 3.b. Consequently, this task will be closely coordinated with Subtask 3.b.

Accomplishments

The work on the AFR fixed-bed reactor (FBR) system was continued. Experiments were done at two bed depths and two flow rates with samples of Illinois No. 6, Pittsburgh No. 8, and Upper Freeport bituminous coals. Over the range of bed depths examined, there did not appear to be a large effect on tar yield and composition. We were restricted from using larger bed depths because problems with tar deposition in the gas cell. However, the ability to bypass some of the tar from the cell has recently been added which will allow larger samples to be used.

It was also found that the temperature of the maximum evolution rate of tar and CH_4 unexpectedly decreased with increasing bed depth. This was due to low levels of oxygen contamination. The contamination problems have recently been solved.

Plans

Complete initial set of experiments on secondary reaction effects in thick beds. Continue development of single particle model with BYU. Begin work on tar repolymerization model.

II.F. SUBTASK 2.F. - LARGE PARTICLE OXIDATION AT HIGH PRESSURES

Senior Investigators: Angus U. Blackham and Geoffrey J. Germane
Brigham Young University
Provo, Utah 84602
(801) 378-2355 and 6536

Student Research Assistants: Gary Pehrson and Michael Sheetz

Objectives

The overall objective for this subtask is to provide data for the reaction rates of large char particles of interest to fixed-bed coal gasification systems operating at pressure.

The specific objectives for this quarter, which was the first quarter of this study, include:

1. Select personnel for work on this study.
2. Review appropriate literature in pertinent areas.
3. Select the experimental approach.
4. Discuss and evaluate equipment design features.

Accomplishments

Two components of this subtask to accomplish the overall objective were suggested in the Phase II Plan (Blackham, 1989): 1) high-pressure, large-particle reactor design, fabrication and preliminary data; 2) experimental reaction rate data for chars from five coals. During the last quarter, personnel to work on this study were selected. The subtask is being closely coordinated with Subtasks 2.b and 3.b.

High-Pressure, Large-Particle Reactor Design

Introduction and Literature Survey - In the Phase II Plan for this subtask (Blackham, 1989), a test facility consisting of a TGA unit encased in a high-pressure shell was proposed. This suggestion followed the essential features of an experimental unit constructed by Sears et al. (1982). This facility is a pressurized thermobalance designed to operate at pressures up to 1000 psig at intermediate temperatures, or to almost 2000 K at one atmosphere.

The maximum conditions attainable simultaneously are reported to be 1570 K at 450 psig. Results are given for a lignite coal reacting with CO_2. The main objective for this equipment was to study coal pyrolysis and gasification reactions continuously at high temperature and pressure. A significant observation of their study was that "data of this nature are practically nonexistent for gasification reactions." In subsequent papers (Tamhankar et al., 1984; Sears et al., 1985) this facility has been used to study chars at up to 16 atmospheres at 1170 K reacting in CO_2 and H_2O. No data on reaction in oxygen were reported. Parikh and Mahalingan (1987) reported the use of a fixed-bed reactor to simulate conditions in the devolatilization zone of a Lurgi gasifier. The entering reactive gas contained 2 percent oxygen and 30 percent steam. The operating conditions were 600-800 K and 30 psig.

Kalson and Briggs (1985) studied the devolatilization of a single lump of coal (15 grams) at 100 kPa (14.7 psia) in the temperature range 700-850 K. The devolatilizer consisted of a 5.25 cm I.D. stainless steel pipe with the sample held in a 4.1 cm O.D. stainless steel screen basket. The basket was suspended on a chain that was raised or lowered within the devolatilizer pipe by means of an electrically controlled winch. It was indicated that the design of the unit could operate at a pressure of 1.7 MPa. It was also noted in their paper that "little systematic information is available for tar production from fixed-bed gasifiers."

Nuttall et al. (1979) reported on a bench-scale, single-particle reactor where internal conditions could be both controlled and monitored by a minicomputer. Coal samples (2.5 cm diameter) were used in devolatilization tests. "The coal particle was placed in a wire mesh basket attached to the force transducer by a stainless steel rod." Temperatures were measured by micro-thermocouples attached to the coal particle. Feldkirchner and Johnson (1968) described the construction of a high pressure thermobalance for study of iron ore in cycles of oxidation and reduction. They built this thermobalance to operate "at elevated pressures and temperatures because none were available commercially." The high pressure system consisted of two tubes joined together with the lower tube placed vertically in an electric furnace. The upper tube contained a microforce transducer of 10 g. capacity for weight measurement. A gold suspension chain is attached on one end to a windlass and on the other end to a nickel wire which supports the sample in a nickel mesh basket. The reactor tube was rated for heating to 1200 K. The complete system could be taken to a pressure of 100 atm.

The references briefly reported above are serving as the basis for our discussions concerning the experimental system to be designed and built for the fixed-bed oxidation studies of this subtask. Additional literature references have also been obtained and are being reviewed.

Selection of an Experimental Approach. On the basis of the experimental approaches reported in the literature, it was concluded that satisfactory reaction tubes can be designed and built which can be inserted into the HPCP reactor of Subtask 2.b. In this way, much of the facility needed for Subtask 2.f. already available. The general features of the large-particle design will consist of three components: a) the reactor tube, b) the balance, and c) the connecting pipe. The balance unit under pressure may include a magnetic bar suspending a platinum wire mesh basket by a long platinum wire. The suspending force can be controlled by a suitable external solenoid to give a record of mass loss of the sample in the basket. Alternatively, the entire balance unit may be encased to put all of the unit under pressure except the electronic control circuits passing through the pressure boundary. The connecting pipe will convey the pressure of the reactor to the balance unit and provide the housing for the long suspending wire. The connecting pipe may have a small pressure-sealed panel than can be easily opened to change samples. The suspending wire will be sufficiently long to place the sample in the optical access path at the lower part of the reactor. Different reactor tubes may be placed in the reactor to provide flexibility in the types of experiments envisioned. A ceramic tube may be necessary at the highest temperatures planned. Quartz tubes will be needed for the optical access for particle or bed temperature measurement. Pyrex tubes may be used at sufficiently low temperatures. A quartz tube with a bonded sintered disk may provide a platform for a bed of large particles.

Discussion and Evaluation of Design. The personnel of Subtasks 3.b. and 2.f. have met a few times during the quarter and discussed the features of the experimental approach outlined above. With a large char particle in a hot reactive gas stream, the surface temperature of the reacting particle may be considerably higher than the gas temperature. The optical system currently under construction for Subtask 2.b. will be used to determine the surface temperatures. Also, it may be necessary to place tiny thermocouples within the particle to follow the changes of temperature. The design of the balance unit will be given first priority. With samples in the 1-5 gram mass range it is desireable to follow changes in mass during reaction to the nearest

milligram. It will be necessary to determine if this can be achieved with hot gas flowing around the sample.

Different sample configurations are being considered: a) a single large particle - spherical, square, or cylindrical; b) a cluster of large particles held in a wire mesh basket; c) a long cylindrical particle with only the ends available to the reacting gas - hence one dimensional reaction; d) a bed of large particles on a sintered disk bonded to the reactor tube. Some checks on preliminary design features using some simple reactor tubes in a crucible furnace or a tube furnace at atmospheric pressure without optical temperature measurement are planned.

Experimental Reaction Rate Data

Experimental work has not yet been initiated.

Plans

During the next quarter, detailed design of the three components of the reactor tube insert will continue. Evaluation of some design features will be made using simple quartz tubes in a crucible or tube furnace at atmospheric pressure. Analytical methods and procedures will be determined for char characterization and for reaction rate calculations. Some large particle chars will be prepared under simple atmospheric pressure conditions.

II.G. SUBTASK 2.G. – SO_x/NO_x SUBMODEL DEVELOPMENT

Senior Investigators: L. Douglas Smoot and B. Scott Brewster
Brigham Young University
Provo, Utah 84602
(801) 378-4326 and (801) 378-6240

Research Assistant: Richard D. Boardman

Objectives

The objectives of this subtask are 1) to extend an existing pollutant submodel in PCGC-2 for predicting NO_x formation and destruction to include thermal NO, 2) to extend the submodel to include SO_x reactions and SO_x-sorbent reactions (effects of SO_3 non-equilibrium in the gas phase will be considered), and 3) to consider the effects of fuel-rich conditions and high-pressure on sulfur and nitrogen chemistry in pulverized-fuel systems.

Accomplishments

Much progress has been made toward verifying the expanded NO_x submodel. Work has primarily focused on evaluating the thermal NO mechanism incorporated into the code using the data collected under independent funding at BYU in a laboratory-scale reactor. Refinements to PCGC-2 have resulted in improved prediction of the temperature and major species concentrations. Subsequently, thermal NO predictions have been made and compared with the data. Additional experimental work has been carried out with independent funding to investigate the chemistry in the near-burner region of the reactor. Important findings have resulted from the joint theoretical and experimental work.

Options available for estimating radical oxygen have been partially investigated for the thermal NO model. Sensitivity of the rate expressions to temperature has been demonstrated. Improved coal gasification cases have been completed which closely match experimental data. An investigation of the expanded fuel NO mechanism is now ready to begin.

NO_x Submodel Development

Evaluation of Thermal NO Mechanism

In the 7th Quarterly Report (Solomon et al., 1988b) the expanded NO_x submodel was presented along with data that were measured at BYU in natural gas and propane diffusion flames. Initial PCGC-2 simulations were presented which demonstrated deficiencies of the code in predicting the basic flame structure. This made it difficult to evaluate the thermal NO mechanism. After making corrections to the radiation submodel, predictions were made which favorably match the measured major species (CO_2, CO, and O_2), temperature, and velocity profiles. Subsequently, thermal NO predictions have been made and compared to the measured NO concentrations.

Refinements were also made to the experimental data (Boardman, 1990; Eatough, 1990) during the quarter. The reactor burner was redesigned to establish a symmetric flame in the combustor. Spatially resolved major species, temperature, velocity, and pollutants species profiles were then measured in the near-burner region where the reactions of interest appear to occur. Concentration of NO, NO_x, HCN and NH_3 was measured to determine if prompt NO formation occurs in the flame region.

Figures II.G-1 and II.G-2 compare predicted and measured major species and temperature for the natural gas/air combustion tests. The major species are shown to closely match the measured data in the near-burner region where temperature is maximum. In the aft region of the reactor, CO_2 is predicted above the measured concentrations while CO is predicted below the measured concentration. The sum of CO_2 and CO always equals the sum of the measured values. In all three radial profiles, predicted oxygen concentrations closely match the measured values. It is important to predict the correct magnitude and trend of the major species since radical oxygen concentrations are estimated from partial equilibrium assumptions involving the major species (Iverach et al., 1973; Sarofim and Pohl, 1973; and Thompson et al., 1981).

$$[O] = K'[O_2]^{1/2} \qquad \text{(II.G-1)}$$

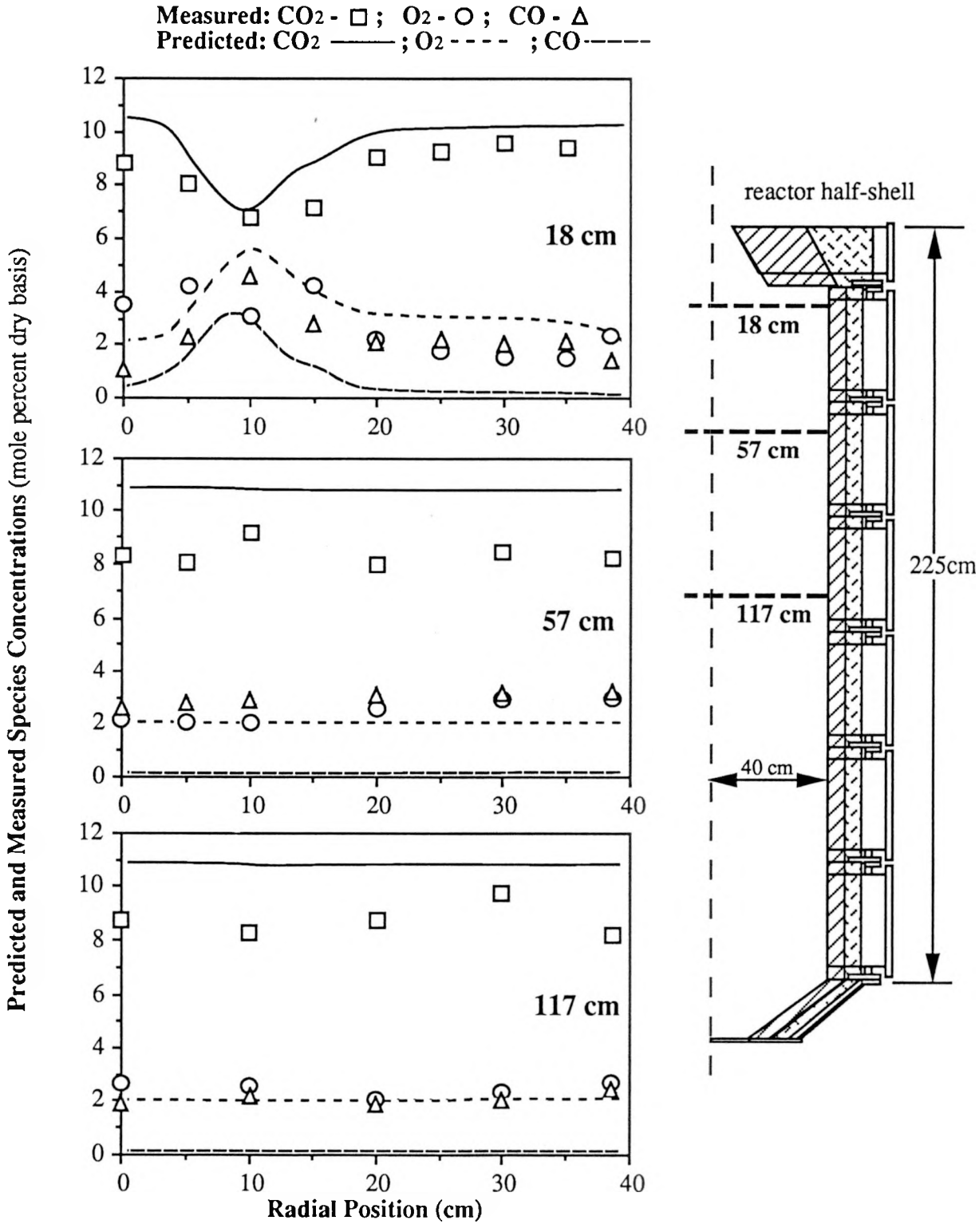

Figure II.G-1. Comparison of measured (symbols) and predicted (lines) major species radial profiles for a 500,000 BTU/hr natural gas/air diffusion flame.
Equivalence ratio = 0.98; Secondary swirl number (theoretical and actual) = 1.5;
Data measured in a BYU Advanced Combustion Engineering Research Center reactor (Eatough, 1989).

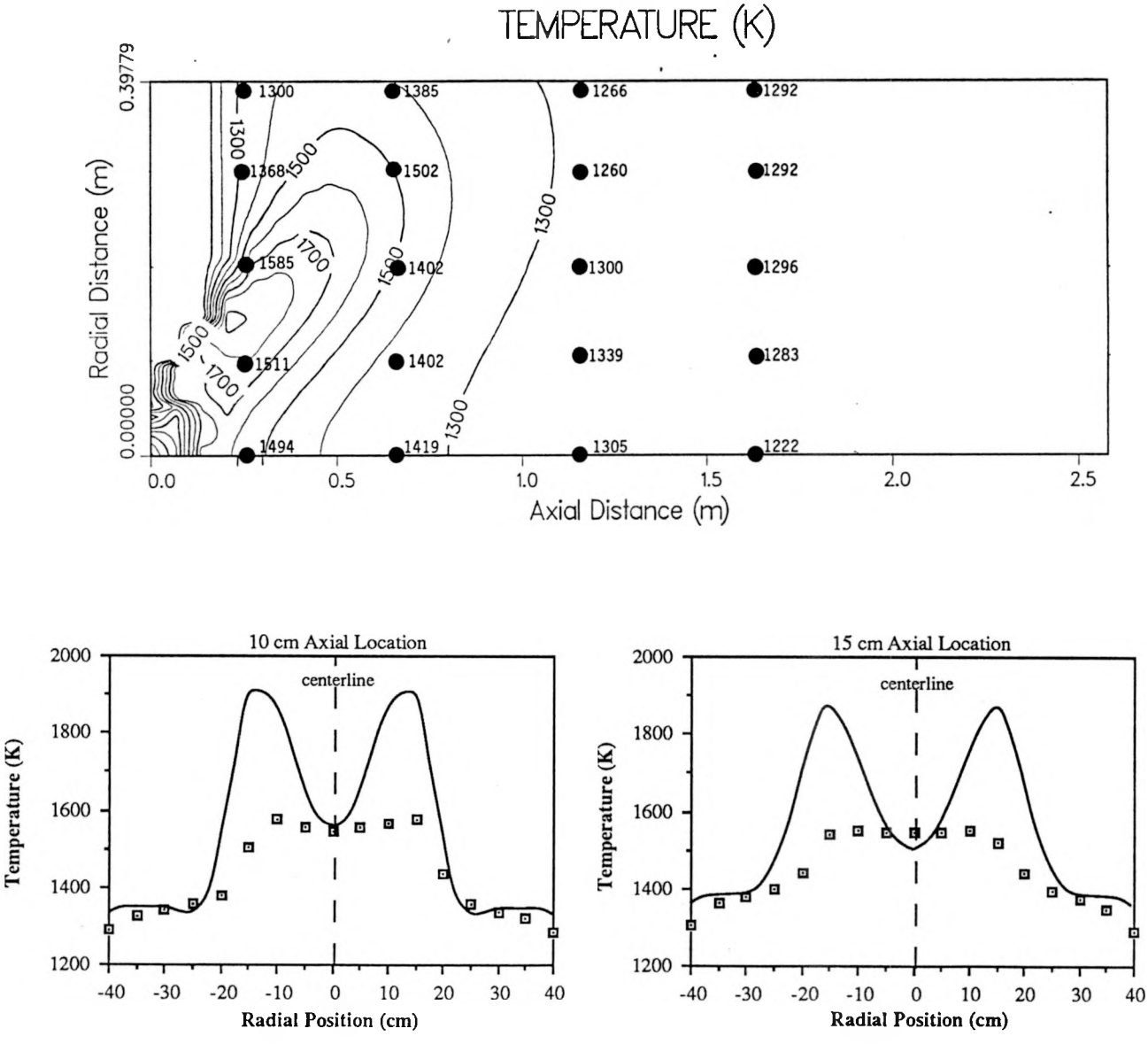

Figure II.G-2. Comparison of measured (symbols) and predicted (curves) temperature profiles for a 500,000 BTU/hr natural gas/air diffusion flame. Equivalence ratio = 0.98; Secondary swirl number = 1.5; Data measured in a BYU Advanced Combustion Engineering Research Center reactor (Eatough, 1990).

$$[O] = K''[O_2][CO]/[CO_2] \qquad \text{(II.G-2)}$$

Figure II.G-2 reveals that the predicted temperature field generally matches the experimental data except in the peak temperature region. A shielded suction pyrometer was used to obtain the measured values, and there is a possibility that the intrusive nature of the probe disturbed the fluid mechanics significantly. This would presumably lead to decreased mixing and decreased reaction in the highly turbulent near-burner region resulting in a low temperature measurement. Furthermore, the measured data are uncorrected for heat loss of the thermocouple pile to the pyrometer shield and probe. According to calculations, a heat balance would adjust the measured temperature upward by as much as 50 K. Despite the early disparities between the predicted and measured temperature profiles, agreement of the temperature along the reactor wall and centerline and at the combustor exit infers the reactor heat balance closes. Any adjustment to the wall boundary temperatures resulted in predicted temperatures fields which did not match the composite temperature field as well. Thus, the predicted temperature field was thought to be suitable for evaluating the NO_x submodel.

Figure II.G.3 presents detailed measurement of nitrogen pollutant species and compares the predicted and measured NO concentrations throughout the reactor. Predicted NO concentrations were made using the extended Zeldovich mechanism. Radical oxygen concentrations were estimated assuming oxygen radicals to be in partial equilibrium with O_2 (Equation II.G-1). When radical oxygen concentrations were estimated using Equation II.G-2, the predicted NO level was an order of magnitude higher (see Figure II.G-5, below). Even when the temperature was artificially adjusted down by 100 K, Equation II.G-2 led to NO predictions well above the measured profiles. It appears that it is most appropriate to use Equation II.G-1 to estimate oxygen radical concentration.

Figure II.G-3 shows the buildup and decay of HCN and NH_3 by interaction of fuel fragments (CH_i's) with molecular nitrogen and intermediate nitrogen species. The goal of the experimental work was to operate at conditions where prompt NO and NO_2 formation would be minimized. This attempt was thwarted due

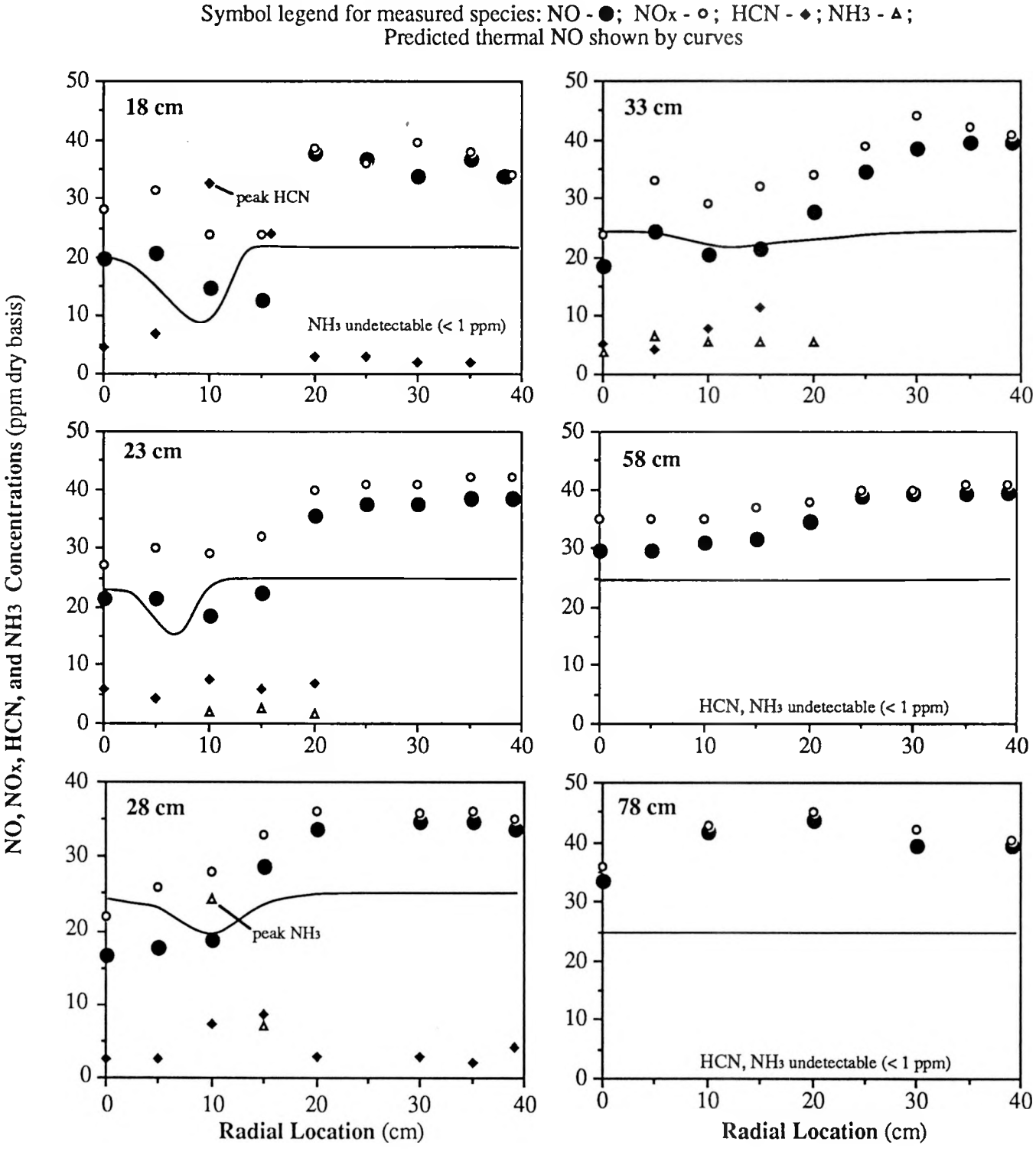

Figure II.G-3. Comparison of predicted thermal NO (——) with measured NO (●) for a 500,000 BTU/hr natural gas/air diffusion flame. Axial location of radial profiles listed in upper left corner. Other measured species (NO_x, HCN, and NH_3) shown to demonstrate complexity of the chemistry. Data measured in a BYU Advanced Combustion Engineering Research Center reactor. Equivalence ratio = 0.98; Secondary air swirl = 1.5

to the locally fuel-rich zone inherent in non-premixed flames. Thus, it is impossible to completely avoid mechanisms of prompt NO formation and decay in hydrocarbon diffusion flames.

Figure II.G-4 illustrates the complex mixing structure established when swirl is imparted to the secondary air stream. A fuel-rich region exists along the flame front where HCN is produced. Figure II.G-3 shows that HCN passes through a maximum at the flame edge. The highest observed HCN concentration occurred on the 18 cm radial profile. Higher values may occur in the reactor quarl. NH_3 builds up as a result of HCN decay. This trend is observed in the experimental data which show initially undetectable quantities of NH_3 and then buildup at later profiles. The highest NH_3 concentration is not observed until 28 cm. These measurements are consistent with measurements of Mitchell et al. (1980) in a laminar methane/air diffusion flame, although a higher level of NH_3 was detected in the experiments of this work.

The detection of relatively large concentrations of cyanide and amine components reveals that NO is formed from HCN and NH_3 oxidation on the fuel-lean side of the flame front. This mechanism of NO formation is termed "prompt NO" since it occurs early in the reactor where radical fuel species are present. NO is also reduced to N_2 by nitrogen intermediates on the fuel-rich side of the flame. Figure II.G-4 depicts the global reactions for the reactions occurring along the flame front. There is a possibility that the formation of NO by the prompt NO reactions is compensated or exceeded by the destruction of NO by nitrogen intermediates in the fuel-rich core.

The nitrogen chemistry is further complicated by the formation of NO_2, which is the majority of the difference between NO_x and NO concentrations shown in Figure II.G-3. NO_2 is formed by oxidation of NO by HO_2 in fuel-rich regions. It is subsequently converted back to NO by reaction with H radicals. The measured data show that NO_2 is formed in the fuel-rich recirculating zone and then is essentially all converted back to NO shortly following uniform mixing in the reactor.

The purpose of these comparisons is to demonstrate the ability of the Zeldovich mechanism to predict thermal NO formation. The predicted thermal NO

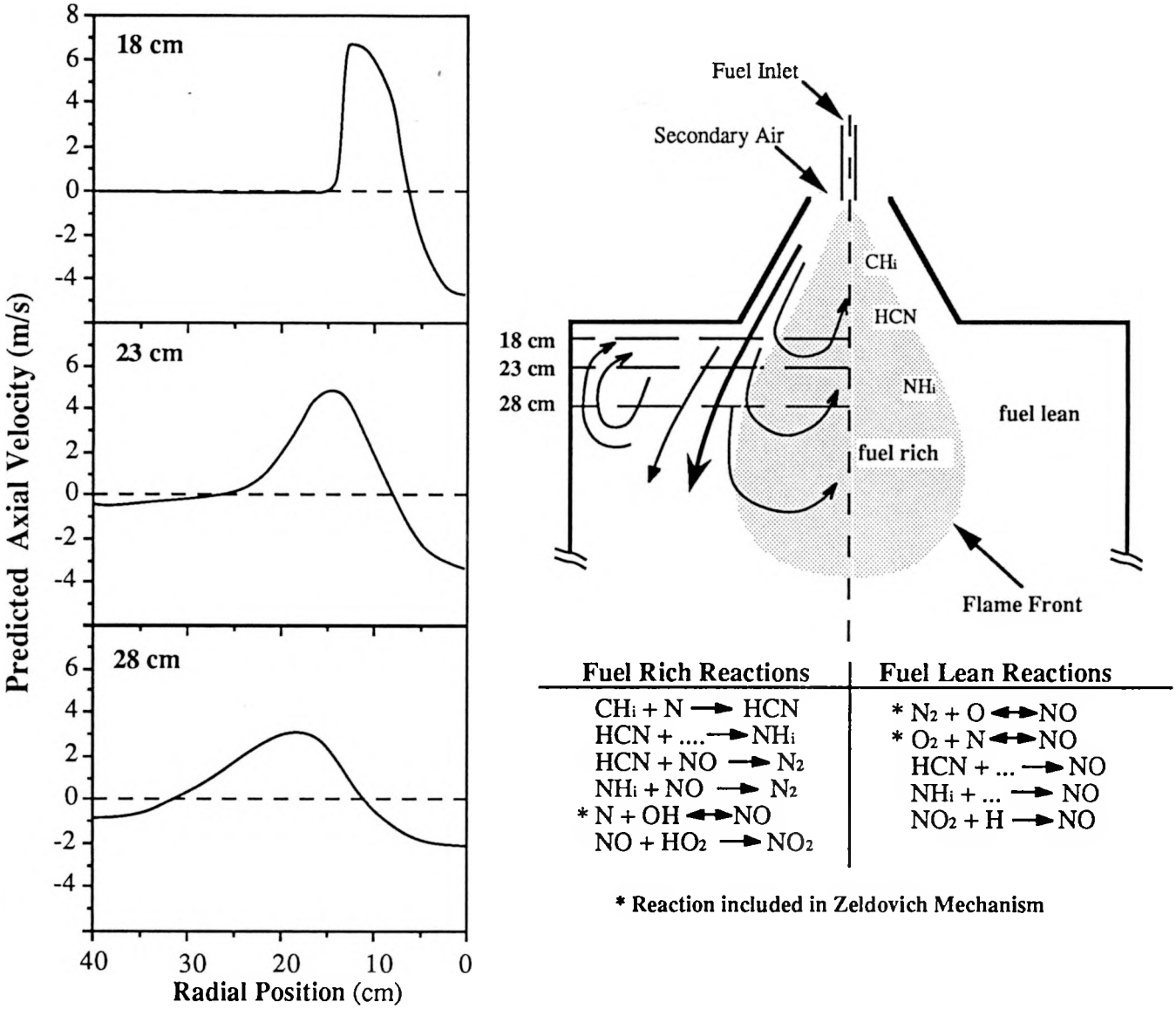

Figure II.G-4. Schematic showing mixing and nitrogen chemistry in the near burner region of a swirling-flow, natural gas/air diffusion flame. Velocity profiles predicted by PCGC-2 show recirculation strength near the wall and at the center region of the reactor.

is lower than the measured concentrations by approximately 30 percent. Whether this difference is due to prompt NO formation remains uncertain. In general, a limitation of using the NO_x model to predict NO formation in gas combustors has been identified. Aside from these complexities, the thermal NO appears to predict NO concentrations on the order of the measured values.

The sensitivity of the thermal NO mechanism to temperature is demonstrated in Figure II.G-5. Predictions were made using the base solution with uniform adjustment to the temperature field. The single point at [0.0, 485] was made using Equation II.G-2 to estimate radical oxygen concentrations. This demonstrates one application of the code to predict the effect of increasing the reactor temperature.

The greatest utility of the code will be realized if the thermal NO mechanism can match observed trends that were measured during parametric variation of equivalence ratio and secondary swirl number. These predictions are currently being made and will be reported in the next quarterly report. Additional work is in progress to predict data measured in a separate natural gas-fired combustor that were obtained from TECFLAM in West Germany.

Fuel NO Mechanism Evaluation - Subsequent to revisions in the radiation submodel of PCGC-2, a lignite coal gasification case has been predicted. Work is ready to begin during the next quarter to evaluate the available options of the expanded fuel NO mechanism. Additional cases for coal combustion will be evaluated using the improved code.

SO_x-Sorbent Reactions Submodel Development

Simulations of gasification cases are in progress to determine the validity of using an equilibrium approach when predicting SO_x species under fuel-rich conditions. These results will be presented and discussed in the next quarterly report.

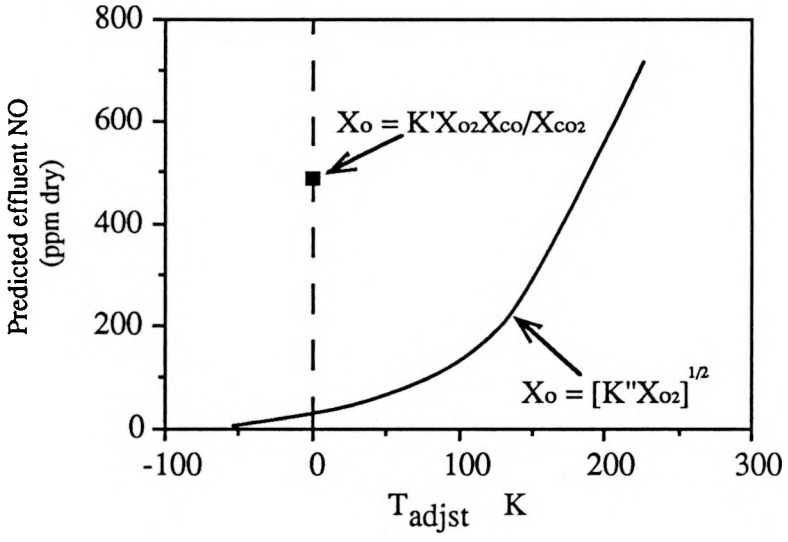

Figure II.G-5. Predicted thermal NO concentrations using the extended Zeldovich mechanism. T_{adjst} represents a uniform temperature adjustment to the predicted field of temperatures shown in Figure II.G-2 (T_{adjst} = 0.0 matches the predicted temperature field). Symbol at [0.0, 485] was predicted using Equation II.G-2.

Plans

Work during the next quarter will continue to focus on evaluation of the NO_x submodel. The evaluation of the revised and expanded NO_x submodel will be completed and reported in the next quarterly report. Emphasis will be given to predicting NO trends with increasing stoichiometric ratio and swirl number variation. Comparisons will also be completed for the data procured from TECFLAM (KäB, 1989). Concurrently, low rank coal combustion and gasification simulations will be made to further investigate the empirical fuel and thermal NO mechanism adapted from Mitchell and Tarbell (1982). The expanded version of the original fuel NO mechanism of Smith et al., (1982), which now includes NH_3 as a reaction center, will also be tested. A comparison of predicted and measured SO_2 and H_2S species will be made for the coal gasification simulations completed during the NO_x model evaluation. Modifications to PCGC-2 to generalize the feed inlets will then begin.

SECTION III. TASK 3. COMPREHENSIVE MODEL DEVELOPMENT AND EVALUATION

Objectives

The objective of this task is to integrate advanced chemistry and physics submodels into a comprehensive two-dimensional model of entrained-flow reactors (PCGC-2) and to evaluate the model by comparing with data from well-documented experiments. Approaches for the comprehensive modeling of fixed-bed reactors will also be reviewed and evaluated and an initial framework for a comprehensive fixed-bed code will be employed after submission of a detailed test plan (Subtask 3.b).

Task Outline

This task is being performed in three subtasks. The first covers the full 60 months of the program is devoted to the development of the entrained-bed code. The second subtask is for fixed-bed reactors is divided into two parts. The first part (12 months) was devoted to reviewing the state-of-the-art in fixed-bed reactors. This led to the development of the research plan for fixed-bed reactors, which was approved. The code development is being done in the remaining 45 months of the program. The third subtask is to generalize the entrained-bed code to fuels other than dry pulverized coal and will be performed during the last 24 months of the program.

III.A. SUBTASK 3.A. - INTEGRATION OF ADVANCED SUBMODELS INTO ENTRAINED-FLOW CODE, WITH EVALUATION AND DOCUMENTATION

Senior Investigators - B. Scott Brewster and L. Douglas Smoot
Brigham Young University
Provo, UT 84602
(801) 378-6240 and 4326

Research Assistant - Susana K. Berrondo

Objective

The objective of this subtask is to improve and validate an existing 2-D code (PCGC-2) for entrained coal gasification and combustion to be more generally applicable to variation in coal rank and operating conditions. The approach being followed is to 1) incorporate detailed, coal-chemistry submodels being developed under Task 2 into PCGC-2, 2) validate the code with carefully chosen experimental data, 3) improve robustness for a wide range of operating conditions, and 4) improve user-friendliness by implementing the improved code on a workstation with a graphical user interface. The code will be applied to systems of practical interest in Task 4.a.

Accomplishments

Several improvements were made in PCGC-2 during the last quarter. A major error was discovered and corrected in the radiation submodel. This correction apparently resolved the previously reported problem with unreasonably high temperature predictions in some cases. A new option was also added to the code for solving the radiation submodel for gaseous combustion (no particles). Other improvements were made in the full energy equation option, the SIMPLE-based numerical algorithm used for solving the fluid flowfield, and the tri-diagonal matrix solver used by SIMPLE. Converged solutions were then obtained for several cases being used in Subtask 2.g to evaluate the extended NO_x submodel, and for the gasification case chosen previously as a standard test case. Additional model validation data were also obtained from AFR, and work continued on modeling

the TWR reactor facility. Development of a user-friendly, graphical interface on the Sun workstation was also continued.

PCGC-2 Improvements

During the past quarter, PCGC-2 was applied to several cases being used to evaluate the extended NO_x submodel (see Subtask 2.g). In these cases, maximum and effluent gas temperatures known to be as much as 1000 degrees higher than the actual temperatures were predicted. In the detailed investigation that followed, a new option was added to code to solve the radiation submodel in gaseous combustion cases (no particles). Several errors were also discovered and corrected in the code, and several minor improvements were made to make the code more user-friendly. The most significant error was found in the radiation submodel and was apparently responsible for the unreasonable temperature predictions. This error involved calculating the blackbody emissive power (E_b) as $2\sigma T^4$ rather than $4\sigma T^4$. In addition to correcting this factor-of-two error, the code was changed to calculate E_b for the particle phase from gas temperature rather than particle temperature. This latter change makes the calculation of E_b consistent with the calculation of the radiation flux field, which substitutes gas temperature for the particle temperature since Eulerian particle temperature information is not available.

Other corrections and improvements were made in the full energy equation option, the SIMPLE-based numerical algorithm used for solving the fluid flowfield, and the tri-diagonal matrix solver used by SIMPLE. In the full energy equation option, a counter counts the number of times properties are requested at enthalpy levels that are outside the table limits. The user must insure that the limits are wide enough to cover the necessary range. During the past quarter, it was discovered that this feature was not working properly at the low end. The user was being told that physical properties were being requested from the table at enthalpies that corresponded to temperatures less than the lowest inlet temperature to the reactor, which was true due to the nature of the interpolation algorithm, but these properties were not being used in the interpolation process (e.g. their weighting factors were zero). Hence, the code was modified to not include these requests in the total number of requests (if any) outside the table limits.

Also, it was discovered that the code had been inadvertantly modified in recent history to under-relax the pressure corrections in the SIMPLE algorithm. Since this procedure is not standard practice, it was removed. Also, it was found that the convergence acceleration parameter recommended by Van Doormaal and Raithby (1984) for the tri-diagonal matrix solver used in SIMPLE, and which was incorporated into PCGC-2 during the past year, was causing instability in the solution algorithm in some cases. It was found that a more conservative implementation of this feature is desirable for code robustness, and the code was modified appropriately. This modification led to the ability to converge several cases that previously would not converge. At least two of these cases are being applied to validate the extended NO_x submodel (Subtask 2.g).

PCGC-2 Validation

Work continued on validating the code for selected cases. Results for a gaseous combustion case being used to validate the thermal NO_x submodel are shown in Figure III.A-1. For this validation, it is critical to correctly predict the gas temperature. Predicted centerline temperature is shown for the simulation of natural gas combustion in the laboratory-scale BYU-ACERC reactor. These results illustrate the importance of including the radiation submodel in gaseous combustion cases and the effect of the corrections to the radiation submodel described above. In addition to the results without radiation and the corrected and uncorrected results with radiation, results are shown assuming no local heat losses (adiabatic assumption). Experimental data are shown for comparison. Radiation plays a significant role in the predictions for this gaseous combustion case. The prediction with the corrected radiation submodel is up to 700 K lower than the prediction without the correction, and agrees closely with the data.

During the last quarter, additional data obtained from the TWR facility were received from AFR. These data include thermocouple measurements of gas temperature (with and without coal), video camera measurements of particle velocity, and tomography measurements of a Montana Rosebud subbituminous coal flame. The tomography measurements were obtained by FT-IR and include particle and gas temperature, particle and soot concentration (percent blockage), and CO_2 concentration (absorbance). The TWR simulation for gas only (no coal) and

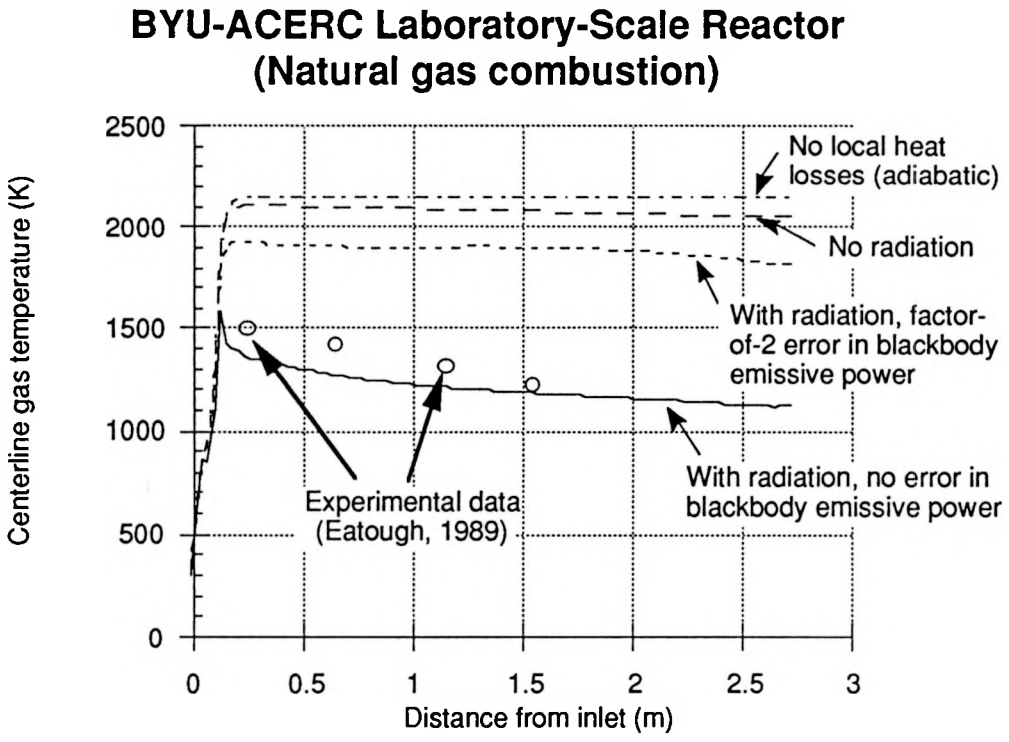

Figure III.A-1. Predicted centerline temperature profiles for combustion of natural gas in the BYU-ACERC laboratory-scale reactor compared with experimental data.

Montana Rosebud coal combustion were repeated with the corrections that have been made to the code during the past quarter.

Figure III.A-2 shows radial temperature profiles for air only (no coal). A similar figure was presented in the 3rd Annual Report (Brewster and Smoot, 1989); however, the experimental data shown previously had not been corrected for radiative heat loss from the thermocouple. The data in Figure III.A-2 are corrected for two assumed values of thermocouple emissivity. The values for ϵ=0.5 are thought to be more accurate, since the thermocouples were oxidized. As shown before, the predicted values agree reasonably well with the experimental data, with predictions accounting for both laminar and turbulent viscosities.

Figure III.A-3 shows a similar plot for combustion of Montana Rosebud subbituminous coal. Again, the measurements were corrected for radiation loss from the thermocouple, assuming two values of emissivity. The values for the higher emissivity (in this case, ϵ=0.9) are again thought to be more accurate. The assumed emissivity is higher in the case of particle combustion due to tar depositing on the thermocouple. Two predictions are shown for alternative geometries simulating the coal injection nozzle. These two geometries may be thought of as limiting cases. In the first case, the nozzle was modeled as a non-protruding 1-mm-i.d. tube with a 2.45-mm wall thickness. In the second case, the nozzle was modeled as a 4.9-mm-i.d. tube with a 0.5-mm wall thickness. A flat profile was assumed for the particles and gas in both cases. The first model geometry is consistent with the physical dimensions of the nozzle duct. The latter model geometry is consistent with the observed diameter of the particle stream as it exits the nozzle. As shown by the dotted lines in the figure, the code predictions are sensitive to the nozzle geometry. The effects of the cold carrier gas persist to a height of 5 cm for the 1-mm nozzle prediction, whereas no effects are seen at that height for the 4.9-mm nozzle prediction.

There are two major discrepancies between the predictions and data in Figure III.A-3. First, ignition is predicted too early as shown in Figure III.A-3b. The observed ignition point is 10 cm above the nozzle (Serio, 1987). However, the fact that the predicted gas temperature exceeds the hot air temperature at a height of 5 cm indicates that ignition has occurred prior to

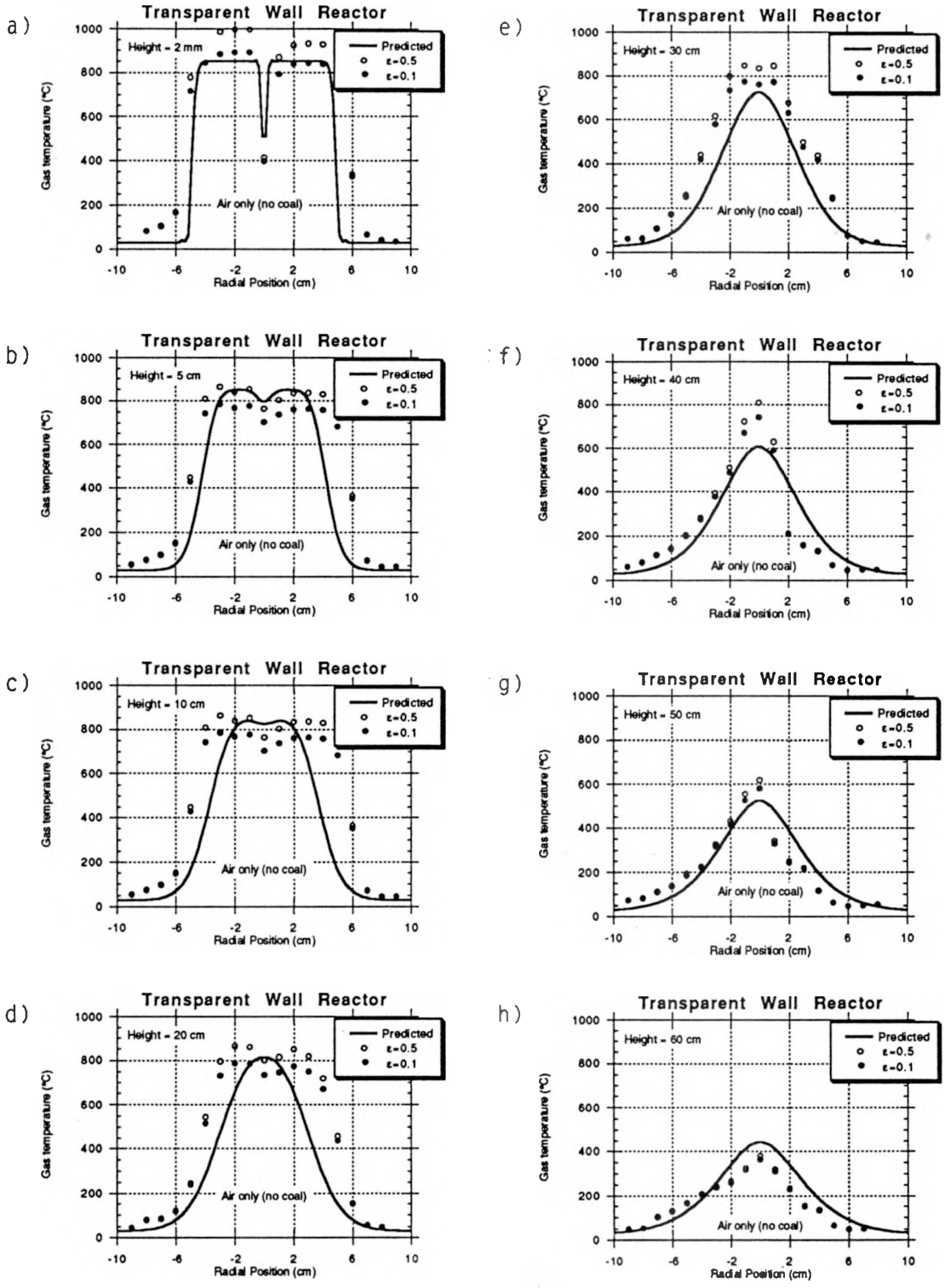

Figure III.A-2. Predicted radial temperature profiles for transparent wall reactor with no coal in primary stream compared with measured values, corrected for radiation loss from the thermocouple (Markham et al., 1990).

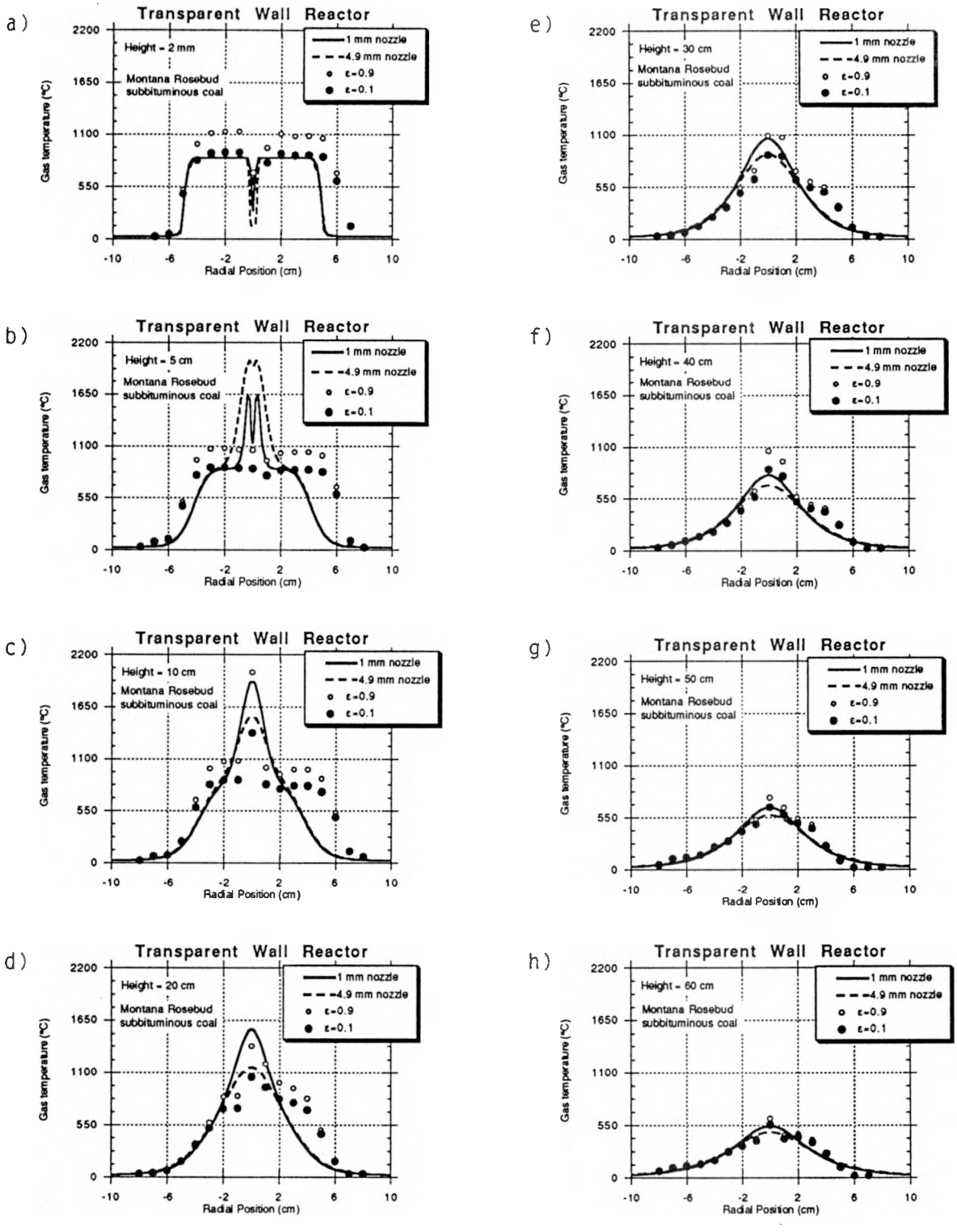

Figure III.A-3. Predicted radial temperature profiles for combustion of Montana Rosebud subbituminous coal in transparent wall reactor compared with measured values, corrected for radiation loss from the thermocouple (Markham et al., 1990).

5 cm in the predictions. The second major discrepancy is that the mixing rate between the hot and cold air at a radial location of approximately 5 cm is overpredicted (see Figures III.A-3b, c, and d). Neither of these discrepancies appears correctable by the nozzle geometry assumed for the model.

Other factors that might be responsible for the discrepancies between the predictions and data in Figure III.A-3 include inaccurate knowledge of the boundary (inlet) conditions for turbulence intensity, neglecting the effects of turbulence on gas-phase chemistry, neglecting the effects of gas buoyancy in laminar flow, using the standard k-ϵ turbulence model which is designed for fully turbulent flows, and neglecting the effects of local composition, temperature, and pressure on laminar viscosity. Inlet turbulence intensity could be determined by making calculations using a literature correlation for screen-generated turbulence and confirming the results with measurements from a hot-wire anemometer in the TWR. The effects of turbulence on local gas properties can be investigated by simply turning on a flag in the code. Buoyancy effects can be included by modifying the gas momentum source terms. The k-ϵ model could be extended to include re-laminarization by including the appropriate additional terms. It is not clear at this point whether these terms could all be lumped into the source terms, or whether the solution procedure for the k and ϵ equations would need to be modified. The effects of local composition, temperature, and pressure on viscosity could be included by modifying a flag already in the code.

The transparent wall reactor was designed to operate in the laminar regime. As shown in the 3rd Annual Report, the Reynolds numbers of the cold carrier gas and hot air stream are in the laminar range. The flowrate of the cold air entering from the room is not accurately known, but its inlet velocity has been assumed to be equal to that of the hot air (1.4 m/s). At the assumed flowrate, the Reynolds number was in the turbulent regime (10,000). Recent measurements have indicated that the inlet velocity may be significantly higher (2.3 m/s). A higher inlet velocity of room air may alter the previous conclusions about the relative importance of laminar and turbulent mixing. At any rate, the flowrate of room air needs to be accurately known for the simulation, and the laminar option should be reinvestigated, especially with the modifications described above. Based on the inlet Reynolds numbers, it is likely that the reactor is

operating in transitional flow. It may be desirable to adjust the velocity of the room air in future experiments to match that of the hot air by varying the velocity of the exhaust fan which draws the room air into the reactor.

Graphical User Interface

Work continued on developing a graphical user interface (GUI) for PCGC-2. Menus associated with the panel buttons were added to allow the user to browse through the available options without having to open a window. The menus also allow the user to jump directly to the desired option. A multiple units options has been added which allows the user to provide the required data in several choices of units. The data are then automatically converted to SI units and written to the main data file to be read by PCGC-2.

Work continued on the grid generation option to make it more user-friendly. Input data consistency checks and helpful error messages were added. The windows created by the grid generation option are shown in Figure III.A-4. The GUI reads the main PCGC-2 data file, allows the user to make any changes, and then generates a grid based on the data in the main data file. The user can review the grid data file thus generated in a scrollable window, change the data, and create a new grid. After creating a suitable grid, it can be saved for use by PCGC-2.

Plans

The evaluation of the full energy equation option in PCGC-2 will continue during the next quarter. Both gaseous and particle combustion cases will be checked for enthalpy conservation. Simulation of the TWR will continue and the following possible actions will be considered: Increasing the room air flowrate in the simulation to match the measured velocity, calculating the laminar viscosity locally, incorporating buoyancy effects in the gas phase, locating a correlation for screen-generated turbulence in the literature and using it to predict the turbulence intensity boundary condition, and incorporating an extension to the k-ϵ model to handle re-laminarization. Work will also continue on the graphical interface to extend it to a network-based windowing system. The interface will also be extended to include a database of thermodynamic data which the user can use to modify the thermo file.

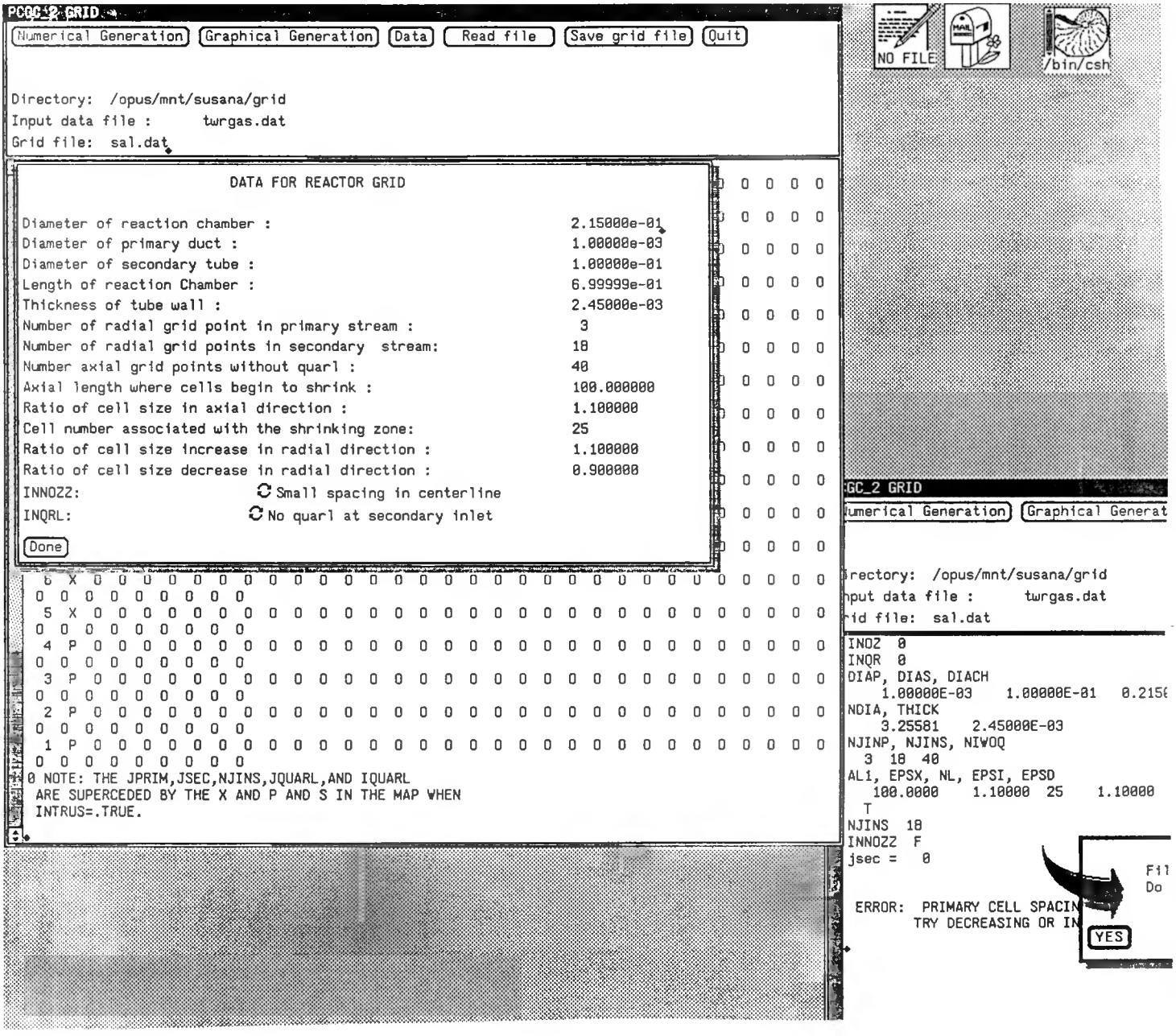

Figure III.A-4. Windows created by grid generation option in graphical user interface for PCGC-2 on Sun-4 workstation computer.

III.B. SUBTASK 3.B. - COMPREHENSIVE FIXED-BED MODELING REVIEW, DEVELOPMENT, EVALUATION, AND IMPLEMENTATION

Senior Investigators - Predrag T. Radulovic and L. Douglas Smoot
Brigham Young University
Provo, Utah 84602
(801) 378-3097 and (801) 378-4326

Graduate Research Assistant - Michael L. Hobbs

Objectives

The objectives of this subtask are: 1) to develop an advanced fixed-bed model incorporating the advanced submodels being developed under Task 2, particularly the large-particle submodel (Subtask 2.e.), and 2) to evaluate the advanced model.

Accomplishments

During the last quarter, work continued on coding chemical and physical submodels and on model validation. Improved temperature profiles and pressure profiles have been obtained from the one-dimensional fixed-bed code. The fixed-bed model considers separate gas and solid temperatures, partial equilibrium in the gas phase, variable bed void fraction, coal drying, devolatilization based on chemical functional group composition, oxidation and gasification of residual char with an ash layer, and axially variable solid and gas flow rates. Predictions and comparisons to experimental data include effluent gas compositions and temperatures, temperature profiles, and axial pressure variation. Additional predictions with comparison to limited data include carbon conversion, particle size effects, and species concentration profiles. The relative importance of char oxidation resistances to bulk film diffusion, ash diffusion, and chemical reaction are identified. For the cases examined, chemical resistance dominates in the cool regions at the bottom and top of the reactor while ash diffusion resistance competes with chemical resistance through most of the reactor. The importance of adequate treatment of devolatilization, gas phase chemistry, and variable bed void fraction is identified. A paper describing the one-dimensional model and the model validation was submitted to the 23rd International Symposium on Combustion. This paper is included in Appendix B.

A review meeting was held in order to specify final features of the one-dimensional model. Further work was performed on the well-mixed, partial-equilibrium model. This model provides an initial estimate of the effluent composition and temperature for the one-dimensional model. A draft of a paper describing the well-mixed, partial-equilibrium model was prepared. Work continued on a review paper on fixed-bed gasification and combustion.

Plans

The development of the fixed-bed code will continue next quarter with emphasis on integrating the large-particle, FG-DVC devolatilization submodel. The equations describing devolatilization need to be solved simultaneously with the conservation equations. AFR's assistance will be needed in understanding all of the comprehensive model equations as well as the submodel equations and solution algorithm.

SECTION IV. TASK 4. APPLICATION OF INTEGRATED CODES

Objective

The objectives of this task are to evaluate the integrated comprehensive codes for pulverized coal and fixed-bed reactors and to apply the codes to selected cases of interest to METC.

Task Outline

This task will be accomplished in two subtasks, one for the entrained-bed lasting 45 months and one for the fixed-bed lasting 36 months. Each of these subtasks will consists of three components: 1) Simulation of demonstration cases on BYU computers; 2) Implementation on a work station at AFR; and 3) Simulation of demonstration cases on the workstation.

IV.A. SUBTASK 4.a. - APPLICATION OF GENERALIZED PULVERIZED COAL COMPREHENSION CODE

Senior Investigator - B. Scott Brewster and L. Douglas Smoot
Brigham Young University
Provo, UT 84602
(801) 378-6240 and 4326

Objective

The objectives of this subtask are 1) to implement the comprehensive entrained-bed code developed in Task 3 at AFR and 2) to simulate reactors of interest to METC.

Accomplishments

No work was conducted on this subtask during the past quarter.

Plans

No work is planned for this subtask during the next quarter.

IV. B. SUBTASK 4. B. - APPLICATION OF FIXED-BED CODE

Senior Investigators - Predrag T. Radulovic and L. Douglas Smoot
Brigham Young University
Provo, Utah 84602
(801) 378-3097 and (801) 378-4326

Graduate Research Assistant - Michael L. Hobbs

Objectives

The objective of this subtask is to apply the advanced fixed-bed[1] code developed in Subtask 3.b to simulate fixed-bed gasifiers of interest to METC.

Accomplishments

Fixed-bed data collection

During the last quarter, work continued on collecting fixed-bed design and test data by direct contact with the organizations and the individuals involved in fixed- or moving-bed gasification or combustion research or in research on non-reacting fixed- or moving-beds. Seventy-eight answers to the fixed-bed data questionnaire have been received, thirty-four have been positive, and eighteen sets of data have been obtained to date. However, some of the most important data sets have not yet been obtained. Requests for data were sent again to a number of individuals and organizations who had not responded to the first request. It is known that several U.S. coals have been tested in SASOL, South Africa, between 1974 and 1982: Kentucky No. 9 bituminous, Powder River Basin subbituminous, Texas lignite, and North Dakota lignite (Simbeck et al., 1983). The test data have been requested from SASOL, Fluor Engineering, and The Department of Energy and an answer has been received from SASOL. SASOL has referred the request to Lurgi, which in turn has declined to provide the test data, claiming confidentiality. Great Plains Gasification Project is another important potential source of test data. The test data have been requested but only a suggestion to obtain "Great Plains Coal Gasification Plant Public Report" has been received. Help from DOE/METC is being sought in collecting some of fixed-bed gasification test data. Work also continued on collecting fixed-bed experimental data from the open literature. The computerized data search was updated.

Fixed-bed code validation

Further testing and validating of the advanced fixed-bed code developed in Subtask 3.b was performed. The test case was the same as one used before - the test run of the Wellman-Galusha gasifier with Jetson high volatile B bituminous coal. Details of testing and evaluating the code are presented under Subtask 3.b. A paper presenting these results was submitted to the 23rd International Symposium on Combustion and given in Appendix B. Key results are summarized below.

The predicted temperature and composition at the bottom and the top of the reactor are in good agreement with the measured values. The predicted temperature profile agrees reasonably well with limited experimental data, but the agreement could be better. The predicted carbon conversion and gas composition profiles seem qualitatively correct, but there are no measured profiles to compare with. Good agreement is obtained between the predicted and measured pressure variations for linearly varying bed void fraction. There is need for further improvement of the advanced fixed-bed code.

Plans

During the next quarter, work will continue on collecting fixed-bed design and test data. The fixed-bed design and test data will be collected both from the open literature and by direct contact with the organizations and individuals involved in fixed- or moving-bed gasification or combustion research or in research on non-reacting fixed or moving beds. Efforts will continue to identify additional test cases for simulation and validation. Further testing and validation of the code will be performed.

REFERENCES

Best, P.E., Solomon, P.R., Serio, M.A., Suuberg, E.M., Mott, W.R., Jr., and Bassilakis, R., ACS Div. of Fuel Chem. Prepr., 32, (4), 138, (1987).

Blackham, A.U., "Subtask 2.F. - Large Char Particle Oxidation at High Pressures", Research Plan for Measurement and Modeling of Advanced Coal Conversion Processes, Section II.F. under Contract No. DE-AC21-86MC23075, Advanced Fuel Research, Inc. (Contractor), East Hartford, CT, (1989).

Boardman, R.D., "Measurement and Prediction of Nitric Oxide in Stationary Combustors", Ph.D. Dissertation, Brigham Young University, Provo, UT, in preparation, (1990).

Brewster, B.S. and Smoot, L.D., Brigham Young University, "Subtask 3.A. - Integration of Advanced Submodels into Entrained-Flow Code, with Evaluation and Documentation", Measurement and Modeling of Advanced Coal Conversion Processes, 3rd Annual Report, Chapter III.A., Solomon, P.R. et al., Principal Investigators under Contract No. DE-AC21-86MC23075, U.S. Dept. of Energy/Morgantown Energy Tech. Center, Morgantown, WV, (1989).

Calkins, W.H., Hagaman, E., and Zeldes, H., Fuel, 63, 1113, (1984a).

Calkins, W.H., Tyler, R.J., Fuel, 63, 1119, (1984b).

Calkins, W.H., Fuel, 63, 1125, (1984c).

Calkins, W.H., Hovsepian, B.K., Drykacz, G.R., Bloomquist, C.A.A., and Ruscic, L., Fuel, 63, 1226, (1984d).

Eatough, C., Ph.D. Dissertation, Brigham Young University, Provo, UT, in preparation, (1990).

Feldkirchner, H.L. and Johnson, J.L., "High Pressure Thermobalance", Rev. Sci. Instrum. (USA), 39, 1227-9, (1968).

Freihaut, J.D, Proscia, W.M., and Seery, D.J., ACS Div. Fuel Chem. Preprints, 33, (2), 262, (1988).

Grant, D.M., Pugmire, R.J., Fletcher, T.H., and Kerstein, A.R., Energy & Fuels, 3, 175, (1989).

Green, T, Kovac, J. Brenner, D., and Larsen, J., in Coal Structure, (R.A. Myers, Ed.), Academic Press, NY, (1982), Chapter 6, p. 199.

Iverach, D., Basden, K.S., and Kirov, N.Y., "Formation of Nitric Oxide in Fuel-Lean and Fuel-Rich Flames", 14th Symposium (Int) on Combustion, The Combustion Institute, Pittsburgh, PA, (1973), p. 767.

KäB, M.H.B. and Spiegelhalder, R., Flammenprofilmessungen an der TECFLAM-Kohlenstaub-Verbrennungsanlage MeBdaten der Flammen Z3, Stuttgart, West Germany, (1989).

Kalson, P.A. and Briggs, D.E., "Devolatilization and Tar Production in a Bituminous Lump Coal", AIChE J., 31, 1047-50, (1985).

Larsen, J.W. and Kovac, J., ACS Symposium Series, **71**, 36, (1978).

Lucht, L.M. and Peppas, N.A., ACS Symposium Series, **169**, 43, (1981).

Lucht, L.M. and Peppas, N.A., Fuel, **66**, 803, (1987).

Mitchell, J.W. and Tarbell, J.M., "A Kinetic Model of Nitric Oxide Formation During Pulverized Coal Combustion", AIChE J., **28**, 302, (1982).

Mitchell, R.E., Sarofim, A.F., and Yu, R., "Nitric Oxide and Hydrogen Cyanide Formation in Laminar Methane/Air Diffusion Flames", Comb. Sci. Tech., **21**, 157-67, (1980).

Mitchell, R.E., "The Influence of the Mineral Matter Content of Coal on the Temperatures and Burning Rates of Char Particles During Pulverized Coal Combustion", 16th Annual International Pittsburgh Coal Conference Proceedings, Pittsburgh, PA, (September 25-29, 1989).

Nelson, P.F., Fuel, **66**, 1264, (1987).

Niksa, S. and Kerstein, A.R., Fuel, **66**, 1389, (1987).

Nuttall, H.E., Stoddart, W.G., and Chen, W.J., "Pyrolysis of Subbituminous New Mexico Coal", J. Pet. Tech., 418-20, (April 1979).

Parikh, R.S. and Mahalingam, R., "Modeling and Experimental Studies on Devolatilization Yields from a Bituminous Coal", Ind. Eng. Chem. Res., **26**, 2378-84, (1987).

Sanada, Y. and Honda, H., Fuel, **45**, 295, (1966).

Sarofim, A.F. and Pohl, J.H., "Kinetics of Nitric Oxide Formation in Premixed Laminar Flames", 14th Symposium (Int) on Combustion, The Combustion Institute, Pittsburgh, PA, (1973), p. 739.

Sears, J.T., Maxfield, E.A., and Tamhankar, S.S., "Pressurized Thermobalance for Use in Oxidizing Atmospheres at High Temperatures", Ind. Eng. Chem. Fund., **21**, 474-8, (1982).

Sears, J.T., Tamhankar, S.S., Radman, A., and Wen, C.Y., "Influence of Char Properties on Reaction Rates", Chem. Eng. Commun., **38**, 17, (1985).

Serio, M.A., Advanced Fuel Research, Inc., "Subtask 2.c. - Secondary Reaction of Pyrolysis Products and Char Burnout Submodel Development and Evaluation", Measurement and Modeling of Advanced Coal Conversion, Annual Report, Chapter II.C., Solomon, P.R. et al., Principal Investigators under Contract No. DE-AC21-86MC23075, U.S. Dept. of Energy/Morgantown Energy Technology Center, Morgantown, WV, (1987).

Serio, M.A., Solomon, P.R., Bassilakis, R., and Suuberg, E.M., ACS Div. of Fuel Chem. Prepr., **34**, (1), 9, (1989).

Serio, M.A., Solomon, P.R., and Suuberg, E.M., "The Variations in Char Reactivity with Pyrolysis Conditions and Coal Type", to be submitted to Fuel, (1990).

Simbeck, D.R., Dickenson, R.L., and Oliver, E.D., "Coal Gasification Systems: A Guide to Status, Applications, and Economics", Final Report, AP-3109, Research Project 2207, EPRI, Palo Alto, CA, (1983).

Smith, I.W., 19th Symposium (Int) on Combustion, The Combustion Institute, (1982), pp. 1045-1065.

Smith, P.J., Hill, S.C., and Smoot, L.D., "Theory for NO Formation in Turbulent Coal Flames", 19th Symposium (Int) on Combustion, The Combustion Institute, Pittsburgh, PA, (1982), p. 1263.

Solomon, P.R., Serio, M.A., Heninger, S.G., ACS Div. of Fuel Chem. Prepr., **31**, (3), 200, (1986).

Solomon, P.R., Hamblen, D.G., Carangelo, R.M., Serio, M.A., and Deshpande, Energy & Fuel **2**, 405, (1988a).

Solomon, P.R., Chien, P.L., Carangelo, R.M., Best, P.E., and Markham, J.R., 22nd Symposium (Int) on Combustion, The Combustion Institute, (1988b), pp. 211-221.

Solomon, P.R., Serio, M.A., Hamblen, D.G., Smoot, L.D., and Brewster, B.S., Measurement and Modeling of Advanced Coal Conversion Processes, 7th Quarterly Report under DOE-METC Contract No. DE-AC21-86MC23075, Advanced Fuel Research, Hartford, CT, (1988c).

Solomon, P.R., Serio, M.A., Hamblen, D.G., Smoot, L.D., and Brewster, B.S., Advanced Fuel Research, Inc./Brigham Young University, Measurement and Modeling of Advanced Coal Conversion, 9th Quarterly Report under DOE-METC Contract No. DE-AC21-86MC23075, Advanced Fuel Research, Hartford, CT, (1988d).

Solomon, P.R., Serio, M.A., Carangelo, R.M., Bassilakis, R., Gravel, D., Baillargeon, M., Baudais, F., and Vail, G., "Analysis of the Argonne Premium Coal Samples by TG-FTIR", Energy & Fuel, submitted for publication (1989a).

Solomon, P.R., Hamblen, D.G, and Yu, Z.Z., ACS Div. of Fuel Chem. Preprints, **34**, (4), 1280, (1989b).

Solomon, P.R., Serio, M.A., Hamblen, D.G., Smoot, L.D., and Brewster, B.S., "Measurement and Modeling of Advanced Coal Conversion Porcesses", DOE/METC 3rd Annual Report under Contract No. DE-AC21-86MC23075, (1989c).

Solum, M., Pugmire, R.J., and Grant, D.M., Energy & Fuels, **3**, 40, (1989).

Suuberg, E.M., Unger, P.E., and Lilly, W.D., Fuel, **64**, 956, (1985).

Tamhankar, S.S., Sears, J.T., and Wen, C.Y., "Coal Pyrolysis at High Temperatures and Pressures", Fuel, **63**, 1230, (1984).

Thompson, D., Brown, T.D., and Beér, J.M., "Formation of NO in a Methane-Air Flame", 18th Symposium (Int) on Combustion, The Combustion Institute, Pittsburgh, PA, 1981, p. 787.

Van Doormaal, J.P. and Raithby, G.D., "Enhancements of the SIMPLE Method for Predicting Incompressible Fluid Flows", Num. Heat Transf., 7, 147, (1984).

APPENDIX A

"FT-IR EMISSION/TRANSMISSION TOMOGRAPHY OF A COAL FLAME"

Paper Submitted to the 23rd International Symposium of the Combustion Institute, 1990

FT-IR EMISSION/TRANSMISSION TOMOGRAPHY OF A COAL FLAME

J.R. Markham, Y.P. Zhang, R.M. Carangelo, and P.R. Solomon
Advanced Fuel Research, Inc., 87 Church Street, East Hartford, CT 06108

ABSTRACT

Fourier Transform Infrared (FT-IR) Emission/Transmission (E/T) spectroscopy has recently been shown to be a versatile technique for coal combustion diagnostics by allowing for measurements of particle concentrations and temperatures, and gas compositions, concentrations, and temperatures. These measurements are for the ensemble of particles and gases along a line-of-sight in the flame. In this paper, tomographic reconstruction techniques have been applied to line-of-sight FT-IR E/T measurements to derive spectra that correspond to small volumes within a coal flame. From these spectra, spatially resolved point values for species temperature and relative concentrations can be determined. The technique was used to study the combustion of Montana Rosebud subbituminous coal burned in a transparent wall reactor. The coal is injected into the center of an up-flowing preheated air stream to create a stable flame. Values for particle temperature, relative particle density, relative soot concentration, the fraction of ignited particles, the relative radiance intensity, the relative CO_2 concentration and the CO_2 temperature have been obtained as functions of distance from the flame axis and height above the coal injector nozzle. The spectroscopic data are in good agreement with visual observations and thermocouple measurements. The data present a picture of the coal burning in a shrinking annulus which collapses to the center at the tip of the flame. CO_2 temperatures are highest in the rapid burning zone (2300 to 2900 K). The highest particle temperatures in this zone are 1900 to 2000 K, with temperatures up to 2400 K outside the zone.

INTRODUCTION

Better understanding of the coal combustion process would promote more reliable utilization of coals having a diversity of characteristics and would enable improved combustion systems to be designed and developed. Among the processes which are the least well understood and predicted are: ignition, soot formation, swelling, char reactivity, and ash formation. Recently, Fourier Transform Infrared (FT-IR) Emission/Transmission (E/T) spectroscopy was applied to a laboratory scale coal flame to determine ignition, soot formation, particle temperature, particle concentrations, gas temperatures and gas concentrations for a number of coals varying in rank from lignite to low volatile bituminous.[1] Chars and demineralized coals were also included in this study. The study demonstrated that the FT-IR E/T technique is a versatile diagnostic for studying coal combustion. However, it suffers from being a line-of-sight technique.

To correct this shortcoming, tomography techniques have been applied to both the FT-IR emission and transmission spectra to obtain spatially resolved spectra. This method has recently been applied to a stable, well defined co-annular laminar ethylene diffusion flame.[2,3] From the spatially resolved spectra, point values for species temperature and relative concentrations were determined for CO_2, H_2O, alkanes, alkenes, alkynes, and soot. The CO_2 and H_2O temperatures were found to be in good agreement with measurements performed on the same flame by coherent-anti-Raman spectra (CARS),[4] and the soot concentrations were in good agreement with soot concentrations determined by laser scattering.[5]

This paper describes the application of FT-IR E/T tomography to a coal flame produced in a transparent wall reactor. From these spectra, spatially resolved point values have been obtained for particle temperature, relative particle density, relative soot

concentration, the fraction of ignited particles, the relative radiance intensity, the relative CO_2 concentration and the CO_2 temperature.

EXPERIMENTAL

Apparatus

The Transparent Wall Reactor (TWR) facility has been described previously.[1] The coal is injected upwards into a center of a 10 cm diameter upward flowing preheated air stream in the center of a 20 cm diameter x 70 cm tall glass enclosure. Figure 1 shows the temperature in the stream as a function of position measured with a thermocouple in the absence of coal. The preheated air stream provides a stable hot environment for the coal up to a height of 30 cm. Critical to the measurements is the flame stability which relies on a steady particle feeding system. Our feeding system employs mechanical vibration to displace and entrain particles into a carrier gas. Improvements in the vibration system have resulted in a flame which is very stable in shape and position except for the ignition point where verticle fluctuations of $\pm$ 5 mm are observed.

The enclosure has movable KBr windows to allow access to the flame by the FT-IR spectrometer (a modified Nicolet 20SX). As discussed in Ref. 6, emission measurements are made by directing the radiation emitted by the hot sample stream through an interferometer to an "emission" detector. Transmission measurements are made by replacing this detector with a high intensity globar source which, after passing through the interferometer, is directed through the sample area to a "transmission" detector. The emission and transmission measurements are made along the same 1 mm wide by 4 mm high optical path defined with apertures. With this optical geometry, parallel line-of-sight emission and transmission spectra were collected across the coal stream at 1 mm increments along the radius.

MCT infrared detectors were used for both emission and transmission measurements. It is important to avoid possible saturation of the transmission detector due to the direct impingement of flame radiation on the detector. Two methods were employed to verify that this did not occur: 1) reproducible line-of-sight attenuation was observed when the detector was apertured to reduce the overall intensity, and 2) the same intensity was observed in a region of the spectrum that was totally blocked (achieved by flooding the beam path with CO_2) in both the flame on and flame off conditions. Different intensities would indicate saturation.

Sample

The sample used in this experiment was a sieved fraction (200 x 325 mesh) of dry Montana Rosebud subbituminous coal. The characteristics of this coal has been published previously.[1,7] The current sample has an 11% ash content. The coal was fed into the TWR at a rate of 1.6 g/min.

Coal Flame

The flame generated from this coal is shown in Fig. 2 and reproduces the flame analyzed previously by line-of-sight FT-IR E/T measurements.[1] Figure 2a presents a view of the entire length of the flame. Below the ignition point, a few particles that are in the outer edge of the stream (closest to the hot gas) are observed to ignite. At 10 cm the flame ignites. Also indicated is the extent of the coal weight loss at several locations above the nozzle. The particle stream was collected for these determinations with a 1.6 cm diameter water cooled extractor that adds cold helium gas to the hot stream to drop the temperature below 350°C as it is aspirated to a cyclone separator. Percent burnout was determined by

ash tracer with a thermogravimetric analyzer.

A weight loss of 43.2% (DAF) was observed for material collected at the ignition point. TGA analysis on this char indicated that it contains essentially no remaining volatile matter. All of the particles have reached a temperature to completely devolatilize but not significantly burn at this point in the TWR, based on the starting material's volatile content of 42.8% (DAF).[1]

SEM photographs were made of collected char. At ignition, most particles are of the same dimensions as before ignition but a few particles are larger (presumably swollen) and some are smaller (possibly fragmented).

Figures 2b and 2c show close-up photographs of the flame taken with 1/250 sec and 1/2000 sec exposures, respectively. The photos indicate the structure of the flame, with the highest density of ignited particle shrinking from the edge to the center-line with increasing height above the nozzle. The positions where the FT-IR tomographic slices were measured are also indicated. The photographs show the relatively laminar appearance of the flame (Figs. 2a and 2b) while some non-uniformity can be seen along the center line in Fig. 2c. The steadiness in the flame is also indicated by reproducibility of consecutive spectroscopic measurements. Typically line-of-sight measurements deviate by less than 10%. Multiple measurements are performed to average out these deviations.

Measurements were made of the particle velocities by measuring the length of tracks recorded with a video camera. The results are presented in Fig. 3 for both combustion and pyrolysis conditions. For pyrolysis conditions, sufficient air was added to make a few particles ignite so that they could be viewed. The figure shows the velocities increasing to the hot gas velocity for pyrolysis and above the hot gas velocity for combustion. The video pictures were also analyzed to determine the relative particle density as a function of position. Below the ignition region, scattering from a He-Ne laser was used to determine the width of the particle stream.

ANALYSIS

Line-of-Sight FT-IR E/T Measurements

The analysis for the line-of-sight FT-IR E/T measurement pertaining to multi-phase reacting streams has been presented previously.[1,6,8-10] It is an extension of the emission/transmission method applied to gases and soot.[11-14]

For a medium containing gases and soot with absorption coefficients α^g_ν and α^s_ν and particles of geometrical cross-sections A at a density of N particles cm^{-3}, the measured transmittance, τ_ν. is given by

$$\tau_\nu = \exp(-(\alpha^s_\nu + \alpha^g_\nu + NAF^t_\nu) L) \qquad (1)$$

where F^t_ν is the ratio of the total cross-section (extinction) to the geometrical cross-section, and L is the path length. The relative concentrations of individual gas species, (related to α^g_ν), soot (related to α^s_ν) and particles (related to NAF_ν) are determined from the regions of the spectra which can be uniquely related to the individual species.

From the radiance R_ν, the normalized radiance $R^n_\nu = R_\nu/(1-\tau)$ is obtained,

$$R^n_\nu = \frac{\alpha^s_\nu R^b_\nu(T_s) + \alpha^g_\nu R^b_\nu(T_g) + NA\,\epsilon_\nu\, R^b_\nu(T_p) + NAF^{s'}_\nu R^b_\nu(T_w)}{\alpha^s_\nu + \alpha^g_\nu + NAF^t_\nu} \qquad (2)$$

where $R^b_\nu(T_g)$, $R^b_\nu(T_s)$, $R^b_\nu(T_p)$ and $R^b_\nu(T_w)$ are the black-body emission spectra at the temperatures T_g, T_s, T_p, and T_w of the gas, soot, particle, and wall, respectively. ϵ_ν is the particle's spectral emittance and $F^{s'}_\nu$ is the cross-section for scattering radiation into the spectrometer. $F^{s'}_\nu$ is taken as negligible in this analysis because the experiment is

performed with room temperature walls and the small diameter of the flame was chosen so that very little scattered radiation from other parts of the flame can enter the spectrometer. The temperatures for individual components are obtained from the normalized radiance as discussed in Refs. 1,6,8-10.

FT-IR E/T Tomography

The reconstruction of spatially resolved FT-IR spectra from multiple line-of-sight spectra has been described in detail elsewhere.[2,3] We have employed the Fourier image reconstruction technique[15] which is capable of handling data from systems of arbitrary shape. Our flame, however, was cylindrically symmetric.

In transmission tomography the projections are of absorbance = $\log_{10}\tau$. The program published by Shepp and Logan was adapted for this work[15] by applying the reconstruction one wavelength at a time.

In spectral regions for which Beer's Law applies, the two-dimensional image reconstructed from line-of-sight absorbance measurements leads to the determination of the spatial dependence of absorbance, and hence relative concentration. Relative concentration can be converted to absolute concentration if appropriate calibration measurements are made.

A straight-forward application of the reconstruction technique to radiance spectra is not possible, because of self-absorption in the sample. In the case of small absorbance encountered in this work (percent transmission > 80%), an emission measurement can be directly corrected by an absorption measurement made along the same path. A self-absorption correction corresponding to that used by Freeman and Katz was employed for the thin sample studied.[16] The Fourier reconstruction program can be applied directly to the

emission thus corrected, to obtain local radiances. These are then converted to normalized radiance and the analysis proceeds as for the line-of-sight spectrum.

Examples of local radiance, transmission and normalized radiance spectra are shown in Figs. 4a, 4b, and 4d. The tomographic reconstruction process enhances noise in data, relative to that in the unprocessed data. In this work the data were smoothed by co-adding data from eight adjacent wavenumber bands. This results in degraded resolution from the 8 cm^{-1} used, although the resolution was still sufficient to quantitatively measure the gas species. The results of the reconstruction were consistent in that the summed absorbance and radiance across the flame diameter agreed with the measured line-of-sight absorbance and radiance, as can be seen in Fig. 4c for absorbance.

In each local absorbance spectrum, characteristic line features associated with carbon dioxide, the major gaseous component within the flame, can be identified (Fig. 4a). The area of this component line above the solid phase continuum was measured to derive the local relative concentration of CO_2. Water is observed in the spectrum but not resolved well enough for quantitative determinations. The shape and amplitude of the solid phase continuum can be analyzed to derive the local relative concentrations of particles or mixtures of particles and soot as described in Ref. 1.

In like manner, each species can be identified in the local radiance spectra (Fig. 4b). The particle/soot emission continuum is subtracted to determine the radiance contribution from CO_2. The corrected local emission and transmission values can then be employed to determine local species temperatures.

Figure 4d shows a normalized radiance spectrum calculated by the local radiance and transmission values. The local particle temperatures are obtained by comparing the normalized radiance to theoretical black-body curves, which are "fit" to the data in regions where the solid phase continuum is not influenced by the gas phase species. Overlayed is a gray-body fit to determine particle temperature. As described in Ref. 1, the black-body

multiplier used for each case is the constant fraction of the theoretical black-body which produces the best match in shape and amplitude to the experimental data. For a completely homogeneous sample of gray-body particles, M would be the particle's emissivity. For this case, some particles may be unignited, or ash particles may be present at a much lower temperature and have a very low emittance. The multiplier than approximates the fraction of particles ignited in each local area times their emissivity.

RESULTS

Tomographic reconstruction has been applied to four sets of 21 parallel line-of-sight E/T measurements, at heights of 6, 12, 16, and 20 cm above the nozzle. One set of measurements was for a region below the visually observed ignition point, where particle heat-up and devolatilization were occurring; one set of measurements was just above ignition and the two others were further up in the flame. The data are presented in Figs. 5 to 7.

Figure 5a presents the height of the continuum blockage determined from the transmittance spectra as percent blockage of the incident IR beam. The total blockage is divided into particles and soot as described in Ref. 1. Soot is observed to appear at ignition as inferred by the change in shape of the continuum, from sloping (particles) to flat (soot and particles). Below the ignition (6 cm above the nozzle) there are particles only (no soot) confined to a radius of about 6 mm. This is in agreement with the boundaries as determined using the He-Ne laser. The multiplier, M (the product of emissivity times the fraction of ignited particles) in Fig. 5b shows a few particles (up to 10%) have ignited at the edge of the coal stream. Such ignited particles can also be seen in Figs. 2a and 2c.

Just above ignition (12 cm above the nozzle), the particles appear to be forced inward into a more dense central stream at the same time that some particles are spread outward. The spreading of the stream is confirmed by the video camera. The outward velocity of

particles can also be seen in Fig. 2b. This spreading is consistent with the location of the ignition zone centered at about 4.75 mm radius, indicated by the 0.5 M value in Fig. 5b (i.e., half the particles ignite) as well as the high level of ignited material shown in Fig. 6a, the high radiance in Fig. 6b and the high CO_2 temperature in Fig. 7a. The increase in gas volume in this zone must create pressure to compress the stream inward and expand the stream outward. The total blockage determined by integrating the blockage times area is shown in Fig. 5a. The integrated particle blockage is increased from 1.0 (by definition) at 6 cm to 1.5 at 12 cm. This suggests that the devolatilization which appears complete at this point may swell or fragment the particles to increase the blockage.

At 16 cm the particle blockage is reduced (0.8) as the material burns out (Fig. 5a) and the ignition zone moves inward (Figs. 5b, 6, and 7a).

At 20 cm, the blockage appears to go back up due to the increased blockage at radiuses above 4 mm. It is likely that the blockage at the edge of the stream is now due to ash as it is no longer luminous. The ignition zone has now moved to the center of the stream.

Figure 6 presents the amount of burning material determined from: a) the multiplier M (Fig. 5b) times the total blockage (Fig. 5a), and b) the total local radiance determined at 4500 cm^{-1} from the local R_ν spectra. These two determinations are in reasonable agreement. Both show the ignition zone decreasing from a radius of about 4.25 mm at 12 cm height to the axis at 20 cm height. The high value of radiance along the center line at 12 cm and 16 cm results from the very high values of the particle density even though M is low. The regions of high radiance determined spectroscopically agree with visual and photographic determinations of the bright ignition zone and the total luminous zone as shown on the figure.

Figure 7a presents the temperature of CO_2 (dashed line) and total continuum, both particles and soot (solid line). Also presented are measurements with a Pt + PtRh

thermocouple obtained at several points in the flame. The thermocouple temperature has been radiation corrected using a 0.9 emissivity because of the soot and ash coatings which developed on the surface. These readings are in reasonable agreement with the CO_2 temperatures. The particles have a relatively constant temperature between 1900 K and 2000 K in the ignition zone. Higher Temperatures (2200 to 2400 K) are, however, observed outside these zones. The higher temperature at large radius is understandable as due to a higher level of O_2. The higher temperature at smaller radius for 12 cm matches the CO_2 temperature, but the higher temperature along the center line at 16 cm is puzzling. Note that prior to ignition, the ignited particles are only at 1700 K, but here, the ambient temperature is only 1500 to 1600 K as determined from the CO_2 temperature.

The CO_2 temperatures are also presented in Fig. 6a (dashed line). The maximum CO_2 temperatures (2300 to 2900 K) occur in the regions of high particle radiance where the maximum combustion is occurring. These temperatures are 400 - 1000K hotter than the particles in the same region suggesting that CO is burning to CO_2 away from the particles. CO_2 temperatures are generally lower (below 2000 K) and are closer to the particle temperatures away from the ignition zone. The exception is the center at 16 cm which, as mentioned above, is puzzling. At 20 cm the CO_2 and particle temperatures are within 100 K except along the axis (the ignition zone) where the CO_2 temperature is hotter.

The CO_2 concentrations are presented in Fig. 6b. The relative concentration of CO_2 is determined from the area of the absorbance band. Below ignition the CO_2 concentration is very small. Above ignition the CO_2 level jumps drastically and spreads with increasing height. The shape of the CO_2 concentration at 12 cm is inverse to the shape of the CO_2 temperature and is most likely due to the variation in CO_2 density with temperature.

CONCLUSIONS

Tomographic reconstruction techniques have been applied to FT-IR E/T measurements to derive local values for species temperatures and concentrations within a laboratory scale coal flame. Values for particle temperature, relative particle density, relative soot concentration, the fraction of ignited particles, the relative radiance intensity, the relative CO_2 concentration and the CO_2 temperature have been obtained as functions of distance from the flame axis and height above the coal injector nozzle. The spectroscopic data are in good agreement with visual observations and thermocouple measurements. The data present a picture of the coal burning in a shrinking annulus which collapses to the center at the tip of the flame. CO_2 temperatures are highest in the rapid burning zone (2300 to 2900 K). The highest particle temperatures in this zone are 1900 to 2000 K, with temperatures up to 2400 K outside the zone.

ACKNOWLEDGEMENT

This work was supported under the U.S. Department of Energy, Morgantown Energy Technology Center Contract No. DE-AC21-86MC23075. Richard Johnson is the Project Manager for this program.

REFERENCES

1. Solomon, P.R., Chien, P.L., Carangelo, R.M., Best, P.E., and Markham, J.R.: Twenty-Second Symposium (International) on Combustion, p. 211, The Combustion Institute, (1988).

2. Chien, P.L., Best, P.E., Carangelo, R.M., and Solomon, P.R., "Tomographic Reconstruction of Fourier Transformed Infrared (FT-IR) Spectra at Points within a Coannular Flame", poster session 22nd Symposium (Int) on Combustion, Seattle, Washington, DC, (Aug. 1988).

3. Best, P.E., Chien, P.L., Carangelo, R.M., Solomon, P.R., Danchak, M. and Ilovici, I.: "Tomographic Reconstruction of FT-IR Emission and Transmission Spectra in a Sooting Laminar Diffusion Flame: Species Concentrations and Temperatures", Combustion and Flame, submitted for publication (1989).

4. Boedeker, L.R., and Dobbs, G.M., Comb. Sci. Technol., **46**:301, (1986).

5. Santoro, R.J., Semerjian, H.G., and Dobbins, R.A., Combustion and Flame, **51**:203, (1983).

6. Best, P.E., Carangelo, R.M., and Solomon, P.R.: Combustion and Flame **66**, 47, (1986).

7. Serio, M.A., Hamblen, D.G., Markham, J.R., and Solomon, P.R.: Energy & Fuel, **1**, 138, (1987).

8. Solomon, P.R., Carangelo, R.M., Best, P.E., Markham, J.R., and Hamblen, D.G.: Twenty-first Symposium (International) on Combustion, p. 437, The Combustion Institute, (1987).

9. Solomon, P.R., Best, P.E., Carangelo, R.M., Markham, J.R., Chien, P.L., Santoro, R.J., and Semerjian, H.G.: Twenty-first Symposium (International) on Combustion, p. 1763, The Combustion Institute, (1987).

10. Solomon, P.R., Carangelo, R.M., Best, P.E., Markham, J.R., and Hamblen, D.G.: Fuel **66**, 897, (1987).

11. Altenkirch, R.A., Mackowski, D.W., Peck, R.E., and Tong, T.W.: Comb. Sci. Tech. **41**, 327, (1984).

12. Tourin, R.H.: Spectroscopic Gas Temperature Measurement, Elsevier, NY, (1966).

13. Limbaugh, C.C.: Infrared Methods for Gaseous Measurement: Theory and Practice, (J. Wormhoudt, Ed.), Marcell Dekker, NY, (1985).

14. Vervisch, P. and Coppalle, A.: Combustion and Flame **52**, 127, (1983).

15. Shepp, L.A. and Logan, B.F.: IEEE Trans. Nucl. Science, NS-21, (1974).

16. Freeman, M.P. and Katz, S.J.: Optical Society of Am., **50**, (8), 826, (1960).

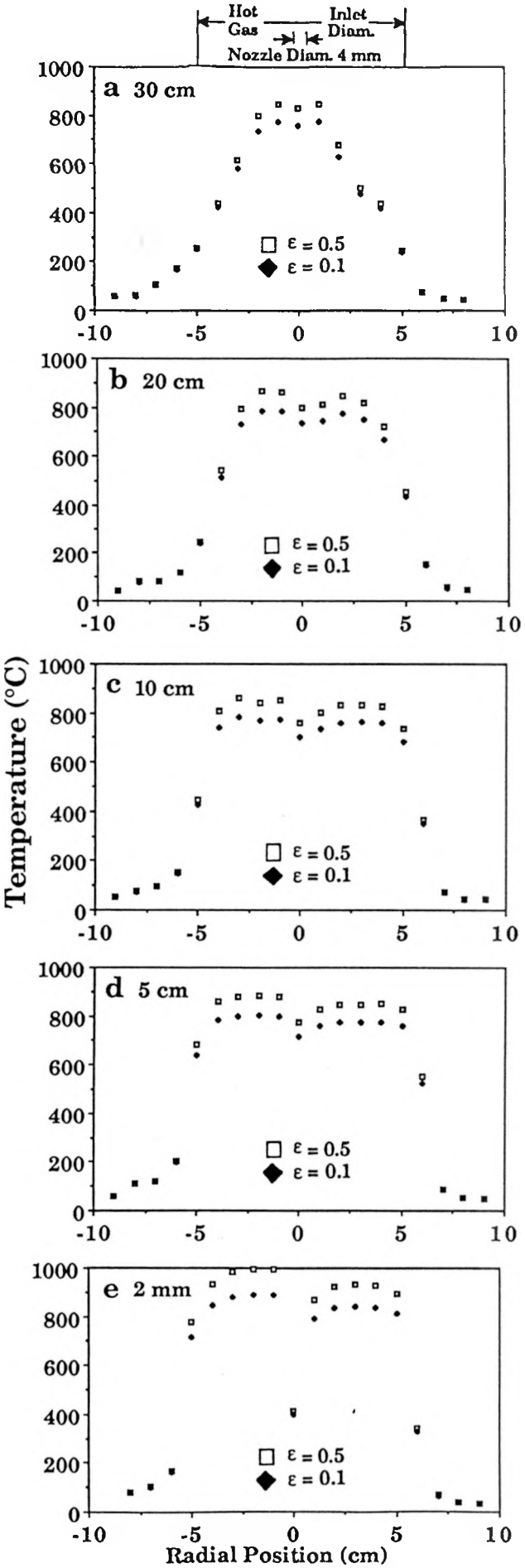

Figure 1. Radial Gas Temperature Profile in the TWR, No Coal Case. ε Represents the Surface Emissivity used to Correct the Type K Thermocouple Measurements for Radiation Loss.

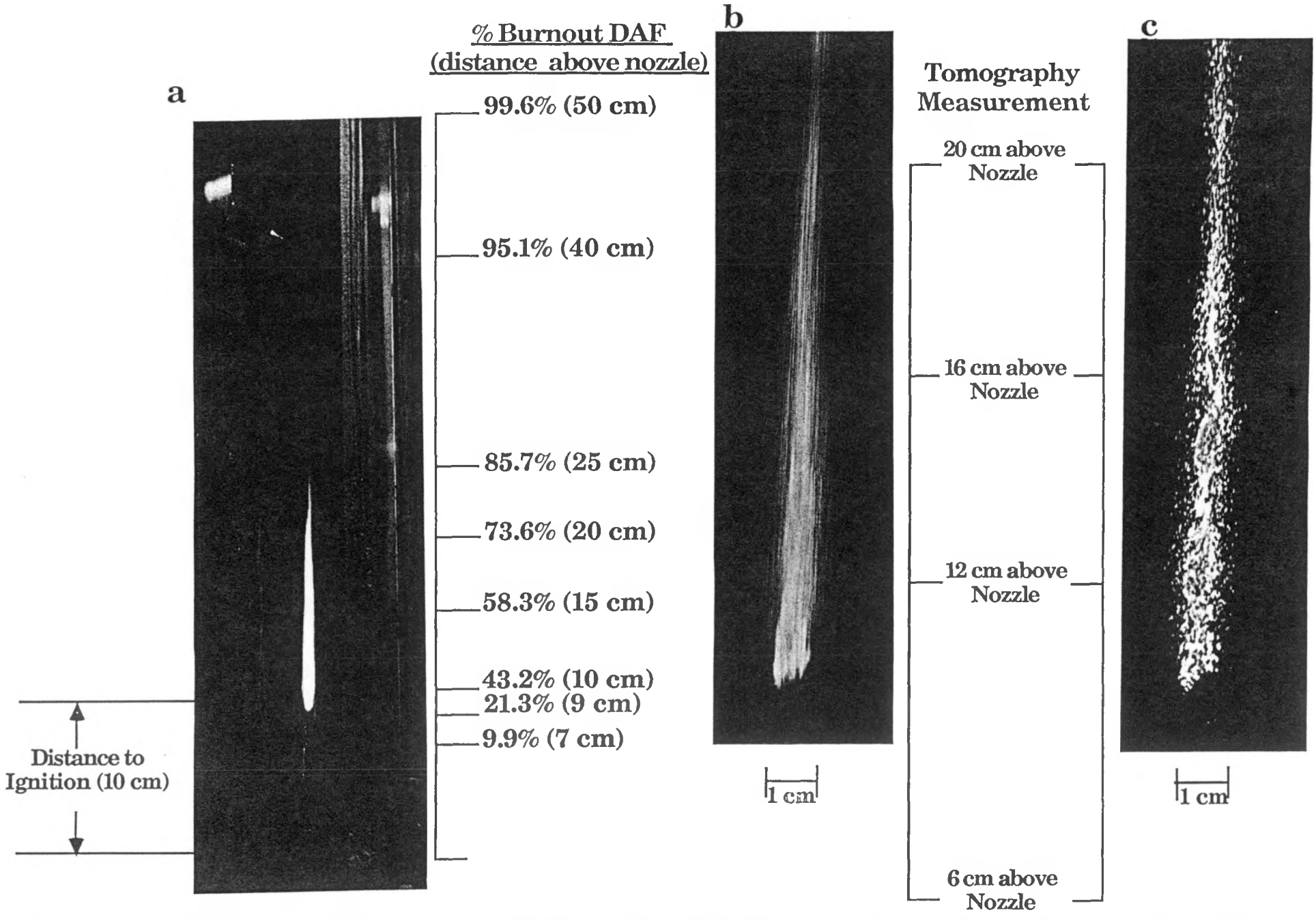

Figure 2. Photographs of Coal Flame in the TWR from Rosebud Subbituminous Coal. a) Flame with% Burnout Values at Indicated Height from Nozzle, b) Long Film Exposure and c) Short Film Exposure Close-ups to Show Density Variation of Ignited Particles Through the Flame. Position of FT-IR Tomographic Measurements are also Indicated.

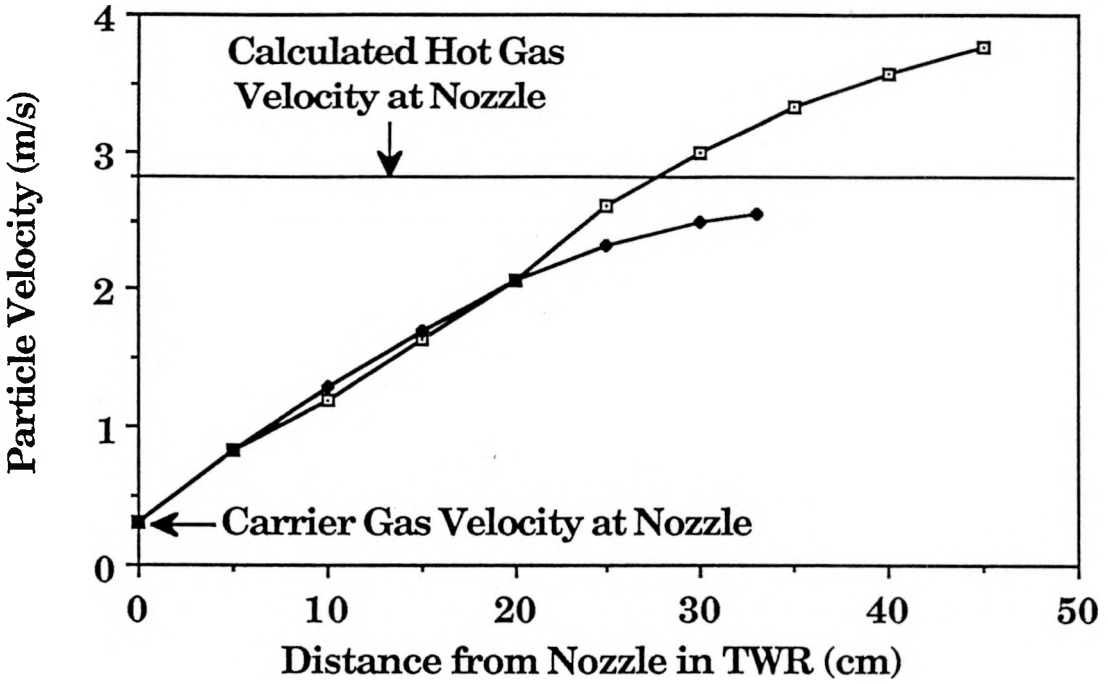

Figure 3. Particle Velocity in the TWR for Pyrolysis (◆) and Combustion (⊡) Conditions

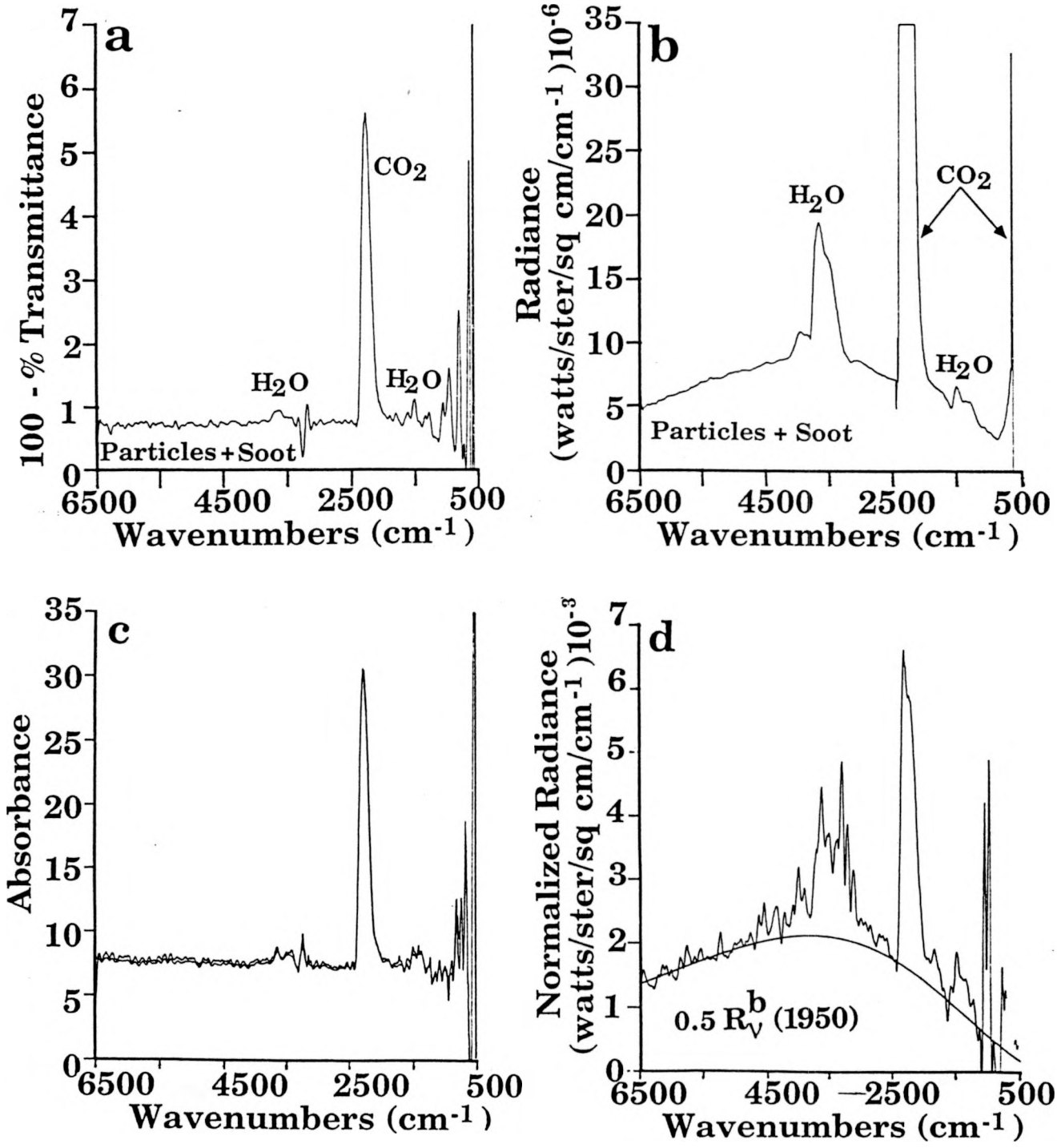

Figure 4. Results of Fourier Reconstruction of the IR Spectra of a Rosebud Coal Flame in the TWR. a) 100-% Transmittance and b) Radiance Measurement at a Radial Position 4mm from the Axis and 2cm Above Ignition. c) Summed Reconstruction of Absorbance Across the Flame Diameter Compared to Line-of-Sight Absorbance. d) Normalized Local Radiance Spectrum with Temperature Determined for the Solid Continuum.

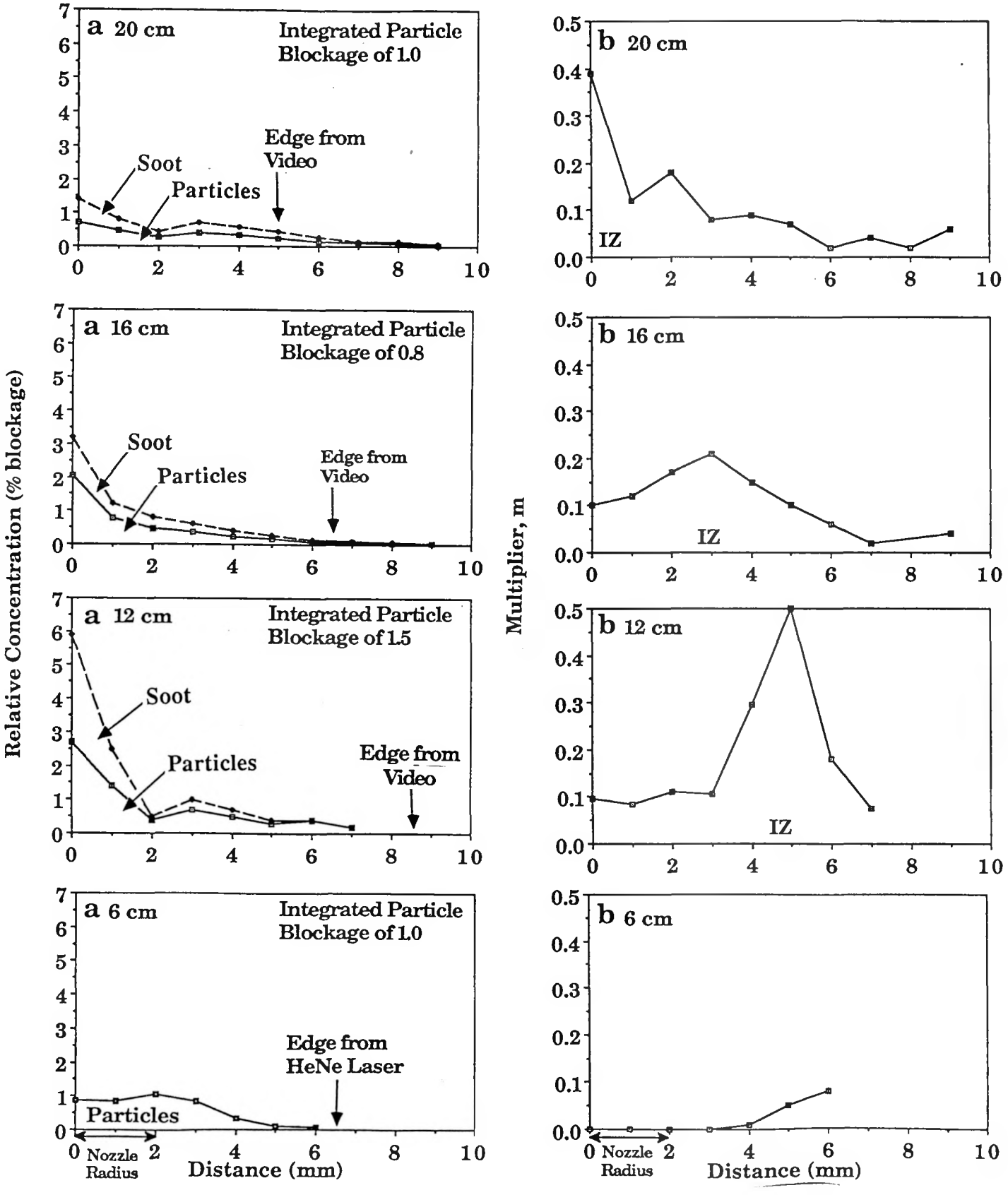

Figure 5. Radial Distributions of a) Particle Concentration and Total (Particle + Soot) Concentration, and b) Multiplier (Black-body Intensity) used for Temperature Determinations at Indicated Distances above the Nozzle for a Rosebud Coal Flame in the TWR. The Region in which the Multiplier, M is a Maximum is Designated by IZ (the Ignition Zone). The Arrows in a) Define the Edge of the Particle Stream Measured with the Video Camera or HeNe Laser.

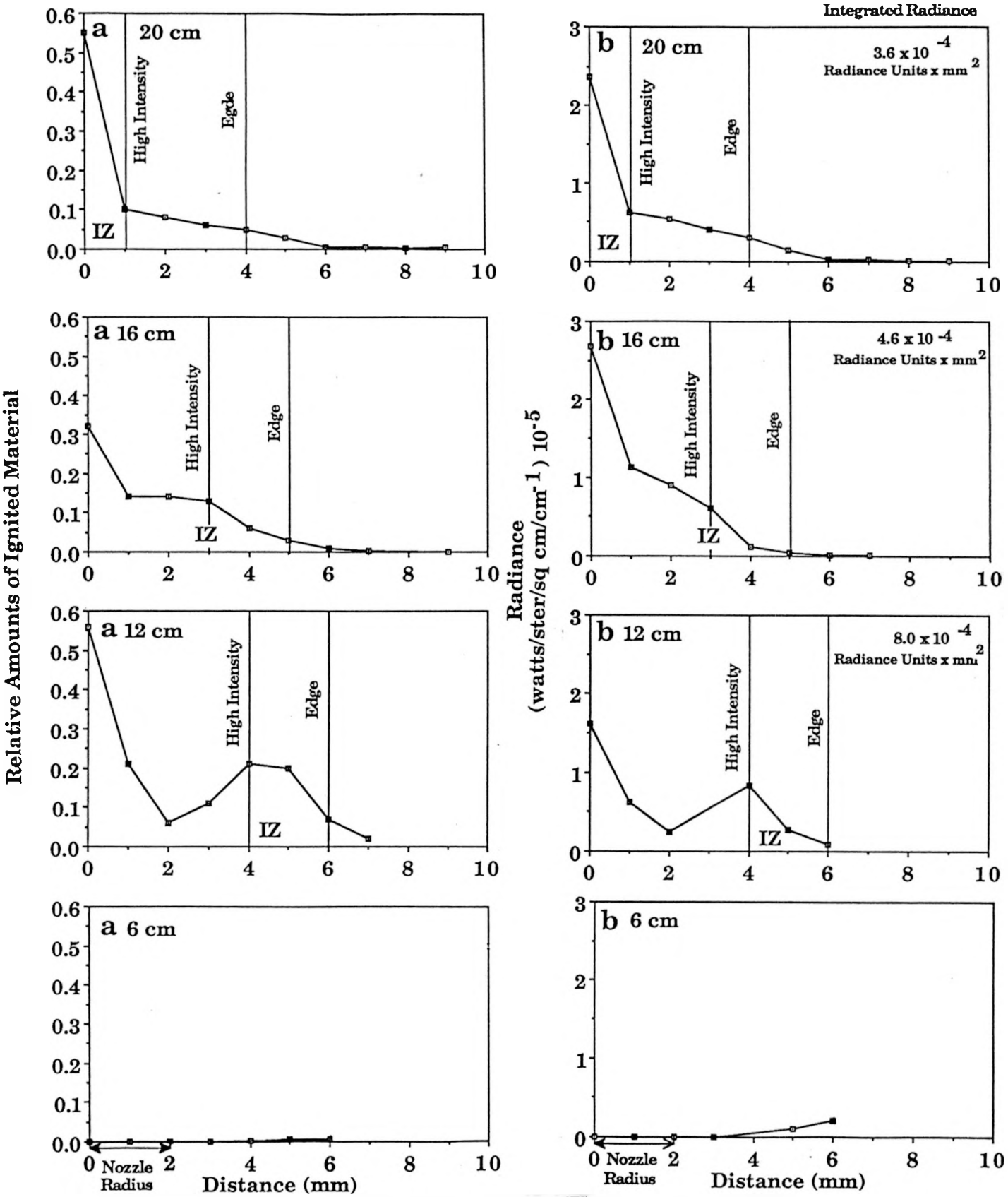

Figure 6. Radial Distributions of a) Relative Amounts of Ignited Material, and b) Radiance Level Measured 4500 cm-1, and at Indicated Distances above the Nozzle for a Rosebud Coal Flame in the TWR. The Ignition Zone (IZ), where the Multiplier, M is at a Maximum and the Edges of Low Intensity and High Intensity Burning Regions are Indicated. Integrated Radial Radiance is also shown in b.

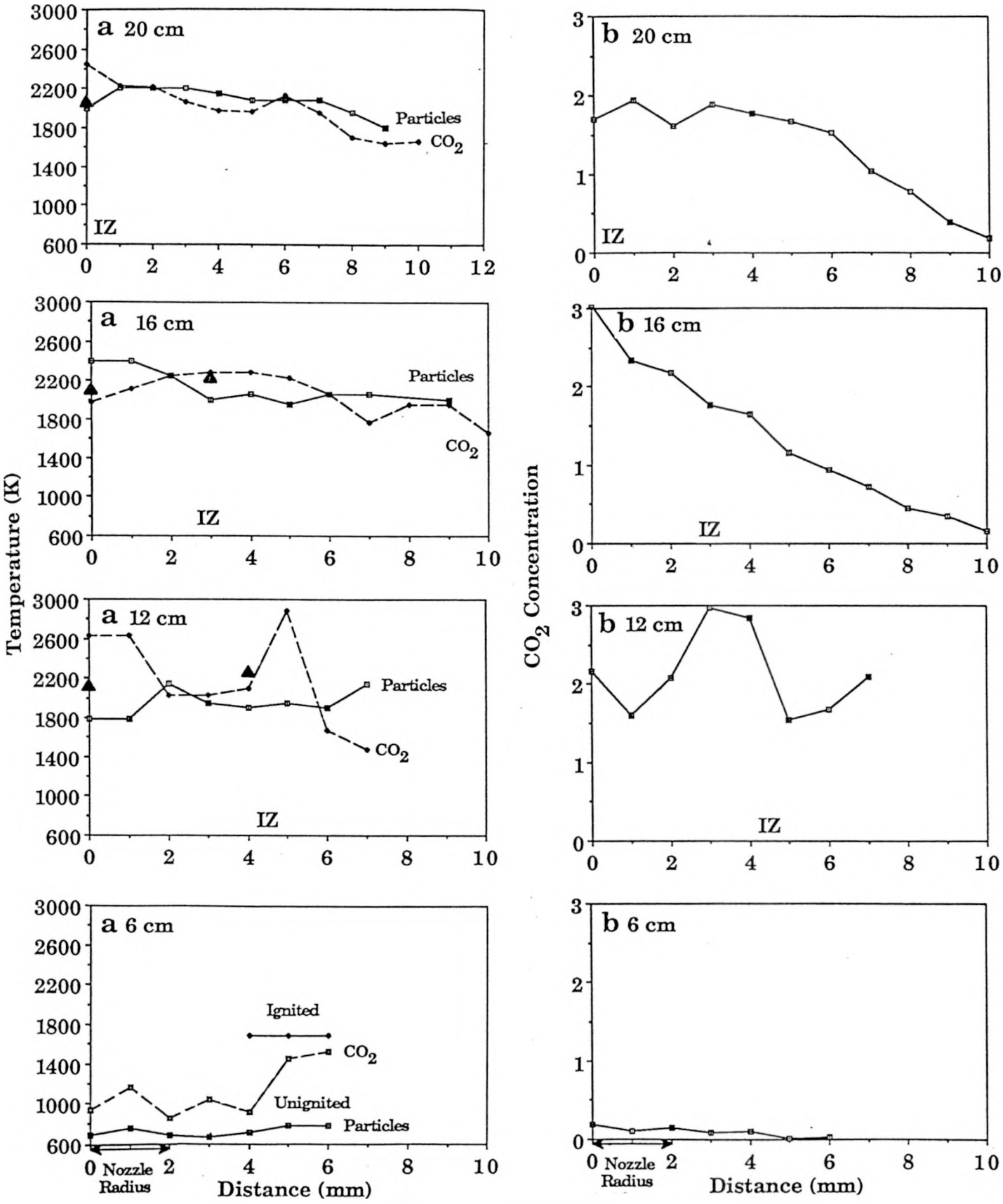

Figure 7. Radial Distributions of a) Particle (solid) and CO2 (dashed) Temperature, and b) CO2 Concentration at Indicated Distances above the Nozzle for a Rosebud Coal Flame in the TWR. Thermocouple Measurements, ▲ are indicated in a) along the Center Axis and at the Edge of the Ignition Zone (IZ), where the Multiplier, M is a Maximum.

APPENDIX B

"CHEMICAL AND PHYSICAL PROCESSES IN COUNTERCURRENT FIXED-BED COAL GASIFICATION"

Paper Submitted to the 23rd International Symposium of the
Combustion Institute, 1990

Submitted to the 23rd International Symposium on Combustion

Subject Matter: Coal Combustion, Combustion in Practical Systems, Modeling and Simulation

CHEMICAL AND PHYSICAL PROCESSES IN COUNTERCURRENT FIXED-BED COAL GASIFICATION

M. L. Hobbs, P. T. Radulovic and L. D. Smoot§
Advanced Combustion Engineering Research Center
Brigham Young University
Provo, Utah 84602
(801) 378-4326

Word Count:

Text:	3400
References:	675
Acknowledgement:	100
Figures:	1400
Tables:	200
Total:	**5000**

(Excluding References and Acknowledgement)

§ The author to whom the correspondence should be directed

CHEMICAL AND PHYSICAL PROCESSES IN COUNTERCURRENT FIXED-BED COAL GASIFICATION

M. L. Hobbs, P. T. Radulovic and L. D. Smoot
Advanced Combustion Engineering Research Center
Brigham Young University, Provo, Utah 84602

The objective of this paper is to investigate and model chemical and physical processes in slowly moving beds (i.e. fixed beds) of gasifying coal. A one-dimensional model of countercurrent fixed-bed gasification has been developed and results have been compared to experimental data obtained from a large scale gasifier. The steady-state model considers separate gas and solid temperatures, partial equilibrium in the gas phase, variable bed void fraction, coal drying, devolatilization based on chemical functional group composition, oxidation and gasification of residual char with an ash layer, and axially variable solid and gas flow rates. An accurate initial estimate of the effluent composition and temperature from a two-zone, partial equilibrium model has been found essential for this highly nonlinear problem. Predictions and comparisons to experimental data include effluent gas compositions and temperatures, temperature profiles, and axial pressure variation. Additional predictions with comparison to limited data include carbon conversion, variable particle size, and species concentration profiles. The relative importance of char oxidation resistances to bulk film diffusion, ash diffusion, and chemical reaction are identified. For the cases examined, chemical resistance dominates in the cool regions at the bottom and top of the reactor while ash diffusion resistance competes with chemical resistance through most of the reactor. The importance of adequate treatment of devolatilization, gas phase chemistry, and variable bed void fraction is identified.

Introduction

Commercial coal gasification has been used to obtain synthetic fuel as well as petrochemical feedstocks for over 200 years. The most important commercial gasification process is fixed-bed gasification. Eighty-nine percent of gasified coal is by fixed-bed, ten percent is by entrained-bed, and only one percent is by fluidized-bed.

A demonstration, Wellman-Galusha fixed-bed gasifier[1] is shown schematically in Fig. 1. Coal is fed to the top of the reactor from two coal lock hoppers and moves downward under gravity, countercurrent to the rising gas stream. The dry ash is removed at the bottom of the reactor. The influent or blast gas is composed of air saturated with steam. The steam-to-air ratio is used to control the ash temperature.

Figure 1 shows the reactor divided into four overlapping zones: i) drying, ii) devolatilization, iii) gasification, and iv) combustion. As the coal slowly descends, the hot gases produced in the gasification and combustion zones exchange energy with the cool solid. Water and

volatile matter are released when the solid reaches a sufficiently high temperature. After drying and devolatilization, the char enters the gasification zone where carbon reacts with steam, carbon dioxide and hydrogen. Endothermic reactions in this section produce carbon monoxide and hydrogen. The slightly exothermic reaction of hydrogen with carbon produces methane. Differentiation between the "gasification zone" and "combustion zone" can be determined by the presence of free oxygen. Combustion and gasification reactions can occur simultaneously in the "combustion zone". Combustible gases such as carbon monoxide or hydrogen may react with oxygen. Solid residence time in the drying, gasification and oxidation zones may be on the order of several hours. Residence time in the ash layer may be even higher depending on the thickness of this zone. The large solid residence times indicate significant settling resulting in variable axial velocities. Gas residence times are on the order of seconds.

Amundson and Arri[2] applied a detailed char model to a countercurrent reactor. Soon afterward, Yoon et al.[3], Desai and Wen[4], and Stillman[5] presented detailed models of a fixed-bed gasifier. Even though the model of Yoon et al. in 1978 was rather sophisticated, simpler global models continued to be developed.[6,7,8] Cho and Joseph[9] extended Yoon's model to include unequal gas-solid temperatures. Yoon's model was further extended by Kim and Joseph[10] to account for transient affects. Yu and Denn[11] extended Yoon's model to two space dimensions. More recent models include the one-dimensional, steady-state model of Earl and Islam[12], and the two-dimensional, transient models of Thorsness and Kang[13] and Bhattacharya et al.[14]. Khanna and Seinfeld[15] show recent advances in catalytic fixed-bed models which have many of the features of coal gasification/combustion fixed-bed models.

No major advancements have been reported in comprehensive fixed-bed gasifier or combustor modeling in the past few years. An assessment of fixed-bed models indicates common assumptions such as equal gas/solid temperatures, axially uniform gas/solid phase plug flow, uniform bed porosity, instantaneous devolatilization (with volatile yield from proximate analysis and composition assumed to be constant), char oxidation parameters from small particle data, and little or no gas phase chemistry. The model presented in this paper relaxes all of these assumptions.

Fixed-bed Model

Model Foundations

The foundation of the model is the conservation equations for mass and energy. The source terms in the continuity and energy equations are described by various physical and chemical submodels. Input parameters are reactor dimensions, operating conditions, inlet solid and gas temperature, pressure, concentrations, and flow rates and wall temperature. Calculated quantities include axial variation in gas temperature, solids temperature, pressure, species concentration, gas

flow rate, solid flow rate and wall heat loss. Plug flow is assumed in both the solid and gas phase with variable axial velocities. Gas phase pressure drop is calculated with the Ergun equation[16] for packed beds. An effective heat transfer coefficient is used for heat loss to the wall, including both stagnant and dynamic contributions as well as conduction and diffusive radiation. Large coal particle devolatilization occurs simultaneously with char oxidation and gasification. A shell progressive shrinking core model[13] describes oxidation and gasification. Equilibrium is used to calculate gas concentrations and temperatures. Turbulence is not treated formally in the slowly moving bed with low gas velocities, but is included implicitly through model correlations such as the effective heat transfer coefficient.

Table 1 summarizes general assumptions, conservation equations and boundary conditions for the one-dimensional, fixed-bed model. Reaction source terms represent coal drying and devolatilization, and char oxidation and gasification. These chemical and physical processes are shown in Fig. 2. Drying is assumed to be water vapor diffusion-limited. Devolatilization is described by assuming that the organic portion of the coal particle is composed of various functional groups: carboxyl, hydroxyl, ether, nitrogen, etc. A detailed functional group model (FG model) has been used to describe the devolatilization process[17,18,19,20]. The kinetics for evolution of each functional group are taken to be independent of the type of coal. Oxidation and gasification reactions consume the nonvolatile portion of the dry, ash-free coal. Three gasification reactants are considered: steam, carbon dioxide, and hydrogen. Volatile functional groups can competitively evolve as light gases or tar. Tar is treated as a single species that has a variable composition dependent on the location in the reactor, and can be treated in full or partial chemical equilibrium or kinetically. Gas temperature is determined by assuming all gas species to be in thermal equilibrium even though chemical equilibrium may not exist. Gas phase composition is determined by Gibbs free energy minimization. Locally varying solid temperature is determined from enthalpy and the elemental composition of the coal. All gas phase transport properties (conductivity, viscosity, diffusivity, etc.) are considered to be functions of temperature and composition.

An accurate initial estimate of the effluent composition and temperature was essential for an effective solution. With effluent conditions specified, the initial value solver LSODE[21] provides rapid, robust convergence.

Conservation Equations

Table 1 summarized the gas and solid overall continuity, gas and solid energy equations, and gas and solid species or elemental continuity equations. The constitutive relations for solid flow have been proposed only recently and no solution for these equations has been attempted.

Drying

The chemical submodels are composed of coal drying and devolatilization, char oxidation and gasification, and gas phase chemistry. Diffusion-limited vaporization of moisture from the coal particle is described by[22]:

$$r_w = k_{wm}\left(\rho_{wp} - \rho_{wg}\right) \tag{1}$$

where k_{wm}, ρ_{wp} and ρ_{wg} represent the moisture mass transfer coefficient, surface moisture concentration and bulk water concentrations respectively. Blowing or transpiration effects influence the rates by approximately 5% for large particles, and while included in the model, have been neglected for the calculations herein.

Devolatilization

Coal devolatilization rates can be described by consumption of solid or by production of light gas and tar:

$$r_i = \rho^o_{sm}\left(1-\varepsilon^o\right)\left(1-\Omega^o_{ash}-\Omega^o_{moisture}\right)\frac{d\omega_{i,\,(char,\,tar,\,or\,gas)}}{dt} \tag{2}$$

where ρ^o_{sm} is measured apparent density of the feed coal, ε^o is the bed void fraction of the feed coal, Ω^o_{ash} and $\Omega^o_{moisture}$ are the proximate ash and moisture fractions of the feed coal, and $\omega_{i,(char,\,tar,\,or\,gas)}$ is the weight fraction of the i^{th} functional group in the char, tar, or gas. The time derivatives in Eq. (2) were calculated by assuming that light gases do not evolve from the gaseous tar:

$$\frac{d\omega_{i,gas}}{dt} = \left(1-x^o+x\right)k_i Y_i \text{ and } \frac{d\omega_{i,tar}}{dt} = k_x x Y_i \tag{3}$$

$$\frac{d\omega_{i,char}}{dt} = -\frac{d\omega_{i,gas}}{dt} - \frac{d\omega_{i,tar}}{dt} \tag{4}$$

$\omega_{i,gas}$, $\omega_{i,tar}$, and $\omega_{i,char}$ represent fractional amounts of a particular functional group component that has evolved as light gas, tar or is remaining in the solid. Normally distributed Arrhenius rate coefficients for 19 functional groups and tar, k_i and k_x, where obtained from Solomon et al.[20] for the organic functional groups depicted in Fig. 2. The X and Y values represent the two-dimensional description of coal[18]. The Y dimension is divided into fractions according to the chemical composition of the coal. The initial fraction of a particular functional group component is represented by Y_i^o, and the sum of Y_i^o's equals 1. The evolution of each functional group into the gas is represented by the first order decay of the Y dimension, $\frac{dY_i}{dt} = -k_i Y_i$. The X dimension

represents non-tar-forming char, tar-forming-char, and tar. The evolution of tar is represented to be the first order decay of the X dimension, $\frac{dx}{dt} = -k_x x$. The potential tar forming fraction, x^o, was adjusted herein to match experimentally determined tar yields, though it can also be predicted.

Oxidation and Gasification

A shrinking core model with a developing ash layer, commonly referred to as the shell progressive char oxidation model[13], is used for the calculations presented in this paper. The reaction rate for a single coal particle can be derived as[23]:

$$r_p = \frac{A_p \upsilon_s M_p C_{ig}}{\left(\frac{1}{k_r \zeta} + \frac{1}{k_m} + \frac{1}{k_{ash}}\right)} \tag{5}$$

where the resistances in the denominator represent surface reaction, molecular diffusion through the gaseous film and diffusion through the ash layer. Equation (5) neglects the effects of diffusion-induced convective transport and assumes that the reactions are first order in oxidizer concentration. Quantities A_p, ν_s, M_p, C_{ig}, k_r, ζ, k_m, and k_{ash} represent the external surface area of the particle, the stoichiometric coefficient to identify the number of moles of product gas per mole of oxidant, char molecular weight, molar concentration of oxidizer or gasification agent in the bulk gas phase, Arrhenius chemical reaction rate constant, particle area factor to account for internal surface burning, bulk mass transfer coefficient, and ash layer mass transfer coefficient, respectively.

The last resistance in the denominator of Eq. 5 can be determined using an effective mass transfer coefficient[13]:

$$\frac{1}{k_{ash}} = \frac{(1-F)d}{2D_{eff}} \tag{6}$$

where F, d, and D_{eff} represent the fraction of original carbon, coal particle diameter, and effective diffusivity, respectively. Walker et al.[24] and Laurendeau[25] discuss methods for calculating effective diffusivities. Park and Edgar[26] show the effect of a developing ash layer on the burning rate of a core sample of coal. The core burning rate can be predicted by using an effective diffusivity based on the molecular diffusivity multiplied by a constant ($D_{eff} = \phi D_m$). The constant, ϕ, is based on the porosity of the developing ash layer. Thorsness and Kang [13] have used 0.35 for ϕ which is based on the ash porosity. Wang and Wen[27] have measured porosity of a fire clay ash which varied from 0.44 to 0.75. Laurendeau[25] shows that ϕ can be estimated by the ash porosity divided by two. The value two is an estimate of the tortuosity squared. Since ϕ is a function of ash porosity and developing pore structure, ϕ was chosen as 0.18 for this study.

The single particle model can be related to the bed by use of the particle number density and unreacted core particle surface area. The particle diameter, unreacted core diameter and number density were obtained by mass balance, assuming spherical particles:

$$d = \left[(1-\Omega^o_{ash})d_u^3 + \Omega^o_{ash} d_o^3\right]^{1/3} \tag{7}$$

$$d_u = F^{1/3} d_o \tag{8}$$

$$n = \frac{6(1-\varepsilon)}{\pi d^3} \tag{9}$$

where the subscripts o and u represent initial and unreacted core respectively. A simple swelling model has been included to represent particle swelling during devolatilization:

$$d = d^o\left[1+\gamma\left(\frac{V}{V_\infty}\right)\right] \tag{10}$$

where γ, V, and V_∞ represent the swelling factor (chosen as 0.25 for Jetson bituminous coal with a free swelling index of 2), volatiles content, and the ultimate volatiles content, respectively.

Heat and Mass Transfer Coefficients

The heat transfer coefficient for particle to gas heat transfer was obtained following Gupta and Thodos[28]:

$$h_{sg} = \frac{2.06RT}{\varepsilon P}\mathrm{Re}^{-0.575}\mathrm{Pr}^{-0.667} \tag{11}$$

This correlation is based on evaporation of water from a packed-bed of spheres. For a reacting bed of particles, Cho[29] indicates the solid to gas heat transfer coefficient to be smaller than that predicted by Eq. (14). The mass transfer coefficient used in Eq. (5) is also obtained from Gupta and Thodos[28]:

$$k_m = \frac{2.06G}{\varepsilon\rho_g}\mathrm{Re}^{-0.575}\mathrm{Sc}^{-0.667} \tag{12}$$

where G is the superficial mass velocity of the flowing gas.

The bed-to-wall heat transfer coefficient for the gas and particle phase can be determined from the overall bed-to-wall effective heat transfer coefficient which is discussed by Froment and Bischoff[30]:

$$h_w = \frac{2.44k_r^o}{D^{1/3}} + \frac{0.0333k_g\mathrm{Pr}\,\mathrm{Re}}{d} \tag{13}$$

where k_r^o, D, and k_g represent the static contribution of the effective radial conductivity, reactor diameter, and gas thermal conductivity respectively. The static contribution of the effective radial conductivity includes diffusive void-to-void radiation and solid diffusive radiation terms. More information regarding heat and mass transfer correlations for packed-beds can be found in Froment and Bischoff[30], Kunii and Smith[31], and Solomon et al.[32].

Chapman-Enskog theory has been used to calculate multicomponent gas mixture viscosity and diffusivity[33]. The JANAF tables were used to calculate gas-phase enthalpy, entropy, and heat capacity[34]. Solid enthalpy and heat capacities were determined using Merrick's correlations[35]. Most fixed-bed models in the literature assume that the solid and gas properties (i. e. conductivity, heat capacity, viscosity, molecular weight) are not functions of pressure, temperature or composition. However, it was found that gas properties are strong functions of temperature with maximum values occurring near the temperature peak .

Experimental Data

Detailed experimental data were sought for model evaluation. Unfortunately, only limited detailed data exist, at least in the open literature. There are no published data available for separate gas and solids temperatures or gas composition in the bed. The most extensive set of fixed-bed data that includes limited profile data was compiled by Thimsen et al.[1]. Data for seventeen coals (bituminous, subbituminous, and lignite), peat, and coke were reported. The data include gasifier operation data, coal data, tar and water yield, ash and dust data, and gas composition. Some profile data for temperature and pressure were also reported. The most comprehensive set of data for gasification of Jetson high-volatile-B bituminous coal was selected for use in this study. The general schematic for this reactor and operating conditions were presented in Fig. 1.

Data and Model Comparisons

Compositions and Temperatures

The measured and predicted effluent gas composition and temperature are compared in Fig. 3a. The agreement is acceptable, considering that the predictions did not account for the processes which occur in the space above the coal bed. The measured and predicted influent gas composition and temperature are compared in Fig. 3b. Again the agreement is reasonable. The measured and predicted carbon conversion near the grate are also in close agreement.

The measured and predicted temperature profiles are presented in Fig. 4a. The jump near the bottom of the gasifier is caused by heterogeneous oxidation. The drop near the reactor top is caused by devolatilization. The oxidation jump is evident both in the measured and in the predicted profiles. The predicted maximum temperature is high compared to measurements. However, it was reported[1] that the temperature probe was retracted from the reactor if any thermocouple junction read 1589 K (the temperature limit of the materials of the probe) which did not allow peak temperature measurements in the combustion zone of most fuels. The predicted devolatilization temperature drop seems large and steep, although there are no measured data at this location for comparison. The difference between the gas and solids temperatures is expected to be greater in this region. The predicted carbon conversion profile is shown in Fig. 4b. The overall shape

seems qualitatively correct, but there are no measured profile data for comparison. The devolatilization jump is probably too high and too steep since axial mass transport of volatile matter was neglected. Figure 4b also shows the change in particle diameter, unreacted core diameter, and ash layer thickness throughout the reactor.

The predicted concentration profiles for major and minor species are shown in Fig. 5 assuming local gaseous chemical equilibrium. The blast gas is composed of air and steam. The oxidation of carbon was assumed to form CO at the surface of the char. The CO reacts in the gas phase to produce CO_2. The CO_2 peak occurs concurrently with the temperature peak. After oxygen depletion, the CO_2 reacts with the char to form CO, which begins to increase after the peak. Any CO or H_2 produced by steam gasification in the presence of oxygen was further oxidized in the gas phase to form CO_2 and H_2O. These highly exothermic reactions can partially explain the high predicted temperature peak. Assuming partial equilibrium in the gas phase may improve the temperature predictions.

Several minor species are produced in equilibrium in the reactor which decay to low values before reaching the reactor exit. These include NO, OH, and SO_2 which form in the high temperature and oxygen-rich environment near the bottom of the reactor. The devolatilization zone shows an increase in CO, H_2, and CH_4. In fact, all the CH_4 is attributed to devolatilization reactions. Normally, CH_4 is not produced at low pressures typical of this gasifier. The concentrations of N_2, CO_2 and H_2O decrease in the devolatilization zone of the reactor due to dilution effects.

Figure 6 shows the predicted carbon consumption by char oxidation and gasification reactions. The temperature peak occurs just before all oxygen is consumed in the oxidation reaction. Before oxidation is complete, steam and CO_2 gasification reactions begin. Hydrogen reacts with oxygen in the oxidation zone to form steam. Figure 6 also shows chemical, ash, and film resistances. Chemical resistance dominates at the top and bottom of the reactor where the temperatures are low. After the initial coal heats up to high temperatures, film resistance dominates at the top of the reactor. The ash resistance here is near zero since the ash layer is very small. Once the ash layer is sufficiently thick, ash diffusion competes with chemical reaction resistance. This competition occurs throughout most of the reactor. Although confidence in mass transfer coefficients is greater than chemical reaction coefficients, ash porosity is unknown throughout the reactor, and the effective ash diffusivity is difficult to predict. The effective diffusivity was assumed to be equal to the molecular diffusivity multiplied by a constant related to typical ash porosity for these predictions.

Pressure Drop

Figure 7 compares measured and predicted variation in pressure with different assumptions regarding the bed void fraction. The bed void fraction was measured at the top (coal feed void fraction is 0.31) and bottom of the gasifier (ash zone void fraction is 0.64). A constant bed void fraction (average of the coal feed and ash zone void fraction, 0.47) and linearly varying bed void fraction were used in the calculation. Qualitative agreement was obtained between the predicted and measured pressure variation for both assumptions. The pressure drop is smaller in the ash zone due to lower gas mass flow rate and larger void fraction possibly caused by ash clinkers. Quantitative agreement was obtained by varying the bed void fraction linearly. The pressure profile is a sensitive indication that both void fraction and gas flow rate are predicted correctly. Accurate values of void fraction and gas flow rate are essential for quantitative profile predictions.

Conclusions

The importance of treating various chemical and physical processes in fixed-bed gasifiers with sufficient detail has been addressed with emphasis on coal devolatilization, char oxidation, gas phase chemistry, and bed void fraction. Calculations have shown that devolatilization in fixed-bed reactors is not an instantaneous process but is an intimate part of the overall fixed-bed process. Similarly, oxidation and gasification do not occur in separate zones, but simultaneously in certain regions of the reactor bed. Competition between endothermic gasification reactions and exothermic oxidation is evident in broad predicted and measured temperature peaks. Detailed gas phase chemistry was necessary to predict the features of temperature and concentration profiles. Variable bed void fraction was also necessary to accurately predict pressure drop and temperature and concentration profiles. An accurate initial estimate of the effluent composition and temperature from a two-zone, partial equilibrium model was essential for this highly nonlinear problem.

Acknowledgment

This work was sponsored principally by the U. S. Dept. of Energy/Morgantown Energy Technology Center under subcontract from Advanced Fuel Research, Inc., East Hartford, CT. (Contract No. DE-AC21-86MC23075, Richard Johnson, project officer) and also in part by the Advanced Combustion Engineering Research Center at Brigham Young University. Funds for this Center are received from the National Science Foundation (Tapan Mukherjee, project officer), the State of Utah, 25 industrial participants, and the U. S. Department of Energy. Consultations with P. R. Solomon and coworkers at Advanced Fuel Research and A. C. Hindmarsh at Lawrence Livermore Laboratory are greatly appreciated.

1 Thimsen, D., Maurer, R. E., Poole, A. R., Pui, D., Liu, B. and Kittleson, D., "Fixed-bed Gasification Research Using U. S. Coals, Volume 1 Program and Facility Description," final report, DOE/ET/10205-1689 (DE85002000), Morgantown Energy Technology Center, Morgantown, West Virginia (1984).

2 Amundson, N. R. and Arri, L. E.: AIChE J., 24, 87 (1978).

3 Yoon, H., Wei, J. and Denn, M. M.: AIChE J., 24, 885 (1978).

4 Desai, P. R. and Wen, C. Y., "Computer Modeling of the MERC Fixed-bed Gasifier," MERC/CR-78/3, U. S. Department of Energy, Morgantown, West Virginia (1978).

5 Stillman, R.: IBM J. Res. Develop., 23, 240 (1979).

6 Kosky, P. G. and Floess, J. K.: Ind. Eng. Chem. Process Des. Dev., 19, 586 (1980).

7 Daniel, K. J., "Transient Model of a Fixed-bed Gasifier," AIChE 88th National Meeting, June (1980).

8 Daniel, K. J. and Shah, R. P., "Evaluation of Scale-up Parameters for an Advanced Air Blown Fixed-bed Gasifier," paper presented at the Joint Power Generation Conference, Phoenix, Arizona, Sep 28-Oct 2 (1980).

9 Cho, Y. S. and Joseph, B.: Ind. Eng. Chem. Process Des. Dev., 20, 314 (1981).

10 Kim, M. and Joseph, B.: Ind. Eng. Chem. Process Des. Dev., 22, 212 (1983).

11 Yu, W. and Denn M. M.: Chemical Engineering Science, 38, 1467 (1983).

12 Earl, W. B. and Islam, K. A.: CHEMCA 85, paper c2b, 289 (1985).

13 Thorsness, C. B. and Kang, S. W., "A General-purpose, Packed-bed Model for Analysis of Underground Coal Gasification Processes," UCID-20731, Lawrence Livermore National Laboratory, University of California, Livermore, California (1986).

14 Bhattacharya, A., Salam, L., Dudukovic, M. P. and Joseph, B.: Ind. Eng. Chem. Process Des. Dev., 25, 988 (1986).

15 Khanna, R. and Seinfeld, J. H.: Advances in Chemical Engineering (J. Wei, J. L. Anderson, K. B. Bischoff, M. M. Denn and J. H Seinfeld, Editors), Vol. 13 p. 113, Academic Press, Inc., New York (1987).

16 Ergun, S.: Chemical Engineering Progress, 48, 89 (1952).

17 Solomon, P. R. and Colket, M. B.: Seventeenth Symposium (International) on Combustion, p. 131, The Combustion Institute, Pittsburgh, Pennsylvania (1979).

18 Solomon, P. R. and Hamblen, D. G.: Chemistry of Coal Conversion (R. H. Schlosberg, Ed.), Chapter 5, Plenum Press, New York (1985).

19 Serio, M. A., Hamblen, D. G., Markham, J. R., Solomon, P. R.: Energy & Fuels, 1, 138 (1987).

20 Solomon, P. R., Hamblen, D. G., Carangelo, R. M., Serio, M. A. and Deshpande, G. V.: Energy & Fuels, 2, 405 (1988).

21 Hindmarsh, A. C.: "ODEPACK, A Systematized Collection of ODE Solvers," in Scientific Computing (R. S. Stepleman, editor), Vol. 1. p. 55, IMACS Transactions on Scientific Computation, North-Holland, Amsterdam (1983).

22 Smoot, L. D. and Smith, P. J., Pulverized-coal Combustion and Gasification (L. D. Smoot and D. T. Pratt, editors), p. 224, Plenum Press, New York (1979).

23 Smoot, L. D. and Smith, P. J., Coal Combustion and Gasification, p. 92, Plenum Press, New York (1985).

24 Walker, P. L., Rusinko, F., and Austin, L. G., Advances in Catalysis (D. D. Eley, P. W. Selwood and P. B. Weisz, Editors), Vol. XI p.134, Academic Press Inc., New York (1959).

25 Laurendeau, N. M.: Prog. Energy Combust. Sci., 4, 221 (1978).

26 Park, K. Y. and Edgar, T. F.: Ind. Eng. Chem. Res., 26, 237 (1987).

27 Wang, S. C. and Wen, C. Y.: AIChE J., 18, 1231 (1972).

28 Gupta, A. S. and Thodos, G.: AIChE J., 9, 751 (1963).

29 Cho, Y. S.: Modeling and Simulation of Lurgi-type Gasifiers, M. S. Thesis, Washington University, Saint Louis, Missouri (1980).

30 Froment, G. F. and Bischoff, K. B., Chemical Reactor Analysis and Design, John Wiley & Sons, New York (1979).

31 Kunii, D. and Smith, J. M.: AIChE J., 6, 71 (1960).

32 Solomon, P. R., Serio, M. A., Hamblen, D. G., Smoot, L. D. and Brewster, S., "Measurement and Modeling of Advanced Coal Conversion Processes," Second Annual Report #523043-24, U. S. Department of Energy, Morgantown Energy Technology Center, Morgantown, West Virginia (October 1, 1987 to September 30, 1988).

33 Bird, R. B., Stewart, W. E. and Lightfoot, E. N., Transport Phenomena, John Wiley & Sons, New York (1960).

34 Stull, D. R. and Prophet, H., JANAF Thermochemical Tables, Second Edition, Nat. Bur. Stand. (1971).

35 Merrick, D.: Fuel, 62, 540 (1983).

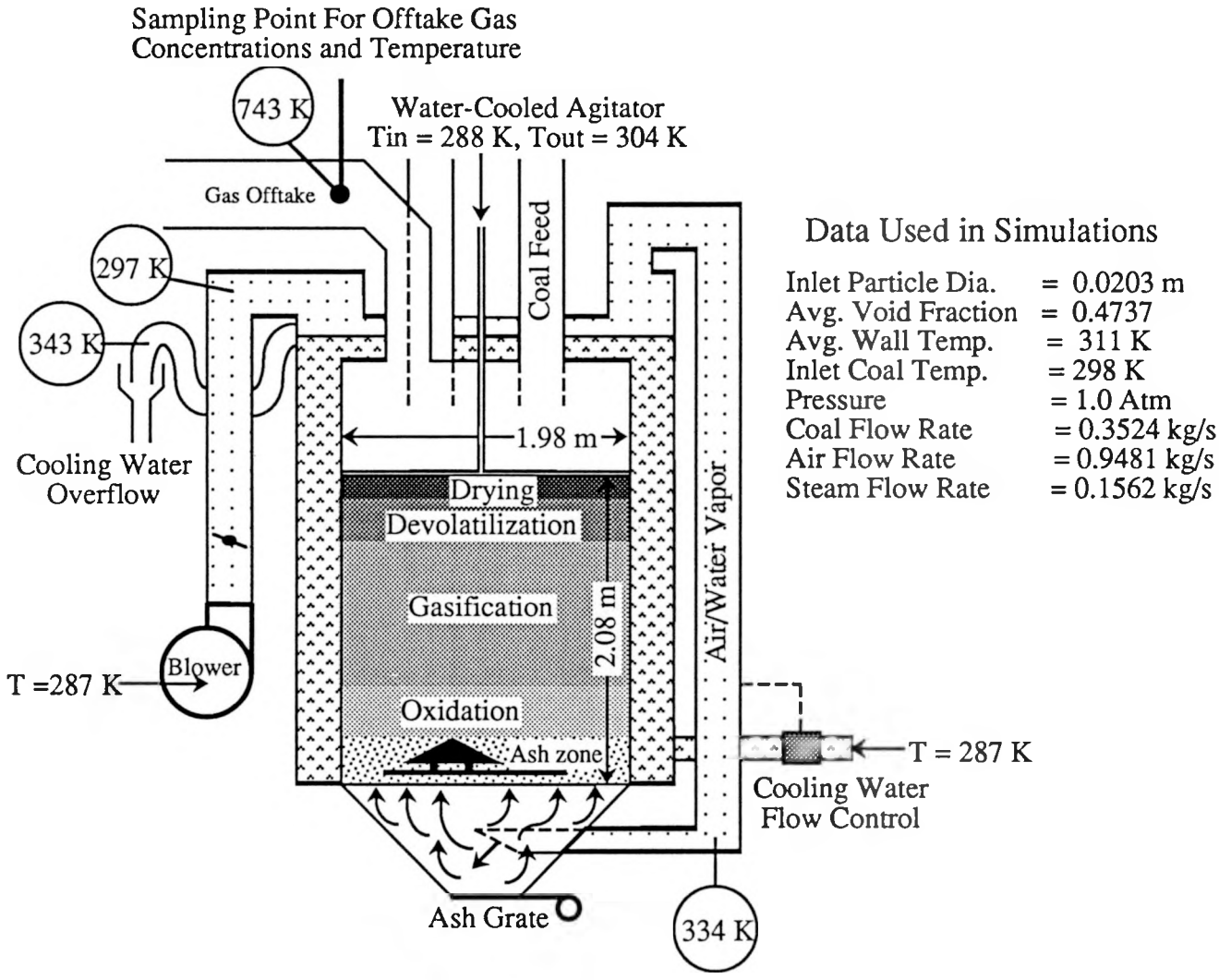

Figure 1. Schematic of typical atmospheric fixed-bed gasifier. Temperatures shown are for gasification of Jetson coal with air. Configuration and data taken from Thimsen et al.[1]

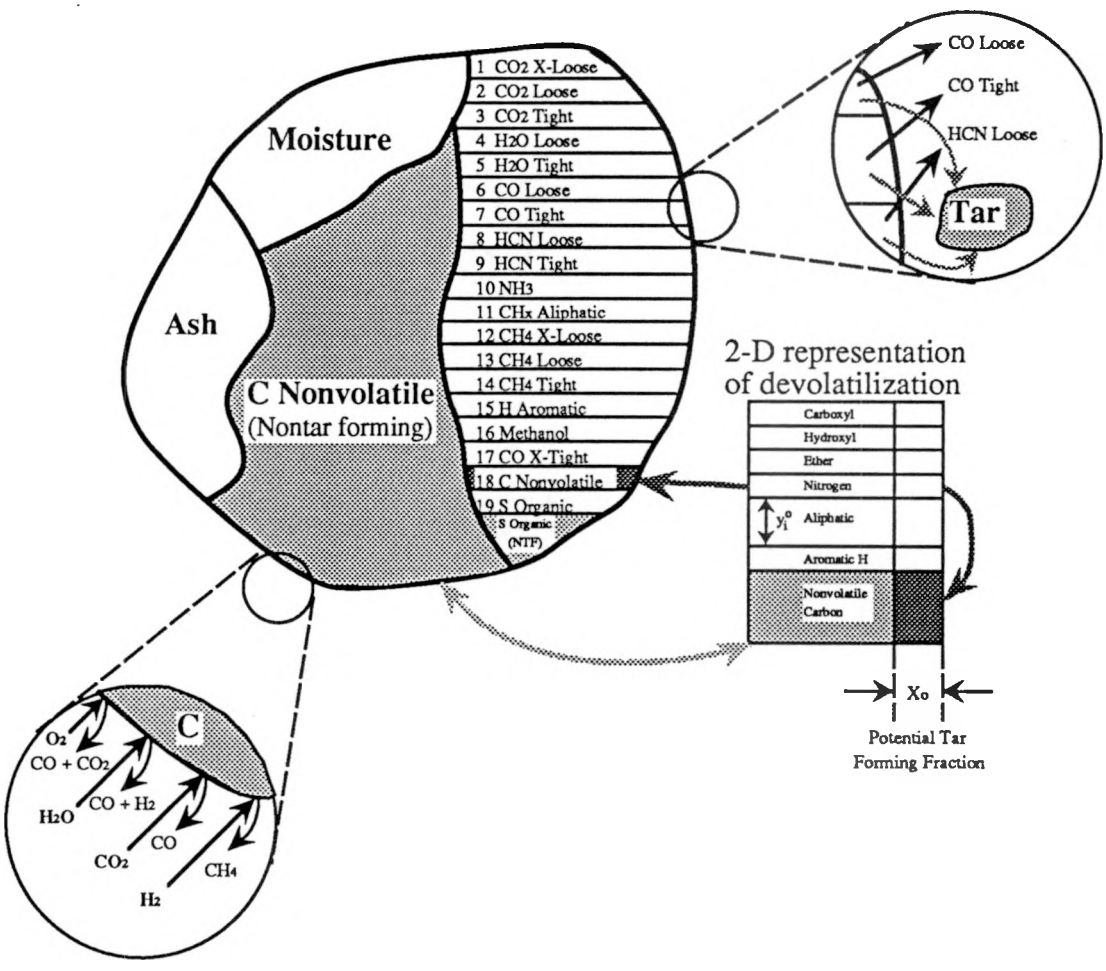

Figure 2. Schematic of coal particle with devolatilization model based on chemical functional groups[17,19] . The potential tar-forming fraction of the nonvolatile carbon functional group evolves as tar. The nontar-forming C and S organic groups evolve via heterogeneous char oxidation or gasification.

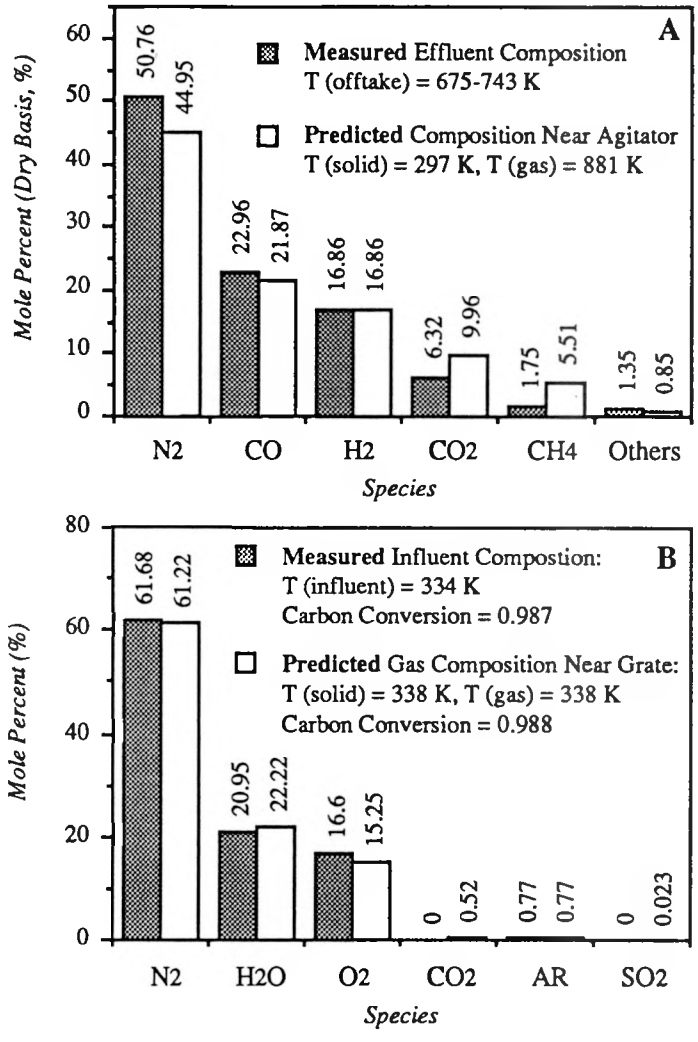

Figure 3. A) Predicted and measured effluent compositions and temperatures, B) predicted and measured influent compositions and temperatures from gasification of Jetson coal in an atmospheric gasifier with air.[1]

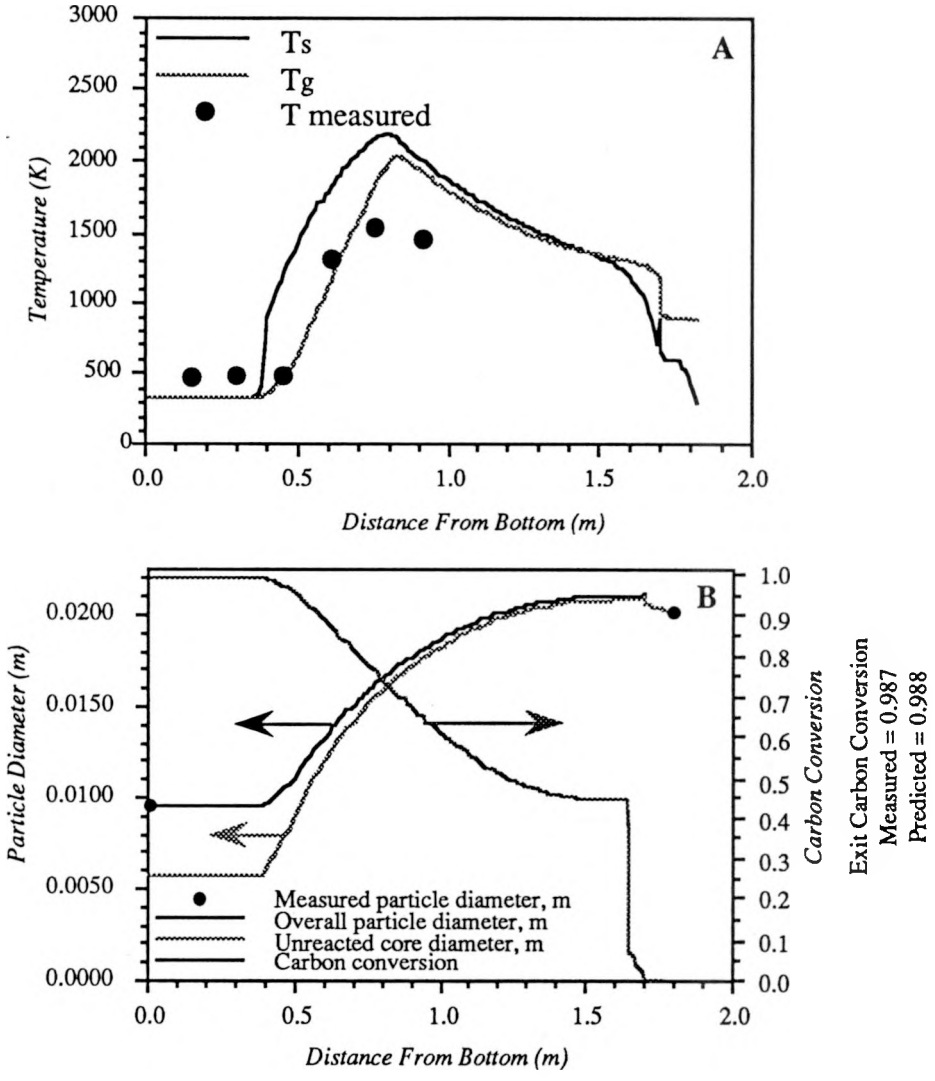

Figure 4. Predicted temperature, carbon conversion, and particle diameter for gasification of Jetson coal in an atmospheric gasifier with air[1]: A) measured and predicted temperature profile, B) predicted carbon conversion, overall and unreacted particle diameter throughout reactor.

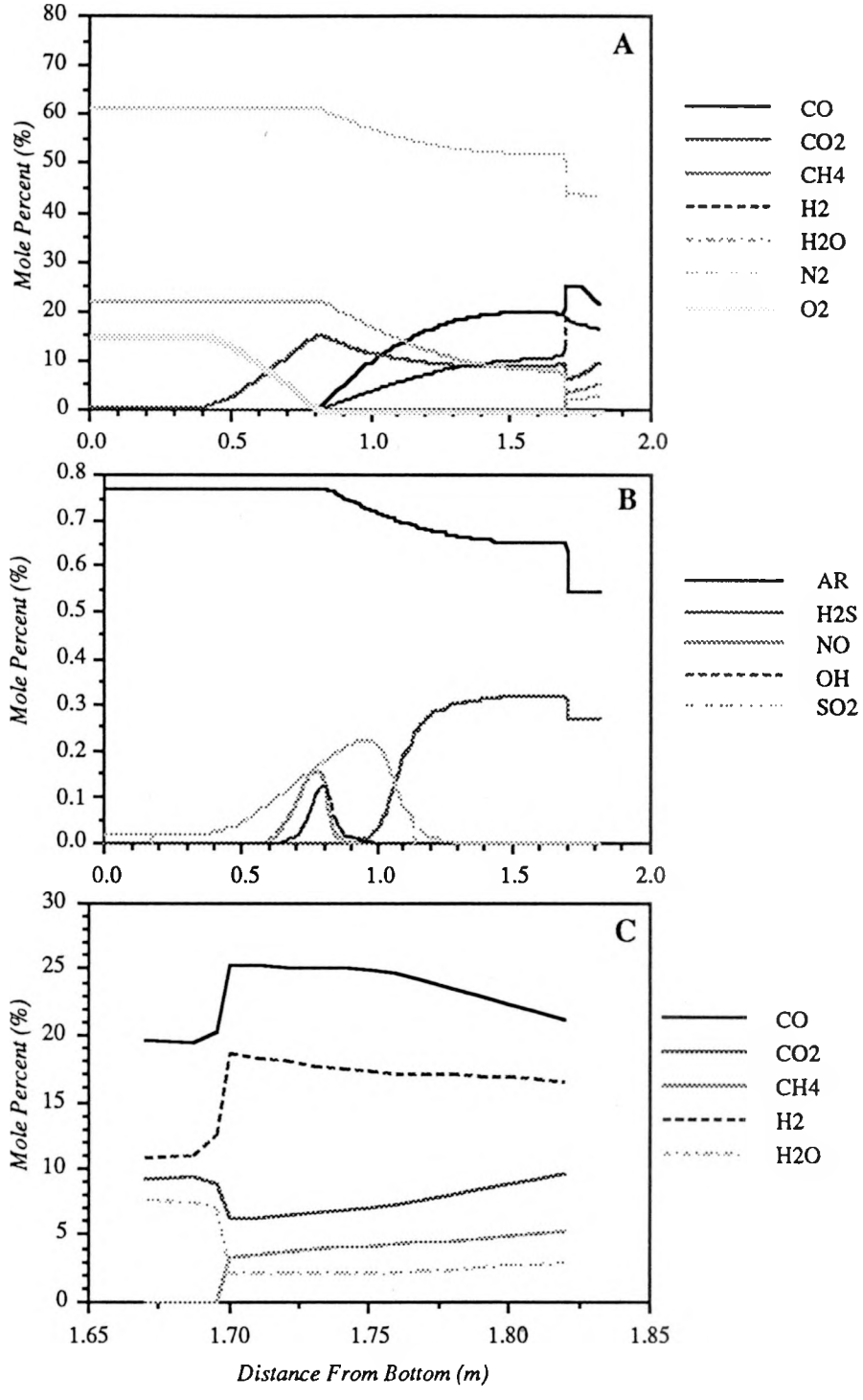

Figure 5. Predicted concentrations for gasification of Jetson coal in an atmospheric gasifier with air: A) major gas species, B) minor gas species, and C) species in devolatilization zone (excluding nitrogen).

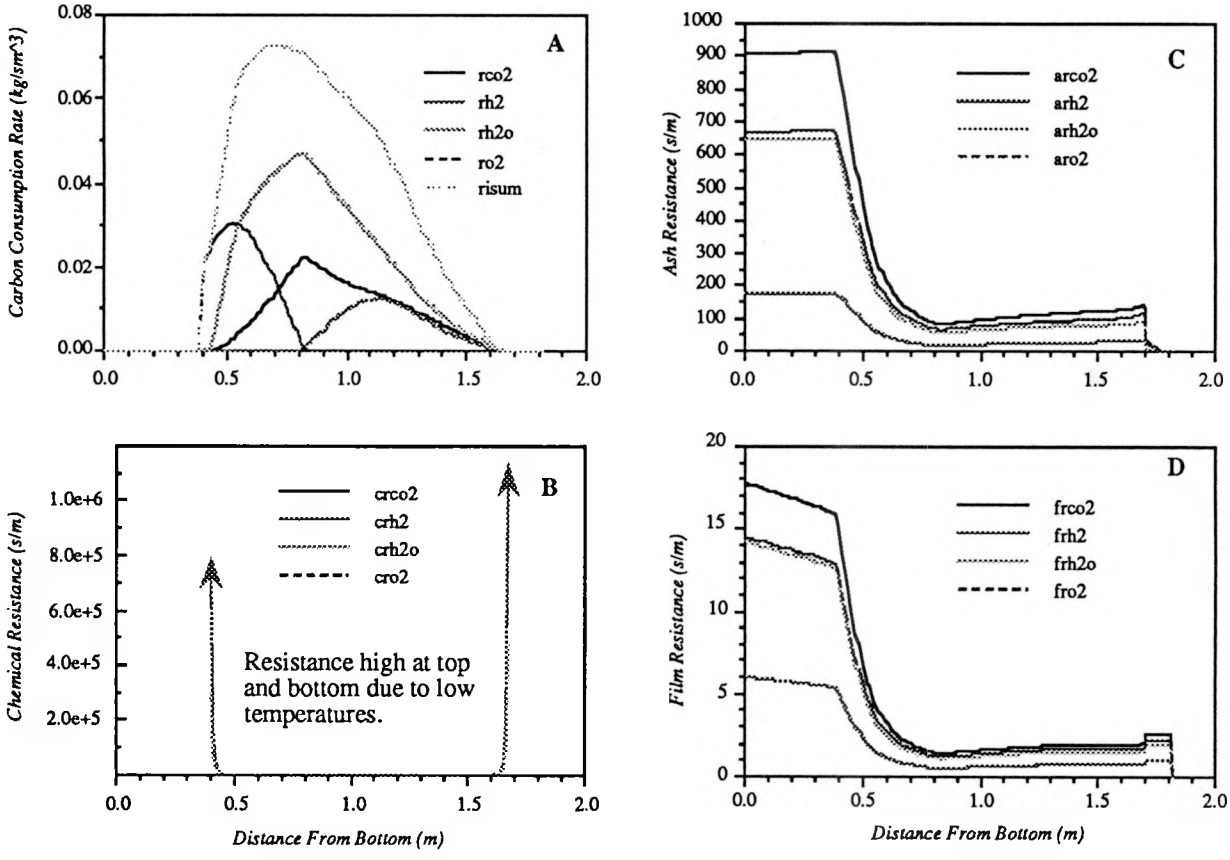

Figure 6. Carbon consumption and resistances for char oxidation and gasification of Jetson coal in an atmospheric fixed-bed gasifier: A) carbon consumption by oxidation and gasification reactions. B) chemical resistance for char oxidation and gasification reactions, C) ash resistance for char oxidation and gasification reactions, D) film resistance form char oxidation and gasification reactions.

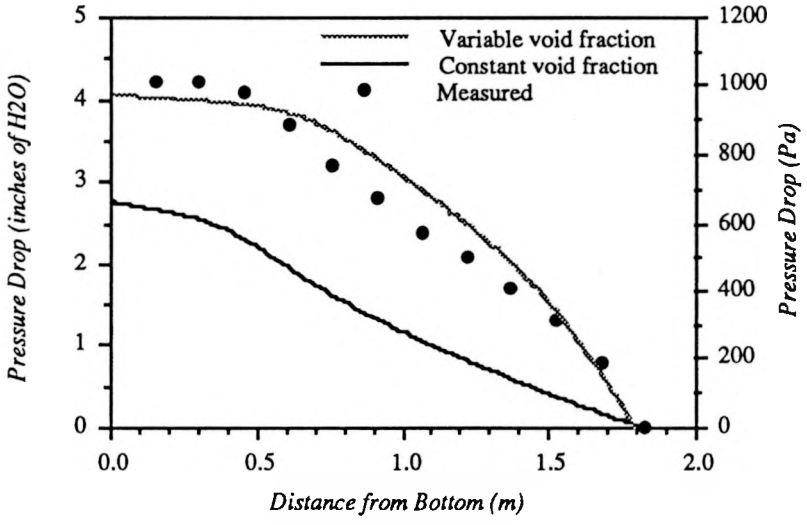

Figure 7. Comparisons of predicted and measured pressure variation in an atmospheric fixed-bed gasifier with (1) constant bed void fraction, 0.47 and (2) variable bed void fraction from 0.31 to 0.64.

Table 1. Assumptions, conservation equations and boundry conditions used in one-dimensional model.

General Assumptions

1. Interdiffusion small compared to chemical reactions.
2. Both particles and gases treated as a continuum.
3. Uniform pressure at control surfaces surrounding particles
4. Negligible viscous heating.
5. Negligible aerodynamic drag.
6. Conduction, radiation and convection to the wall are combined in an effective bulk heat transfer term.
7. Negligible work performed by moving particles.
8. Work due to body forces is small compared to chemical reaction terms.
10. Negligible Soret and Dufour effects.
11. Moving-bed is sufficiently 1-dimensional.
12. Steady state solution will be sought.
13. Negligible axial diffusion.
14. The ideal gas law is valid.
15. Negligible PV-work.
16. Neglibible viscous dissipation.
17. Turbulence effects are implicitly included (See #6).
18. The solid phase internal energy is equal to the solid phase enthalpy.

Equations

Gas & Solid Overall Continuity

$$\begin{cases} \frac{dW_g}{dz} = A\sum_{i=1}^{n} r_i \\ \frac{dW_s}{dz} = -A\sum_{i=1}^{n} r_i \end{cases}$$

Gas & Solid Energy Equation

$$\begin{cases} \frac{dW_g h_g}{dz} = A\left(Q_{sg} - Q_{gw} + \sum_{i=1}^{n} r_i h_{ig}\right) \\ \frac{dW_s h_s}{dz} = A\left(-Q_{sg} - Q_{sw} - \sum_{i=1}^{n} r_i h_{ig}\right) \end{cases}$$

Gas Component Continuity

$$\frac{dW_g \omega_{i,g}}{dt} = A\sum_{i=1}^{n} \phi r_i$$

Solid Component Continuity

$$\frac{dW_s \omega_{i,s}}{dt} = -A\sum_{i=1}^{n} \phi r_i$$

Boundary Conditions

- Reactor Top: Solid phase composition and temperature.
- Reactor Bottom: Influent gas composition and temperature.